INVESTIGATION OF RAIL BOLT HOLE CRACKS

Arthur D. Little, Inc.
Acorn Park
Cambridge, MA 02140

October 1987

Final Report

Document is available to the U.S. public through
the National Technical Information Service,
Springfield, Virginia 22161

prepared for

U.S. DEPARTMENT OF TRANSPORTATION
FEDERAL RAILROAD ADMINISTRATION
OFFICE OF RAIL SAFETY RESEARCH
WASHINGTON, D.C.

NOTICE

This document is disseminated under the Sponsorship of the Department of Transportation in the interest of information exchange. The United States Government assumes no liability for the contents or use thereof.

NOTICE

The United States Government does not endorse products or manufacturers. Trade or manufacturers' names appear herein solely because they are considered essential to the object of this report.

Technical Report Documentation Page

1. Report No.	2. Government Accession No.	3. Recipient's Catalog No.

4. Title and Subtitle	5. Report Date
Investigation of Rail Bolt Hole Cracks	October 1987
	6. Performing Organization Code
7. Author(s)	8. Performing Organization Report No.
R.A. Mayville, P.D. Hilton and D.C. Peirce	89672
9. Performing Organization Name and Address Arthur D. Little, Inc. Acorn Park Cambridge, MA 02140	10. Work Unit No. (TRAIS)
	11. Contract or Grant No. DTRS-57-83-C-0078
12. Sponsoring Agency Name and Address U.S. Department of Transportation Federal Railroad Administration Office of Rail Safety Research Washington, DC	13. Type of Report and Period Covered Final Report November 1983 - June 1984
	14. Sponsoring Agency Code FRA-RRD-1

15. Supplementary Notes

16. Abstract

This document is a collection of two reports on the rail bolt hole crack. Part I describes the development of a model based on beam-on-elastic foundation analysis to calculate the shear force acting at a given bolt hole location. The model includes the effects of wheel and joint bar forces, joint efficiency factor, and dynamic wheel load amplification. Also described are experiments to derive the stress intensity - bolt hole crack length relationship for rail end loading representative of the joint. The stress intensity was found to be independent of crack length for the range studied: 0.5-3 in. The model and experimental results are used to predict crack growth rates for severe traffic conditions. Part II describes analyses of three stages of bolt hole cracking: initiation, corner crack propagation, and through crack propagation up to and into the rail head. The initiation analysis makes use of the force model of the first report and results in the literature to calculate the mean and alternating stresses at the bolt hole surface. Dynamic load effects are considered and the most common occurrence of a bolt hole crack propagating away from the rail end toward the head is explained. Data are reviewed to show that fretting from the bolt or corrosion is probably necessary to initiate fatigue cracking. Estimates of the number of cycles required to propagate a corner crack to a through crack are given, including the effects of wheel eccentricity and lateral load. Several aspects of through crack propagation were considered. The stress intensity of a crack emanating from the first bolt hole due to bolt bearing is calculated for three crack lengths. Estimates of the stress intensity factors are also provided for various straight and kinked crack geometries in the rail head and along the head-web fillet. In addition, finite element analysis was performed to calculate the shear stresses distribution in a rail cross section (2D) and the stress intensity for a bolt hole crack that has entered the rail head (3D). The appendices to Part II describe the fracture appearance of three bolt hole cracks removed from service and a fixture design that could be used to break open bolt hole cracks.

17. Key Words	18. Distribution Statement
Fretting, Rail, Rail End, Fatigue, Crack Initiation, Crack Growth, Corner Cracks, Bolt Holes, Stress Intensity Factor	DOCUMENT IS AVAILABLE TO THE PUBLIC THROUGH THE NATIONAL TECHNICAL INFORMATION SERVICE, SPRINGFIELD, VIRGINIA 22161

19. Security Classif. (of this report)	20. Security Classif. (of this page)	21. No. of Pages	22. Price
Unclassified	Unclassified	150	

Form DOT F 1700.7 (8-72) Reproduction of completed page authorized

METRIC CONVERSION FACTORS

Approximate Conversions to Metric Measures

Symbol	When You Know	Multiply by	To Find	Symbol
		LENGTH		
in	inches	2.5	centimeters	cm
ft	feet	30	centimeters	cm
yd	yards	0.9	meters	m
mi	miles	1.6	kilometers	km
		AREA		
in^2	square inches	6.5	square centimeters	cm^2
ft^2	square feet	0.09	square meters	m^2
yd^2	square yards	0.8	square meters	m^2
mi^2	square miles	2.6	square kilometers	km^2
	acres	0.4	hectares	ha
		MASS (weight)		
oz	ounces	28	grams	g
lb	pounds	0.45	kilograms	kg
	short tons (2000 lb)	0.9	tonnes	t
		VOLUME		
tsp	teaspoons	5	milliliters	ml
Tbsp	tablespoons	15	milliliters	ml
fl oz	fluid ounces	30	milliliters	ml
c	cups	0.24	liters	l
pt	pints	0.47	liters	l
qt	quarts	0.95	liters	l
gal	gallons	3.8	liters	l
ft^3	cubic feet	0.03	cubic meters	m^3
yd^3	cubic yards	0.76	cubic meters	m^3
		TEMPERATURE (exact)		
°F	Fahrenheit temperature	5/9 (after subtracting 32)	Celsius temperature	°C

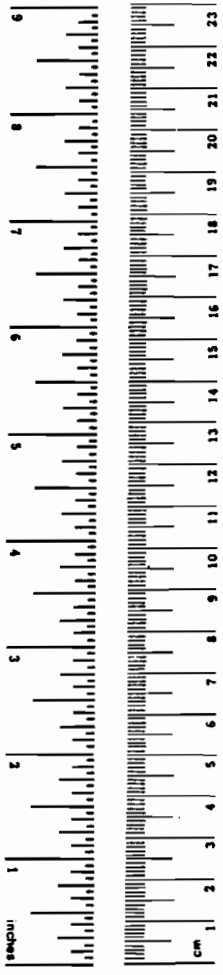

Approximate Conversions from Metric Measures

Symbol	When You Know	Multiply by	To Find	Symbol
		LENGTH		
mm	millimeters	0.04	inches	in
cm	centimeters	0.4	inches	in
m	meters	3.3	feet	ft
m	meters	1.1	yards	yd
km	kilometers	0.6	miles	mi
		AREA		
cm^2	square centimeters	0.16	square inches	in^2
m^2	square meters	1.2	square yards	yd^2
km^2	square kilometers	0.4	square miles	mi^2
ha	hectares (10,000 m^2)	2.5	acres	
		MASS (weight)		
g	grams	0.035	ounces	oz
kg	kilograms	2.2	pounds	lb
t	tonnes (1000 kg)	1.1	short tons	
		VOLUME		
ml	milliliters	0.03	fluid ounces	fl oz
l	liters	2.1	pints	pt
l	liters	1.06	quarts	qt
l	liters	0.26	gallons	gal
m^3	cubic meters	35	cubic feet	ft^3
m^3	cubic meters	1.3	cubic yards	yd^3
		TEMPERATURE (exact)		
°C	Celsius temperature	9/5 (then add 32)	Fahrenheit temperature	°F

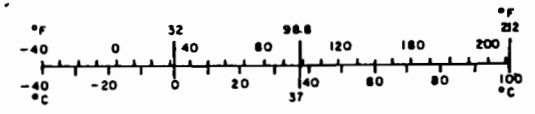

EXECUTIVE SUMMARY

The bolted rail joint represents a discontinuity and, consequently, a weakness of the track structure. Joint bars constantly loosen and bolt hole cracking poses an uncertain danger. Despite the steady replacement of bolted rail by continuously welded rail to alleviate these problems there remains a substantial number of bolted joints. In fact, bolted joints are likely to always be present in such localities as insulated joints and curves for which ease of rail replacement is necessary.

Thus, various means are required to locate bolt hole cracks and to decide whether they must be removed. Technology exists to inspect for bolt hole defects but there is currently no method to determine how fast these cracks grow or when they pose a real threat of fracture.

In order to address these issues, the Federal Railroad Administration (FRA) has organized a research effort to utilize statistics and fracture mechanics to better define rail inspection intervals. An important element of this work is a determination of rail defect geometrics and sizes, rates of growth, and conditions under which fracture and consequent loss of rail integrity occur. This report deals only with the bolt hole crack.

The report is divided into two parts which represent separate investigations. Part I, an Analytical and Experimental Study of Fatigue Crack Growth from Rail End Bolt Holes, deals only with crack growth of a through crack emanating from the first bolt hole toward the rail head and away from the rail end. The crack length range studied was 0.5-3 in. This type of crack is by far the most commonly observed bolt hole crack. The first part of this report is the derivation of a model to calculate the shear force at a bolt hole which is considered the primary driving force for crack growth. The model uses beam-on-elastic foundation analysis to calculate the shear force and bending moment that would exist at the joint center if the rail were continuous. These reactions are then multiplied by the joint efficiency factor k which can range from 0 (no joint) to about 0.8. Next, the joint bar reactions are calculated from equilibrium assuming contact between joint bar and rail under the rail head at the rail end and on the base at a distance from the rail end that depends on the joint type. (These kinematics were observed by Talbot).

Finally, another beam-on-elastic foundation analysis is conducted that includes the joint bar reactions and the wheel load if the wheel is located on the rail of interest. The predicted variation of shear force at the first bolt hole with wheel position along the rail is almost exactly the same as the variation of strain measured on the bolt hole surface for a slowly moving train. This shows that the shear force determines the stress at the bolt hole as expected. The model shows that the shear force at the bolt hole caused by the joint bar reactions and wheel load can be twice the shear force caused by the wheel load alone on continuous rail.

Part I also includes the description of experiments on three-foot rails to derive the stress intensity as a function of bolt hole crack length. The rail specimens were loaded in three-point bending with the end loads applied under the rail head and the center load applied on the rail base to simulate the action of the joint bars. Each rail end contained a bolt hole crack and a prenotch oriented at 45# to the rail axis toward the head away from the end. The rail was cyclically loaded to 80 kips and the crack growth rate measured. Comparison of crack growth rates to the crack growth rate-stress intensity relationship derived from compact tension specimens was used to derive the stress intensity for the bolt hole crack. The stress intensity K_I was 20 ksi!in for a shear force at the bolt hole of 40 kips.

The stress intensity-shear force relation derived from the experiments was used with the shear force model to calculate the stress intensity and crack growth rate for conditions representative of revenue track. For the following conditions

rail size	=	136 lb/yd
foundation modulus	=	3000 psi
static wheel load	=	33 kips
dynamic amplification	=	2
joint efficiency factor	=	0.6

the defect is predicted to grow 1 inch in 6.2 MGT (million gross tons) of traffic. This compares favorably to the value of 9 MGT deduced from a failure analysis of a bolt hole crack under similar conditions.

Part II of this report, Further Studies of Fatigue Crack Initiation and Growth from Rail End Bolt Holes, is a series of analytical and numerical studies on various stages of bolt hole cracking. The crack initiation phase is examined by calculating alternating and mean bolt hole surface stresses and comparing these to fatigue data. Finite element and closed form solutions from the literature are used to determine the relationship between rail shear force and tensile stress on the bolt hole surface. For 132 lb/yd rail with a bolt hole located 3.5 inches from the rail end with diameter 1.12 inch the ratio of maximum tensile stress-to-bolt hole shear force is 0.6 in^{-2}; a 40 kip shear force results in a maximum stress of 24 ksi. The location of maximum tensile stress on the bolt hole surface is always at 45# to the rail axis but the orientation relative to the rail end depends on the wheel location, the joint efficiency factor, and the variation of dynamic wheel load as the wheel crosses the joint. Dynamic wheel load measurements show that the maximum load occurs immediately after the wheel crosses the joint, but there is a second, lower peak when the wheel passes the first bolt hole. When this variation is used in the shear force model for reasonably good joint conditions the location of maximum stress is found to favor crack growth toward the rail head away from the rail end; this is the most commonly observed orientation.

Substitution of the bolt hole stresses into the Goodman equation shows that an endurance strength (completely reversed loading) of approximately 18 ksi is required to explain fatigue. The endurance strength

of rail steel from laboratory specimens for rail web steel is 35 ksi. Data on a similar steel show that fretting can reduce the endurance strength to 22 ksi. Thus, the fretting caused by bolt bearing can explain the initiation of bolt hole cracks.

The next stage of crack growth examined is the propagation of corner cracks from the bolt hole. Closed form expressions for a corner crack emanating from a hole are used to calculate the stress intensity distribution along the crack front for different crack geometries. The applied stress used in these calculations is equal to the shear stress that would exist at the rail neutral axis in the absence of a hole. Combination of the stress intensity solutions with fatigue crack growth data show that a crack that has an initial radius of 0.2 inch requires about 7.5 MGT of heavy traffic to grow through the web. This is approximately the same amount of traffic required to grow a bolt hole crack 1 inch after it completely penetrates the web. A general discussion with some quantitative examples is given on the effects of eccentric and lateral wheel loads on bolt hole corner crack growth. However, the uncertainties associated with actual loading do not enable one to determine the degree to which crack growth is actually influenced.

Several analyses are provided for a through crack that emanates from the bolt hole and approaches the rail head. First, an approximate analysis is given of the effect of bolt bearing on the stress intensity factor. The bearing load is estimated to be 50 kips for a 100#F drop in rail temperature. The Mode I stress intensity due to this load is estimated to be ~ 14ksi!in.

The shear stress distribution over a rail cross section is determined for use in subsequent fracture mechanics analysis of bolt hole cracks that have penetrated the rail head. The elasticity problem is solved by an application of two-dimensional finite element analysis from which the shear stress distribution is found to be closely represented by the solution obtained from simple beam theory.

Three crack geometries are considered for bolt hole cracks that have penetrated the rail head region: a crack that runs along the head-web fillet, a crack that continues at an angle to the rail axis into the rail head, and a crack that turns vertically as it enters the rail head. All of these bolt hole defect types have been observed in service. Each of these crack types is predicted to experience mixed mode loading with increasing stress intensity for longer cracks. The defect that continues to propagate at an angle to the rail axis has the highest K_I and is of sufficient magnitude that residual stresses can cause fracture.

A three-dimensional finite element analysis was conducted to calculate the stress intensity for a bolt hole crack oriented away from the rail end whose end is at the head-web fillet. The boundary conditions include joint bar reactions and the calculations are made for various locations of the wheel with respect to the crack tip. The combined Mode I and Mode II stress intensity factor is equal to 11 ksi in for a 33 kip wheel load when the wheel is just beyond the crack tip. The

analysis also shows that the stress intensity is greatest at the center of the crack in agreement with the crack tunneling observations in the laboratory and field.

Two appendices to Part II are provided on observations of three bolt hole cracks removed from service and a fixture and rail configuration suitable for breaking open field-induced bolt hole cracks in the laboratory. Examination of field bolt hole cracks shows evidence of fretting damage in each case. The rail breaking fixture requires no more than a 100 kip load to break open bolt hole cracks.

TABLE OF CONTENTS

PART I

TABLE OF CONTENTS

PART I

LIST OF FIGURES

LIST OF FIGURES (cont.)

1. INTRODUCTION

Fatigue cracks in railroad rails are eliminated by conducting periodic inspections and removing the plugs or entire rail sections that contain the defect. The inspections are generally conducted once or twice each year with a rail car that utilizes ultrasonics or magnetic induction to locate a defect. The choice of inspection interval is based on experience in which the benefits of removing potentially dangerous and damaging defects are weighed against the costs of running an inspection vehicle and a team to remove all of the defects discovered. Setting inspection intervals would be greatly aided if it were possible to establish the rate at which fatigue cracks grow in service. Some progress has been made toward this end for the transverse detail crack [1].

This report describes the results of analysis of bolted joint mechanics and large scale experiments on rails to provide a methodology for determining the fatigue crack growth rate for a bolt hole crack. It is a continuation of previous work [2] but provides a much more thorough procedure for calculating the tonnage required to grow a bolt hole crack from one length to another.

Only one bolt hole crack geometry is considered: a crack propagating from the first bolt hole toward the rail head away from the rail end. Discussions with railroad personnel and inspection managers indicate that this is by far the most common type of bolt hole crack. The analysis presented in this report supports this assertion.

2. THE MECHANICS OF THE RAIL JOINT

The first step in the fracture mechanics approach to calculating growth rates for rail end bolt hole cracks is to determine the forces and resulting stresses which act at the bolted joint. One of the first and most significant contributions in the understanding of the bolted joint was made by the "Special Committee on Stresses in Railroad Tracks" headed by A.N. Talbot. This joint AREA-ASCE Committee existed between

the years 1918-1940 and performed extensive laboratory and field testing to determine the influence on the stresses in the rail ends and the joint bars of such variables as: joint bar type, bolt tension, foundation modulus, and joint bar length [3]. Both vertical and lateral bending of the bolted joint were studied. Some of the conclusions of these studies are outlined in the following:

- The stresses which result in the rail end and the joint bars can best be described by considering the forces between the joint bars and the rail to be applied at discrete locations as shown in Figure 1. In most cases, the results are best described by the four-force system shown in Figure 1b, but in some cases the results are better described by the six-force system shown in Figure 1c. This conclusion is based on results from mechanical strain gage measurements made at the outer fibers of the rail and the joint bar. The force systems represented in Figure 1 apply for positive and negative bending and for any location of the wheel with respect to the joint. In negative bending the forces are reversed as shown in Figure 1d.

- The joint is a discontinuity in the otherwise continuous rail. The implication of this is that a beam-on-elastic foundation analysis, which works reasonably well for a continuous rail, must be modified for the presence of a bolted joint. The Talbot Committee handled this problem by considering that the joint is only able to carry a certain fraction of the moment that a continuous rail would carry. Their laboratory and field tests indicate that this fraction depends on the condition of the joint but for a good joint varies from 0.6 to 0.8.

- Part of the moment transferred across the bolted joint is carried by longitudinal friction between the joint bar and the rail but that this generally amounts to a small percentage of the total moment.

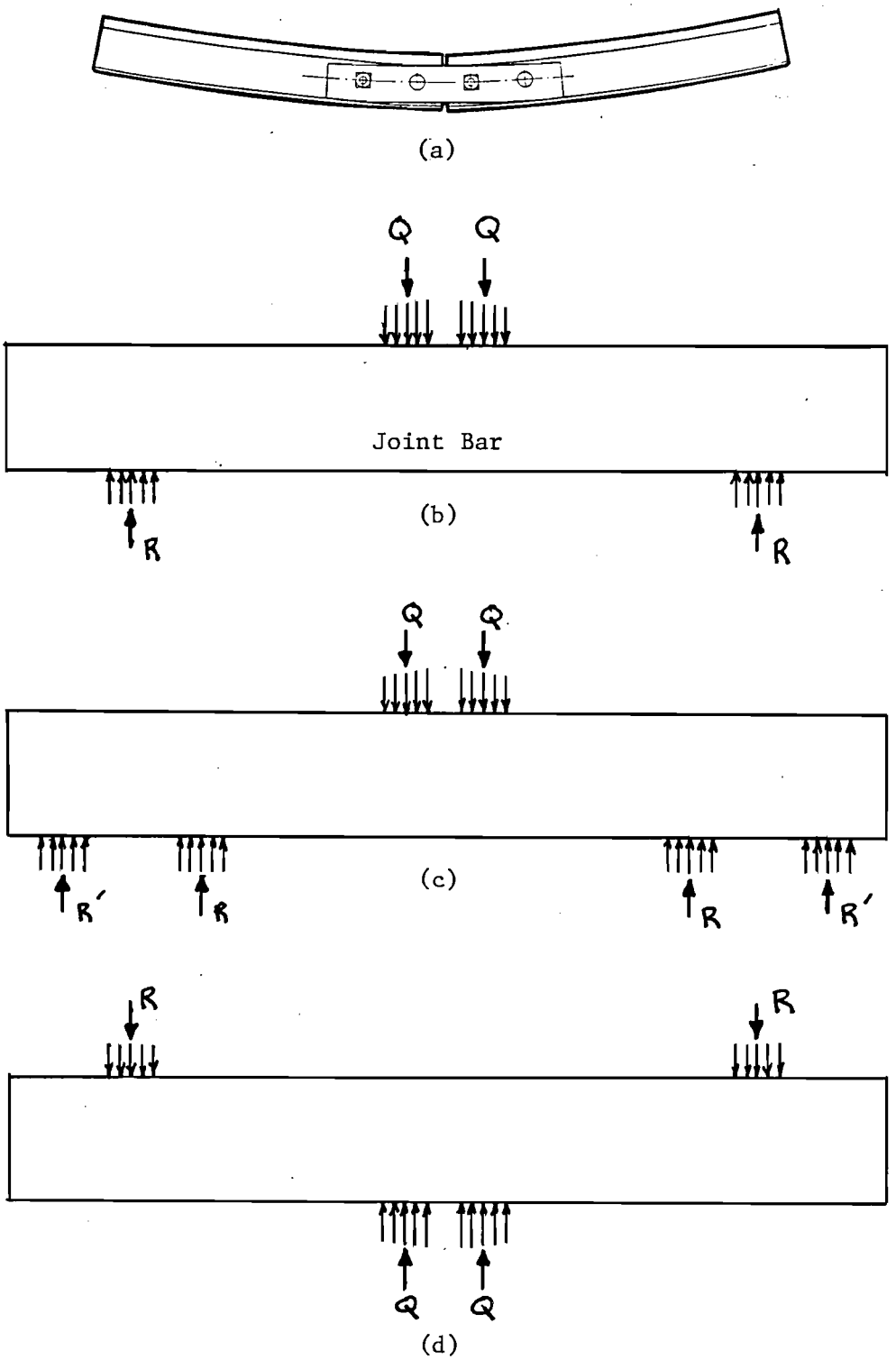

Figure 1: The forces that act on the joint bar under the action of a train wheel: (a) rail and joint bar; (b) four-force system, positive bending; (c) six-force system; (d) negative bending.

The forces between the joint bar and the rail end are applied over discrete locations along the joint bar because of the different curvatures and displacements for the joint bar and the rail end resulting from the joint forces themselves. This is illustrated in Figure 2. The moment at the end of the rail is zero which implies that the curvature there is also zero. On the other hand, the curvature in the joint bar at the rail end is a maximum because the moment in the joint bar is a maximum at the rail ends. The opposite is true near the end of the joint bar: there is a large bending moment and corresponding curvature in the rail but no moment or curvature in the joint bar. The resulting differences in displacement cause contact to occur at the center and near the ends of the joint bar as illustrated in Figure 2. Detailed examinations of the strain variations along the joint bars and rail ends indicated to the Talbot Committee that the centroid of the forces which act at the center of the joint bar, Q, are located approximately 1 in. from the rail end, and that the location of the forces, R, vary considerably from joint to joint. For 36 in. joint bars the distance between the forces Q and R was typically on the order of 10 in. The reason the distance between the forces, Q and R, is about 10 in. instead of 18 in.--half the joint bar length--is not clear. It is probably a result of a much more complex displacement and curvature distribution in the joint than that depicted in Figure 2. This phenomenon has not been investigated in detail in this report.

The Talbot Committee also found that the magnitude of the strains at the outer fibers of the joint bar could be closely approximated by carrying out the following calculations.

1. For the track and train conditions, calculate the bending moment at the joint location using beam-on-elastic foundation analysis under the assumption that the rail is continuous.

2. Multiply this bending moment by the joint efficiency factor, k, to get the actual bending moment carried by the joint bar.

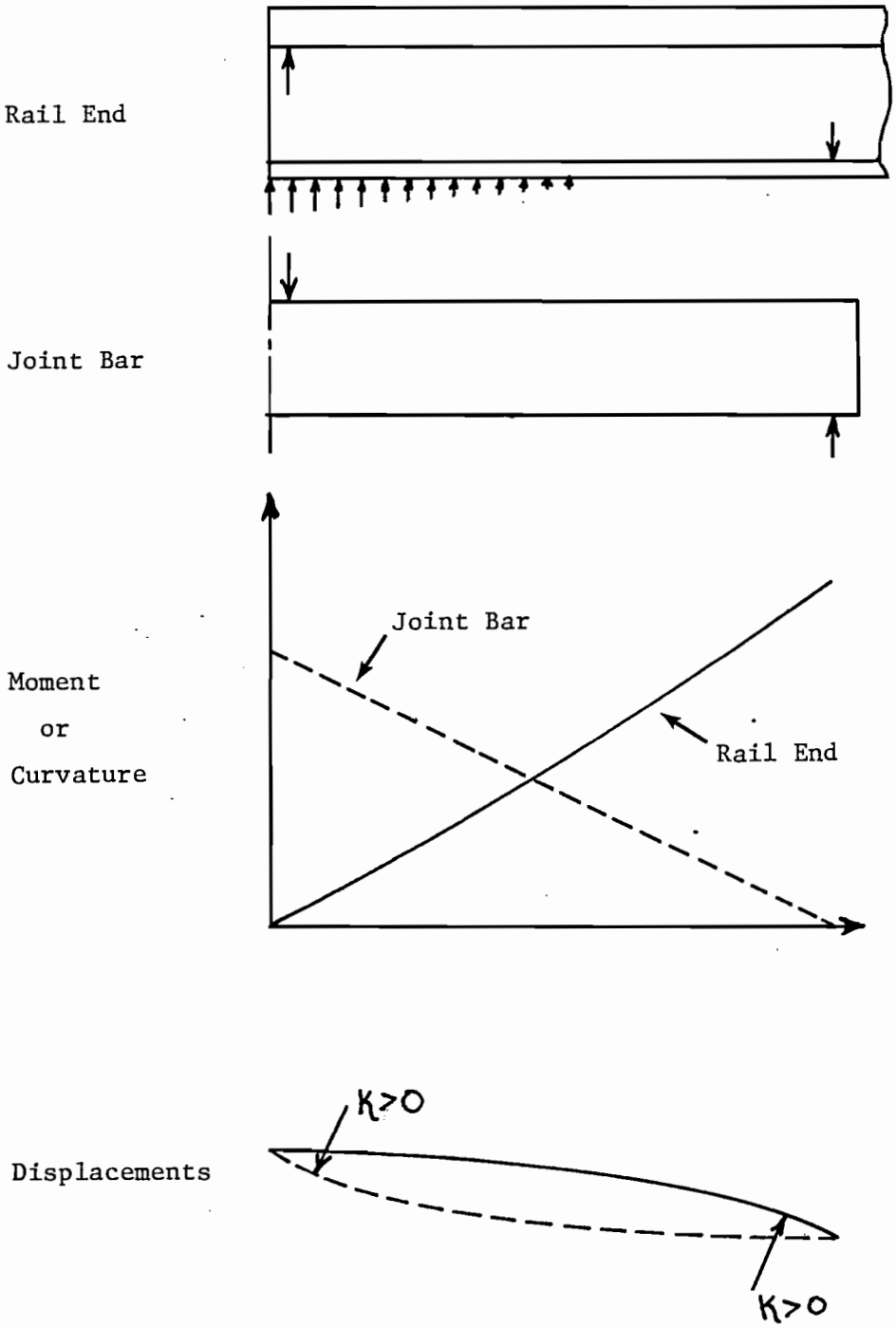

Figure 2: A qualitative explanation for the occurrence of discrete loading points in the bolted rail joint.

3. Assume a value of moment arm, b, calculate the joint bar forces Q and R required to balance this moment and use simple beam theory to calculate the resulting joint bar outer fiber stresses and strains.

The difficulty in conducting this type of analysis for actual track-train conditions is the generally poor knowledge of the dynamic wheel loads, the joint efficiency factor and the distance between the forces, Q and R. There is also the question of whether the force system in Figure 1b or 1c is appropriate.

Dynamic wheel loads can exceed static wheel loads by a factor of two or three. Studies made by Wise, Lindsey and Duncan [4] indicate that the wheel loads increase linearly with train speed near a rail joint. In one example they found the forces to increase by a factor of two as train speed increased from 5 to 60 mph. For dipped joints--that is, joints which have experienced severe batter--dynamic amplification factors on static wheel load of four have been observed [5,6]!

Although the joint efficiency factor does not appear to depend on the bolt tightness [3,7] it must certainly decrease substantially when the bolts become loose enough to carry no load in the absence of a wheel. This is the condition most commonly associated with the occurrence of bolt hole cracks. The theoretical maximum joint efficiency factor has been estimated by Johns, Sampath, Bell and Davies [8] to be given by

$$k_{max} = (I_J/I_R)^{0.25}$$

where I_J and I_R are the moments of inertia of the joint bar pair and the rail. For 132 lb/yd rail and head free joint bars, $k_{max} = 0.76$. It is not difficult to imagine that k can be as low as 0.5 for relatively loose joint bars.

Little work other than that of the Talbot Committee is available to determine the moment arm length b, or whether the four-force or six-

force system shown in Figures 1b and 1c is operative. The evidence collected by the Talbot Committee indicates that b is on the order of 10 in. for 36 in. joint bars.

Consider the implications of the two types of force systems shown in Figure 1. The forces Q, R and R' are calculated according to the method outlined by the Talbot Committee and discussed above except here the shear force at the joint is considered in addition to the moment. Terminology and sign conventions are shown in Figure 3. Again, M and V are calculated from beam-on-elastic foundation theory under the assumption that the rail is continuous and uniform in section at the joint, and then multipled by a joint efficiency factor, k. Therefore, considering equilibrium of the joint bar

$$Q = -[k(\frac{M}{b} + V) - (\frac{c}{b}) R'] . \qquad (1a)$$

$$R = [k(\frac{M}{b} + V) - (\frac{b+c}{b}) R'] \qquad (1b)$$

The forces, Q, R and R' are indeterminant, but there are two things evident from these equations. The first is that if R' is ignored--it is in this investigation--a conservative (high) value for Q is obtained; Q is considered to be one of the primary driving forces for bolt hole crack growth (the other is the wheel load itself). Secondly, Q is greater for higher joint efficiency factors. This would imply that loose joints are less severe in terms of the force Q. However, the condition of the joint--reflected in the value of k--also determines the dynamic loads at the joint. Therefore, although a loose joint, or low k, decreases the force Q, the dynamic loads are probably higher. Based on experience one would expect that the adverse dynamic load effect increases faster than the value of k decreases. This would also suggest that it is more appropriate to specify the effects of joint efficiency and dynamic amplification as a single factor. Note that the dynamic amplification due to a wheel flat is not considered in this analysis.

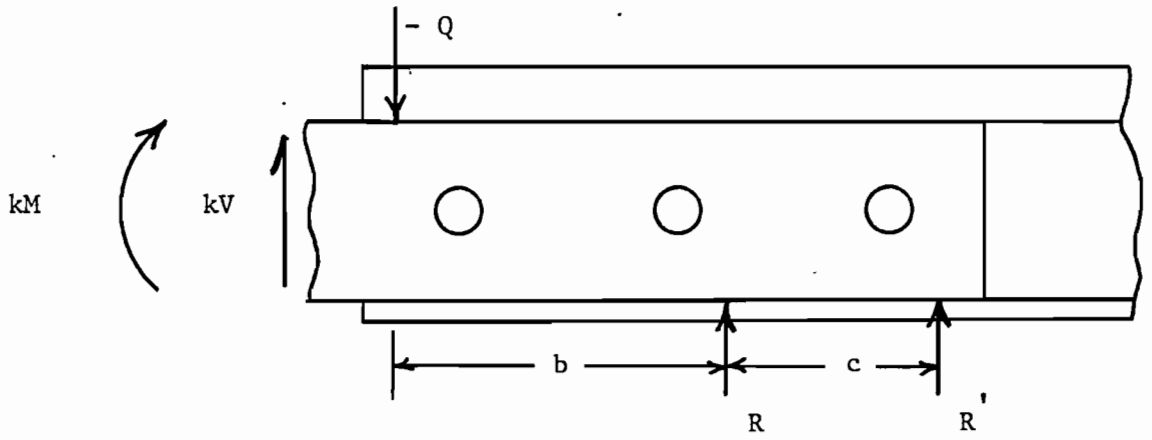

Figure 3: Joint bar forces and sign convention

The goal in studying the mechanics of the rail joint is to calculate a force or stress which can easily be related to the bolt hole cracking behavior. A reasonable choice for this force is the shear force at the rail cross section that contains the bolt hole, because bolt hole cracks generally grow at approximately 45° to the rail axis demonstrating the importance of shear.

A small computer program was written to determine the shear force at any of the three bolt holes in a 36 in. bolted joint for arbitrary track and train characteristics. The steps in the analysis are:

1. Enter the track and train characteristics: foundation modulus, rail moment of inertia, joint efficiency factor, wheel load, wheel spacing for two wheels and dynamic amplification factor. The location of the forces Q and R can also be specified.

2. For a distance, x = X, of the leading wheel from the joint and a distance, x = X + XSP, for the trailing wheel calculate the bending moments and shear forces using the beam-on-elastic foundation equations [9]:

$$M = \frac{W}{4\beta} \exp(-\beta x)(\cos \beta x - \sin \beta x) \qquad (2a)$$

$$V = \frac{W}{2\beta} \exp(-\beta x) \cos \beta x \qquad (2b)$$

where

$$\beta = \left[\frac{u}{4EI}\right]^{0.25}$$

u = foundation modulus
E = Young's modulus for the rail (30×10^6 lb/in^2)
W = wheel load

The value x is always taken as positive. However, V is forced to change sign when a wheel passes the joint; the right-hand side of equation (2b) is assigned a negative value when the wheel is on the rail not containing the bolt hole, and a positive value when the wheel is on the rail containing the bolt hole.

3. The moments and shear forces for the two wheels are summed and multiplied by the joint efficiency factor and the dynamic amplification factor if the wheel has passed the joint.

4. The forces Q and R are determined from equations (1).

5. The problem of a semi-infinite beam-on-elastic foundation is solved in which the applied loads are Q, R, and αW_1 and αW_2 if the wheels are on the rail containing the bolt hole crack; W_1 and W_2 are the two wheel loads.

6. The position of the two wheels is incremented by some distance DX and steps 2-5 are repeated. This process is continued until both wheels have passed the joint.

Figure 4 shows the results of a calculation made by the program with: $u = 2000$ lb/in^2, $I_R = 94.9$ in^4 (136 lb/yd rail), $k = 0.75$ $W_1 = W_2 = 33$ kips, XSP = 66 in., and $\alpha = 1.0$. These parameters are meant to represent a slow moving train over a good joint. The force Q acts at the rail end and the distance between Q and R is 12 in. The results shown in Figure 4 are actually a segment of all the results. They show the variation of the shear force at a distance of 3.5 in. from the rail end, which corresponds to the location of the first bolt hole in a 36 in. joint. The maximum shear force occurs when one of the wheels is over the bolt hole and in this case is equal to 29 kips. The maximum shear force in continuous rail also occurs under the wheel and in this case, from equation (2b) with $x = 0$, is equal to $33/2 = 16.5$ kips. Therefore, it appears that the shear forces in the vicinity of

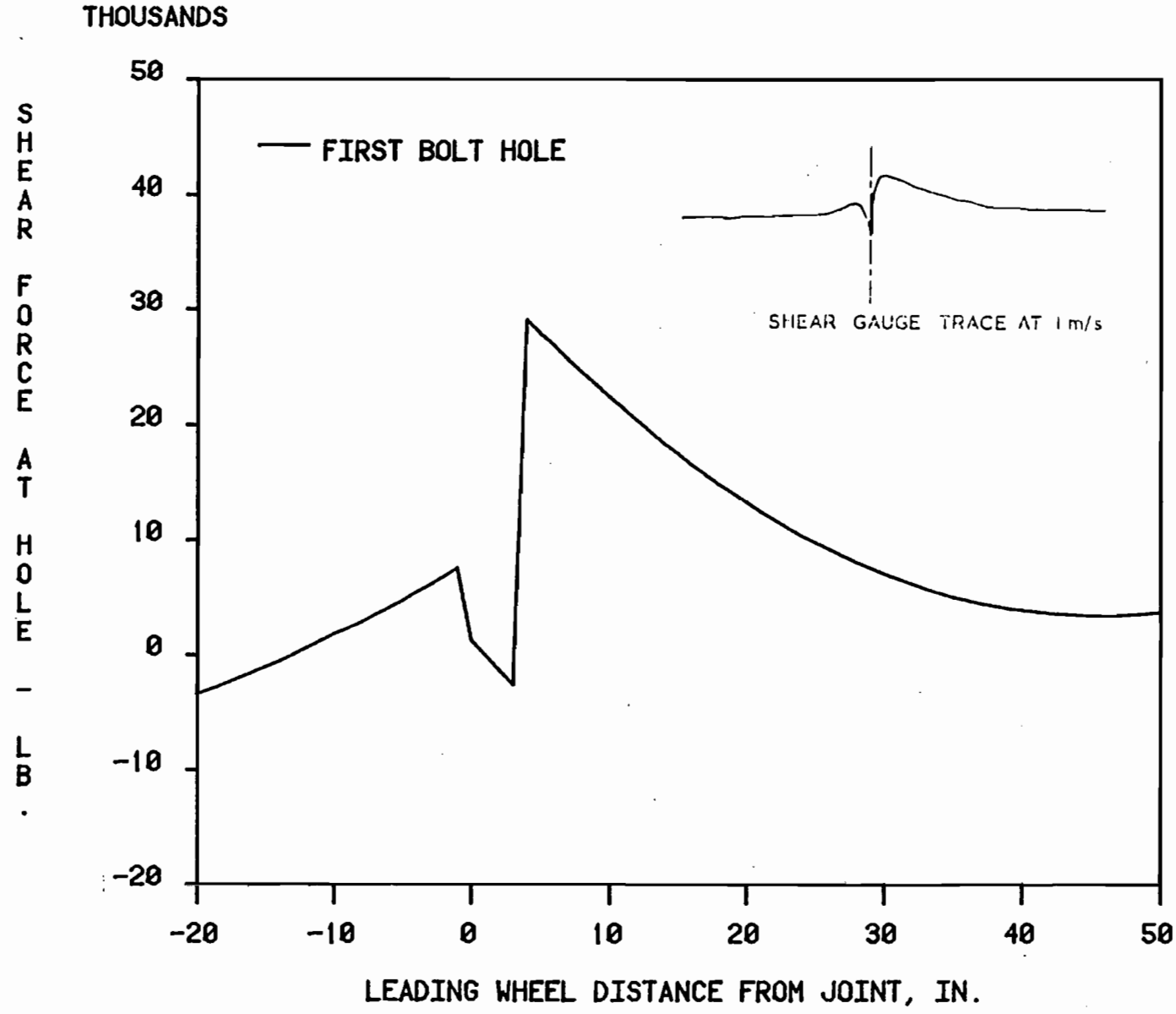

Figure 4: Predicted variation of the shear force at the first bolt hole in comparison to a strain gage measurement from the field.

the bolted rail can be considerably greater than in continuous rail, even if only static wheel loads are considered.

Also shown in Figure 4 is a strain trace obtained from a strain gage mounted on the inside of a bolt hole at 45° to the rail axis for a rail in service with a train passing at 1 m/sec (2.25 mph) [4]. The shear force and the 45° strain should be directly related. The track and train conditions of the field test were not identical to those used in the program calculations, but the similarities in the two curves indicate that the model used to predict bolted joint forces simulates the service behavior quite well.

Figure 5 shows the variation of shear force at each of the three bolt holes in a 36 in. bolted joint under the same conditions as in Figure 4. The shear force is predicted to be greatest in the first bolt hole for a static load. This effect would be accentuated if the maximum dynamic load occurs somewhere between the rail end and the second bolt hole, which is 9.5 in. from the rail end. The greater predicted shear force for the first bolt hole supports the observation that most bolt hole cracks occur at the first bolt hole. The analysis does not provide an explanation for the greater frequency of fatigue cracks from the first bolt hole that grow toward the rail head. This phenomenon may be due to a stress field which is more concentrated at the upper part of the first hole than the lower part as a result of the close proximity of the joint bar force under the rail head at the rail end.

Finally, Figure 6 shows the influence of the joint efficiency factor. The smaller shear force at the bolt hole for $k = 0.5$ is evident from this figure. Also shown is the shear force variation for $k = 0$, which corresponds to the case in which the joint bar is totally ineffective. In this case, the greatest shear force is negative which causes cracking to occur toward the rail head and end or in the diametrically opposed direction. Such cracking is observed in service, but the authors have not confirmed that its occurrence is associated with completely ineffective joints. Not shown in a figure are the effects of rail moment of inertia--rail size--or foundation modulus. These two

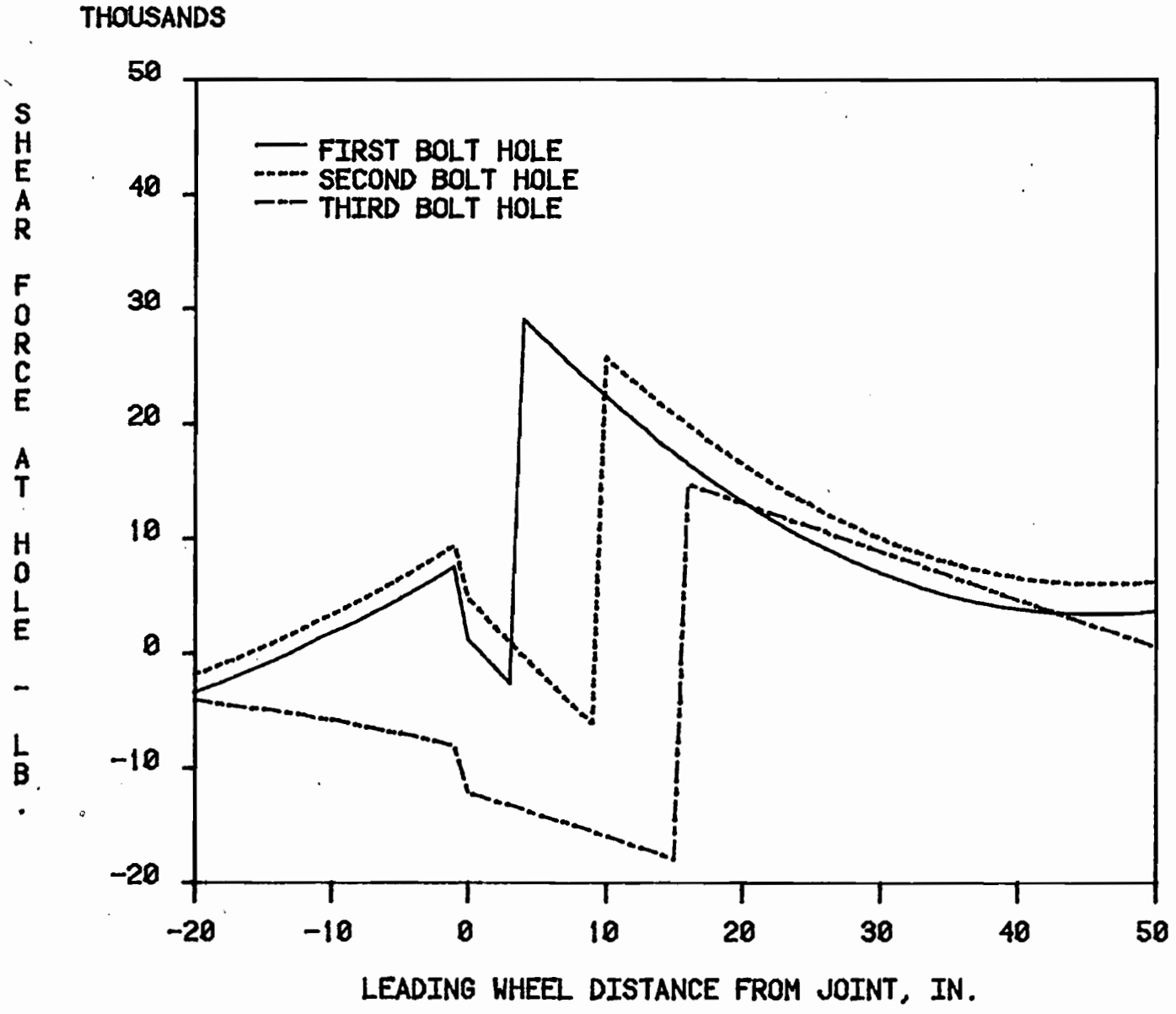

Figure 5: Predicted shear force variation for the three rail end bolt holes in a rail joint with 36 in. joint bars.

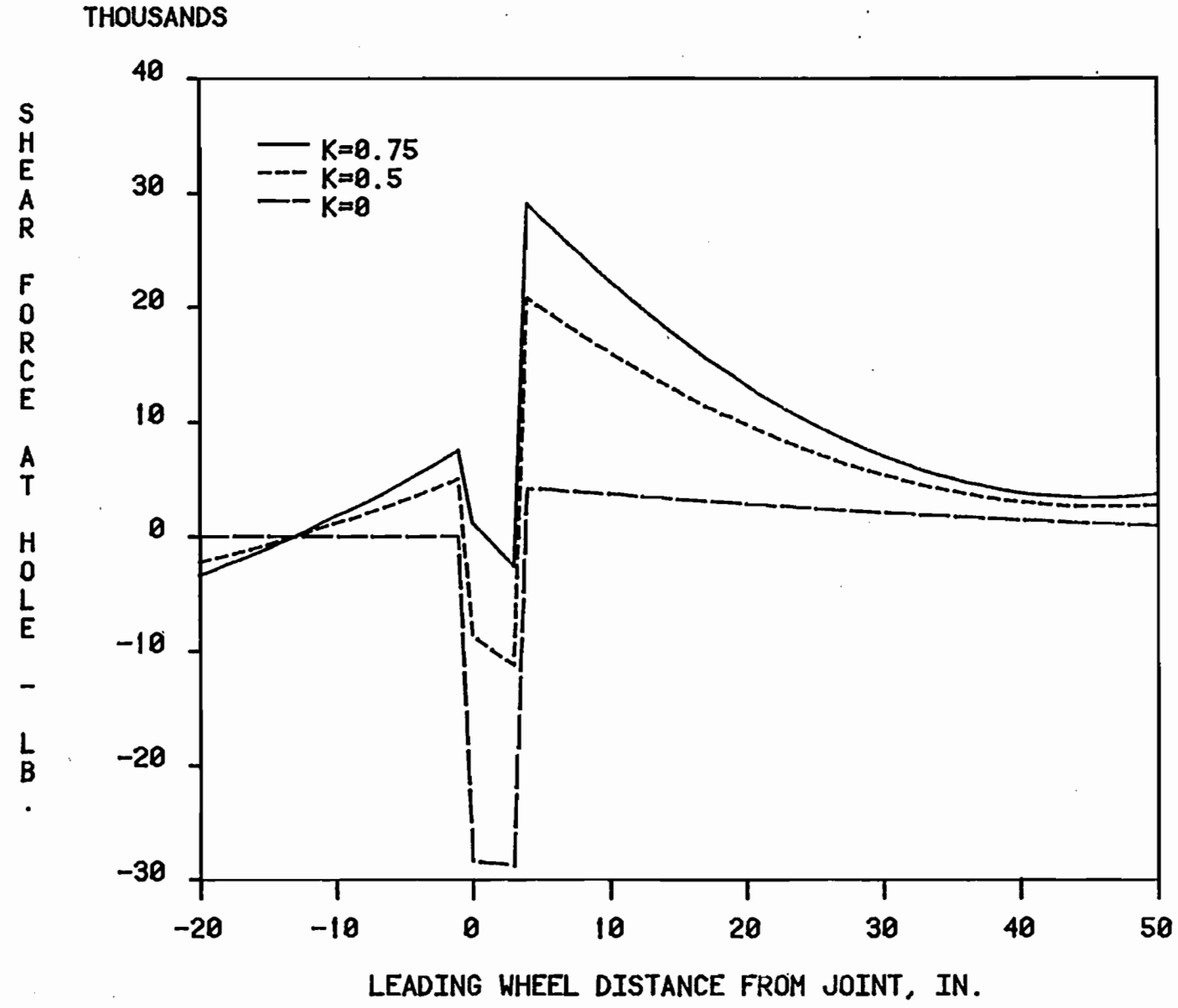

Figure 6: Influence of joint efficiency factor on the shear force variation at the first bolt hole.

parameters affect the shear force through the parameter, β; the shear force is proportional to 1/β and some other terms which depend weakly on b. For example, the ratio of 1/β for u = 3000 lb/in^2 to 1/β for u = 2000 lb/in^2, both for 136 lb/yd rail, is 0.90. Therefore, the shear force for u = 3000 lb/in^2 is about 10% less than that for u = 2000 lb/in^2, all other factors being equal. Consider two rail sizes. The ratio of 1/β for 115 lb/yd rail (I_R = 65.6 in^4) to 1/β for 136 lb/yd rail (I_R = 94.9 in^4), both with u = 2000 lb/in^2, is 0.91. Therefore, the shear force for 115 lb/yd rail is about 9% less than that for 136 lb/yd rail, all other factors being equal. This apparent advantage in using 115 lb/yd rail over 136 lb/yd rail is unfortunately nullified by a higher shear-stress/shear-force ratio for 115 lb/yd rail.

3. DETERMINATION OF K_I FOR THE BOLT HOLE CRACK

Fatigue crack growth rates can be expressed in terms of the alternating stress intensity factor for rail steels under various conditions of geometry and loading. The rate or amount of tonnage required to grow a bolt hole crack a given distance can be determined if the magnitude and variation of ΔK_I with bolt hole crack length can be determined for the track-train conditions of interest.

Analyses

Wells [10] proposed a method to calculate K_I for the rail end bolt hole crack in which the rail web is modeled as an infinite plate in shear. The idealized geometry is shown in Figure 7. The shear stress is a direct result of the shear force at the bolt hole and causes the crack to grow at 45° to the rail axis. The formula for K_I is obtained by superposing the K_I solutions for a biaxial tension and compression stress field which is equivalent to a pure shear stress field. From [11],

$$K_I = F(a/d)\tau\sqrt{\pi a}$$

where

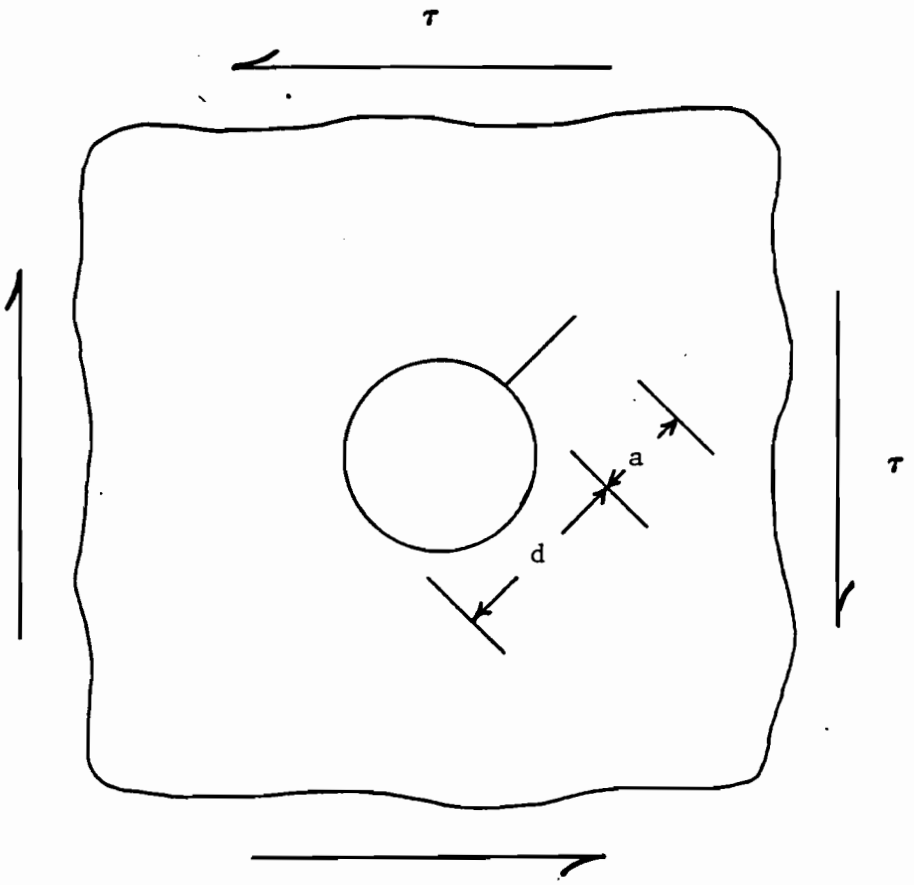

Figure 7: The infinite plate geometry, with a crack emanating from a hole and loaded in shear, used to model the bolt hole crack.

a = crack length

d = hole diameter

F = factor which depends on the ratio, a/d

τ = shear stress

Figure 8 shows the variation of K_I/τ for d = 1.125 in., which is the diameter of a new bolt hole. The infinite plate-in-shear model predicts that K_I rises rapidly for small crack lengths, reaching at a = 0.1 in., a value greater than 70% of the value at a = 2.0 in. K_I is predicted to increase only mildly at greater crack lengths. The solution for the double crack problem--two diametrically opposed cracks--is shown for comparison.

The infinite plate-in-shear model is expected to become inappropriate as the crack extends beyond the neighborhood of the hole. In addition to the variation of the shear force along the rail, the shear stress in the web also varies with the distance from the neutral axis. Simple beam theory can be used to approximate this variation using the equation,

$$\tau = \frac{VQ(z)}{I_R t(z)} \qquad (3)$$

where

z = distance from the neutral axis

V = shear force at the bolt hole

Q = the first moment about the neutral axis of the area bounded by the line z = const. and the extreme boundary of the section,

t = the web thickness at z

The variation of τ/V for a 136 lb/yd cross section using equation (3) is given in Figure 9 and is <u>not</u> constant over any portion of the cross section. (The apparent flat part of the curve at the maximum is only due to the discrete nature of the calculation. Therefore, choice of the maximum value of τ, which occurs at the neutral axis, for use in calculating K_I in the infinite plate model is not expected to be

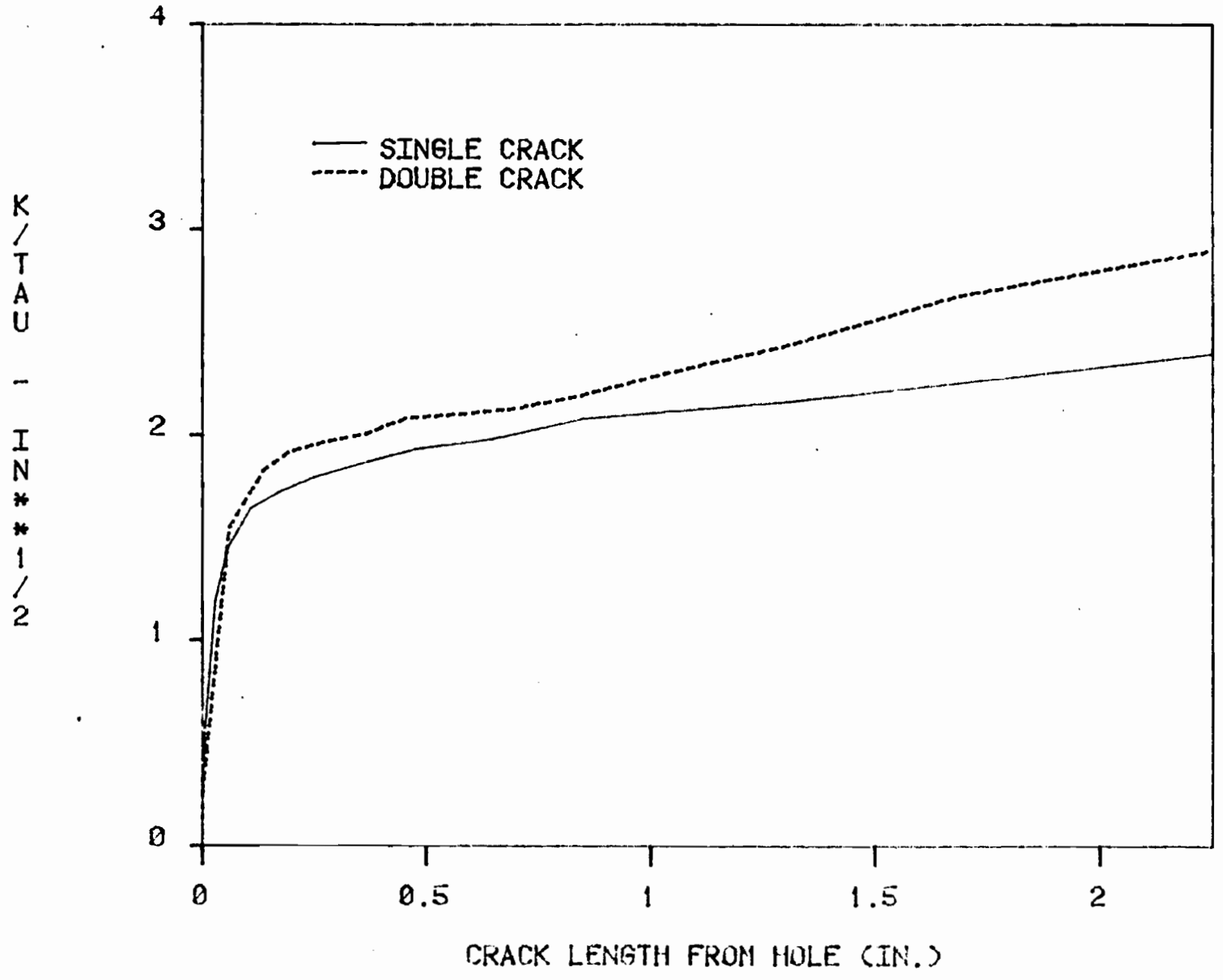

Figure 8: The variation of K_I/τ for a crack or cracks emanating from a hole in an infinite plate in shear (11). (The curves are not smooth because only ten discrete points were used in the computer plot.)

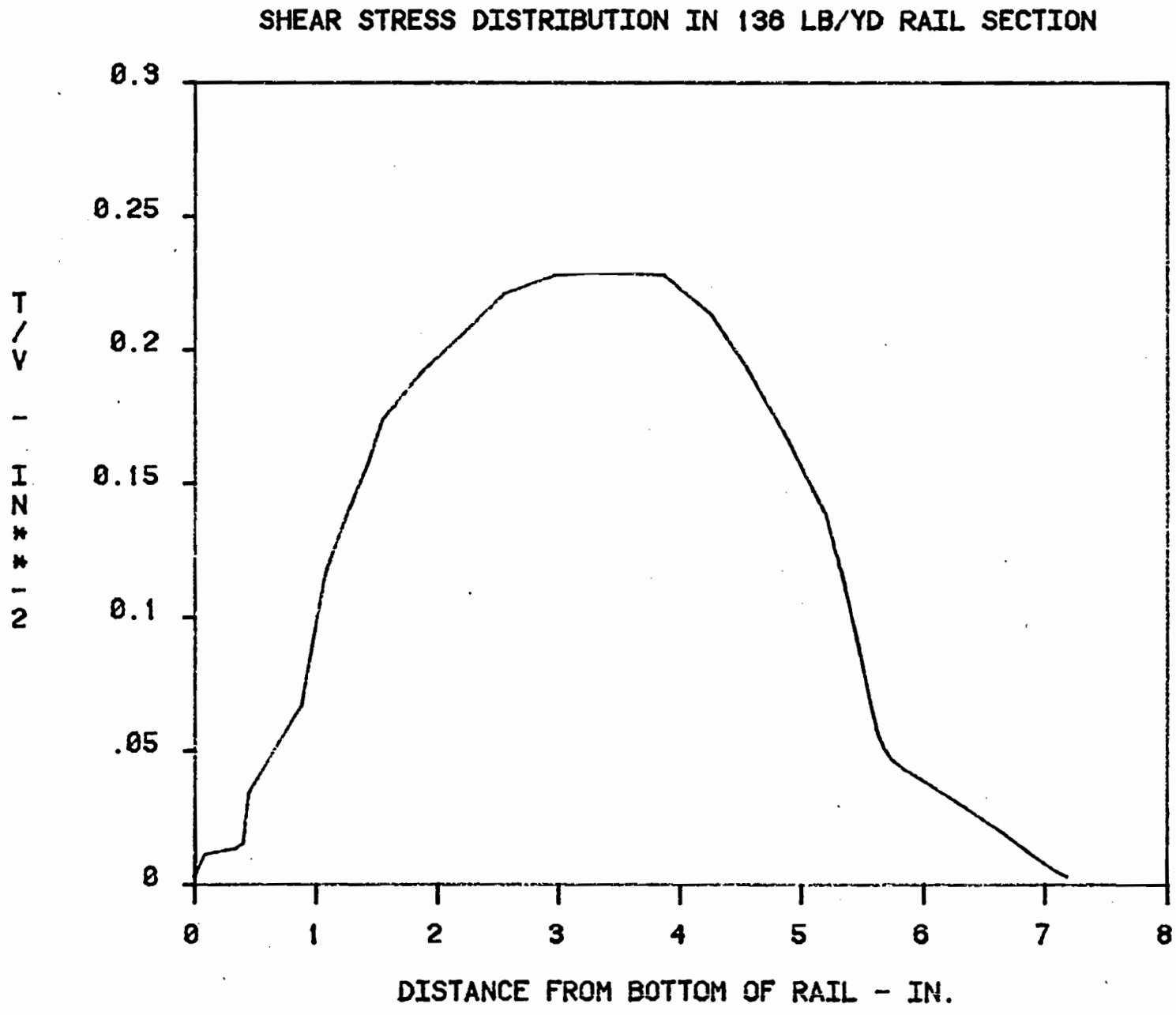

Figure 9: Variation of shear stress along the vertical direction of a 136 lb/yd rail loaded by a shear force. (Computer plot.)

accurate for cracks of any length. In fact, if the variation of the shear stress with crack length, or distance from the neutral axis, is somehow incorporated into the calculation of K_I from Figure 8, it is evident that such a model will eventually predict a decrease of K_I with crack length. Unfortunately, the problem is compounded by the fact that eventually the crack approaches the rail head where an infinite plate model is definitely inappropriate and by the fact that the presence of the crack must alter the distribution of the shear stress through the cross section. A conservative approach to specifying the variation of K_I with crack length would appear to be to use the relation given in Figure 8 with the value of τ at the neutral axis as determined from equation (3).

A few attempts have been made to establish the variation of K_I with crack length with greater certainty, including one by the authors which is reported below. At least two sets of finite element calculations have been made to solve this problem [6,8]. Allen and Morland [6] report the results of what appears to have been a two-dimensional, plane stress finite element analysis for a British 110A lb/yd rail with the bolt hole crack growing toward the rail head away from the rail end. The finite element method was used to calculate the relation between the applied load and displacement for various crack lengths. The stress intensity factor was then derived from the energy release rate compliance relation of linear elastic fracture mechanics. The results from the finite element calculations and the infinite plate-in-shear mold are shown in Figure 10 in terms of the nominal shear stress at the neutral axis. The values of K_I/τ given in Figure 10 are lower than those predicted by the infinite plate-in-shear model, but it is interesting to note that the value of K_I is predicted to decrease as the crack becomes long in comparison to the hole. This is what one expects from the predicted rapid decrease in shear stress. Johns, et al.[8], performed two-dimensional calculations for three bolt hole crack configurations, but unfortunately did not treat the single crack growing toward the rail head, which is of interest in the present report.

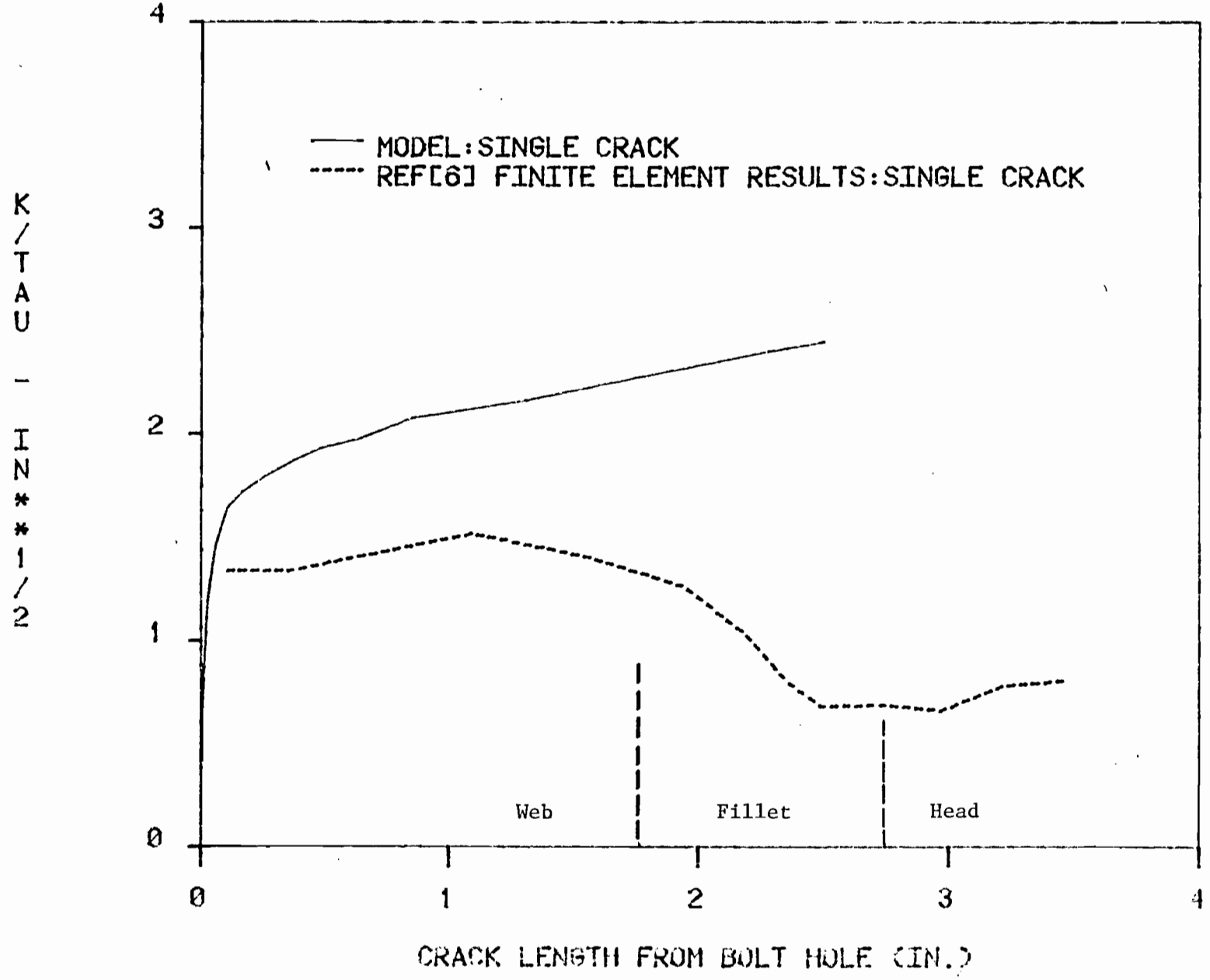

Figure 10: Finite element predictions of K_I/τ for a bolt hole crack in 110 lb/yd rail from (6) in comparison to the infinite plate-in-shear model.

Experiments

An experimental technique was used in this investigation to establish the variation of K_I with crack length for a single bolt hole crack growing toward the rail head away from the rail end. The technique was suggested by James and Anderson [12] and makes use of the relation between crack growth rates and ΔK_I expressed by

$$\frac{da}{dN} = C(\Delta K_I)^m \qquad (4)$$

This relationship is established from a laboratory experiment on a specimen for which the variation of K_I with crack length, a, is known and for which crack growth rates can be measured. The crack growth rate-crack length variation is then obtained for the component of interest and ΔK_I is calculated from (4). James and Anderson applied the technique to through cracks in internally pressurized thick-walled cylinders.

The technique of inferring stress intensity factors from crack growth rates has been applied to the bolt hole crack once already [6, 13]. A 132 lb/yd rail was tested in three-point bending to simulate the shear force at the bolt hole. Details of the loading are not clear, but the rail was loaded at its ends under the base and in the center on the head as illustrated in Figure 11a. The bolt hole had two prenotches diametrically opposed and oriented 45° to the rail axis. The crack lengths were apparently measured optically, and it is not clear how crack growth rates were derived. Accompanying fatigue crack growth rate tests were performed with SEN specimens to obtain the constants for equation (4). Considerable scatter occurred in the SEN tests and the average data were used to derive the K_I/τ relation shown in Figure 12. Also shown in Figure 12 are the predictions of the infinite plate-in-shear model. The experimentally-derived results are seen to be below but reasonably close to the model predictions. The important difference

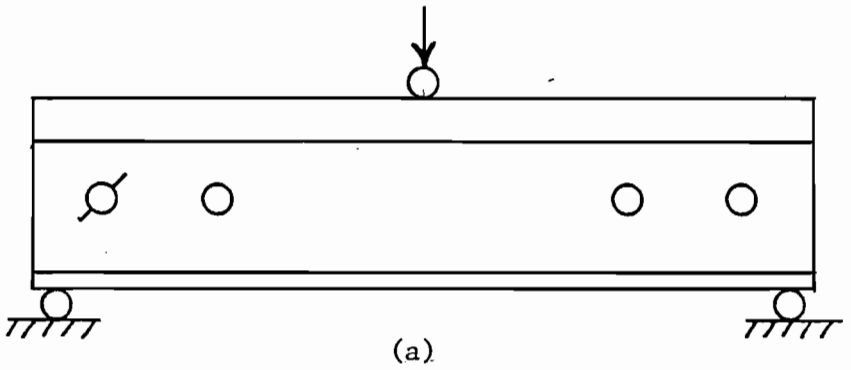

(a)

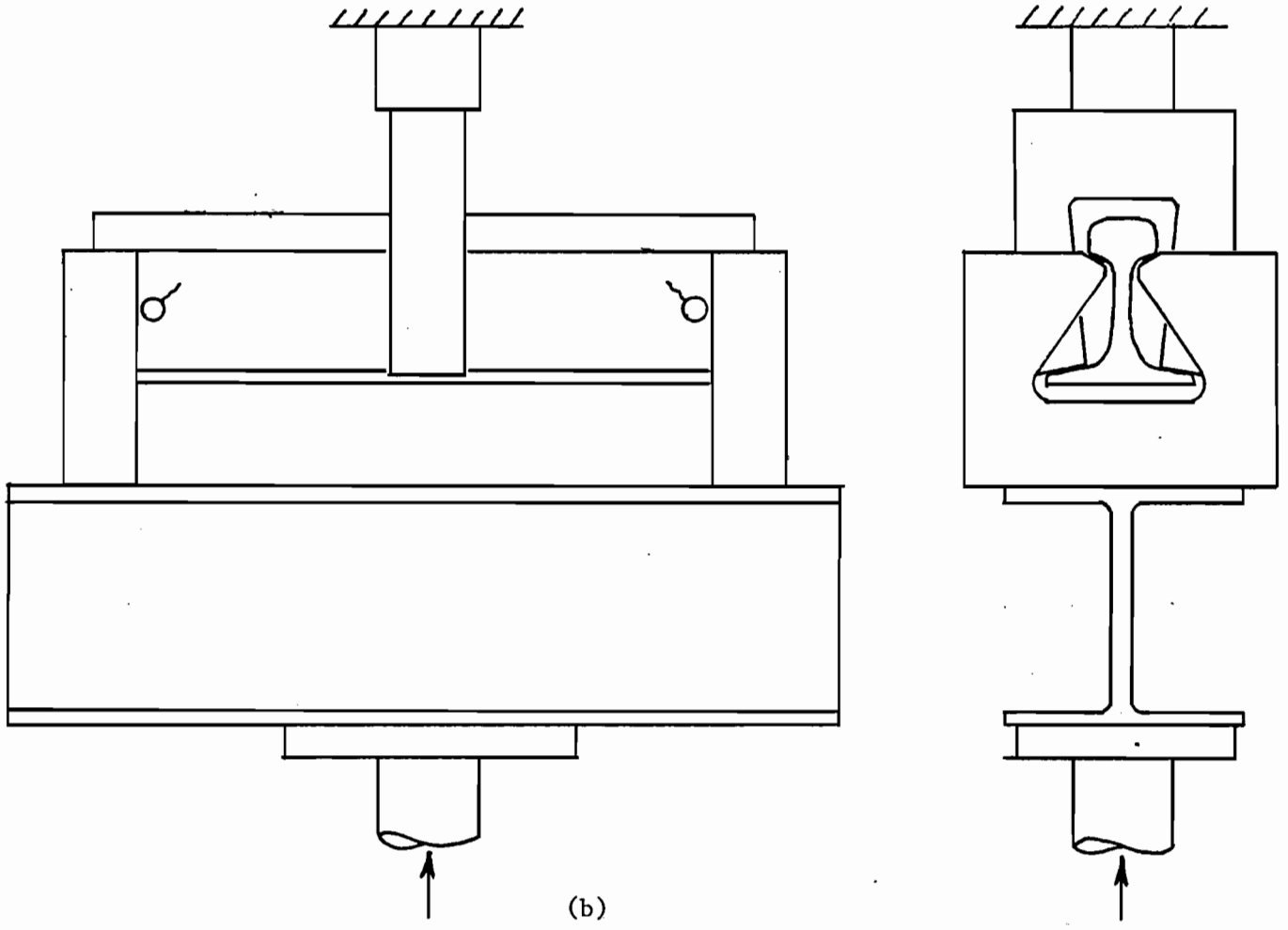

(b)

Figure 11: Three point bend fixtures used to study bolt hole crack fatigue crack growth: (a) fixture type used in (6); (b) fixture used in present investigation.

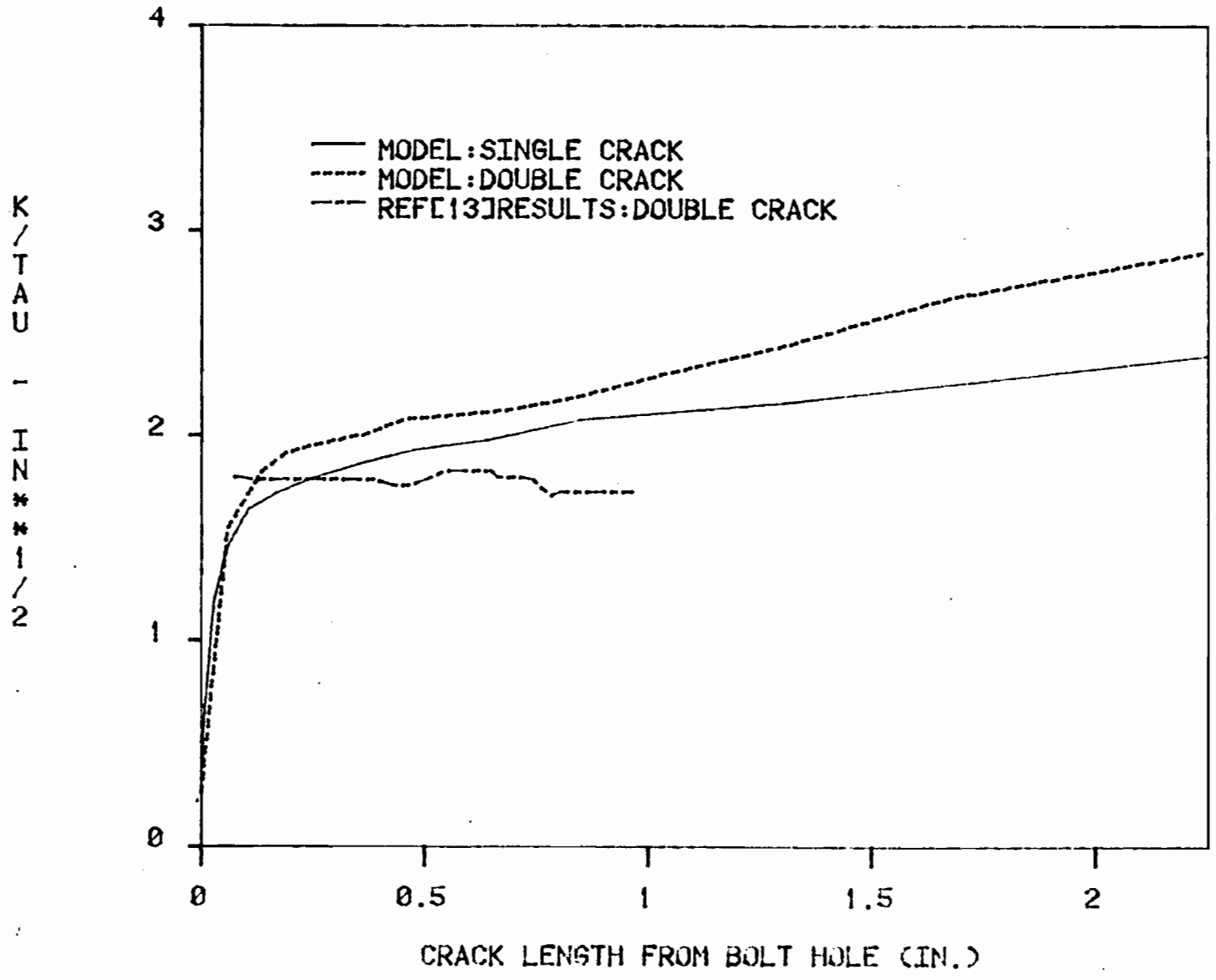

Figure 12: Experimentally - derived K_I/τ values from (6, 13) in comparison to infinite plate-in-shear predictions.

is that the experimentally derived K_I value decreases slightly with increasing crack length in contrast to the model predictions but in line with the expectations based on the variation of shear stress in the section.

Two other experimental investigations [4,14] have been performed on the fatigue of large rail specimens with bolt holes, but the primary goal in these investigations was to generate fatigue initiation data. Wise, Lindsay and Duncan [4] tested 17 in. long specimens with two bolt holes in each end. The loading was three-point bending with an 8 in. center support under the base and two end load points applied to the head. Insufficient information is given to calculate growth rates. More recently, Lindh, Taylor and Rose [14] performed three-point bend tests on 112 lb/yd standard carbon 24 in. rail pieces with two or four bolt holes. Loading was applied in the center under the base and at the ends through the head. One figure is given on fatigue crack growth rates for a specimen which cracked at a hole about 3.5 in. from the center of the specimen; that is, 8.5 in. from the end of the specimen. The central load was 170 kips and cracks growth rate was observed to increase rapidly to final fracture at a crack length of 0.3 in. This indicates that K_I increases rapidly for small cracks as predicted by the infinite plate-in-shear model (see Figure 8).

The experiment conducted in the present investigation was similar to that performed in [6]. The specimens were 36 in. pieces of 136 lb/yd standard carbon rail. A bolt hole was drilled into each end of the rail, 3.5 in. from the rail end with a diameter of 1.125 in. according to AREA specifications. A Chevron prenotch was cut into the edge of each of the holes with a hacksaw so that the crack would grow toward the rail head away from the rail end at 45° to the rail axis. The length of the prenotch was about 0.25 in. on each side of the web. To facilitate optical crack length measurements, a large area was polished along the path where the crack was expected to grow on each side of the web for both bolt holes.

The specimens were loaded in three-point bending with the outside loads applied under the rail head and the center load applied to the top of the rail base. This loading was chosen to simulate the rail joint force system and is illustrated in Figure 11b. The test fixture consisted of a W10 x 68 beam with three solid, machined blocks for the three load supports. The fixture is shown in Figure 13. The W-beam served to transmit a central load to the two end supports. It had a 1.5 in. thick plate welded at the center of the bottom flange to carry the bearing load from the testing machine. Solid machined blocks were chosen for the support because of the large, cyclic bending moments they had to carry in getting around the rail base to the head and because of their relative ease of fabrication. The supports were not attached to the top of the W-beam flange in any way; the minimum fatigue load, 4 kips, provided sufficient friction to keep them from sliding. Hardened bolt heads were inserted in the top of the end supports to provide a single bearing point between the support and the underside of the rail head. Small shims were placed on the underside of the center support adjacent to the rail web to ensure that the forces were applied as close to the web as possible. This latter practice was instituted after fracture of the base of one of the rail specimens occurred; see Figure 14.

The use of a three-point bending fixture with two prenotched bolt holes was seen as being particularly advantageous since each rail specimen was actually two bolt hole crack specimens.

The specimens were tested in a 100 kip electro, servohydraulic testing machine in load control. The load ratio was always maintained at R = 0.05 and tests were run at 8 HZ. In the first test the maximum load was 72 kips and in the second it was 80 kips. Initiation of a sharp crack required about 260,000 cycles in the first test and 160,000 cycles in the second test. Regular crack length measurements were made on only one side of the web for each of the bolt holes. Measurements were occasionally made on the other side of the web and the crack was always found to be growing uniformly with a maximum difference of 0.08

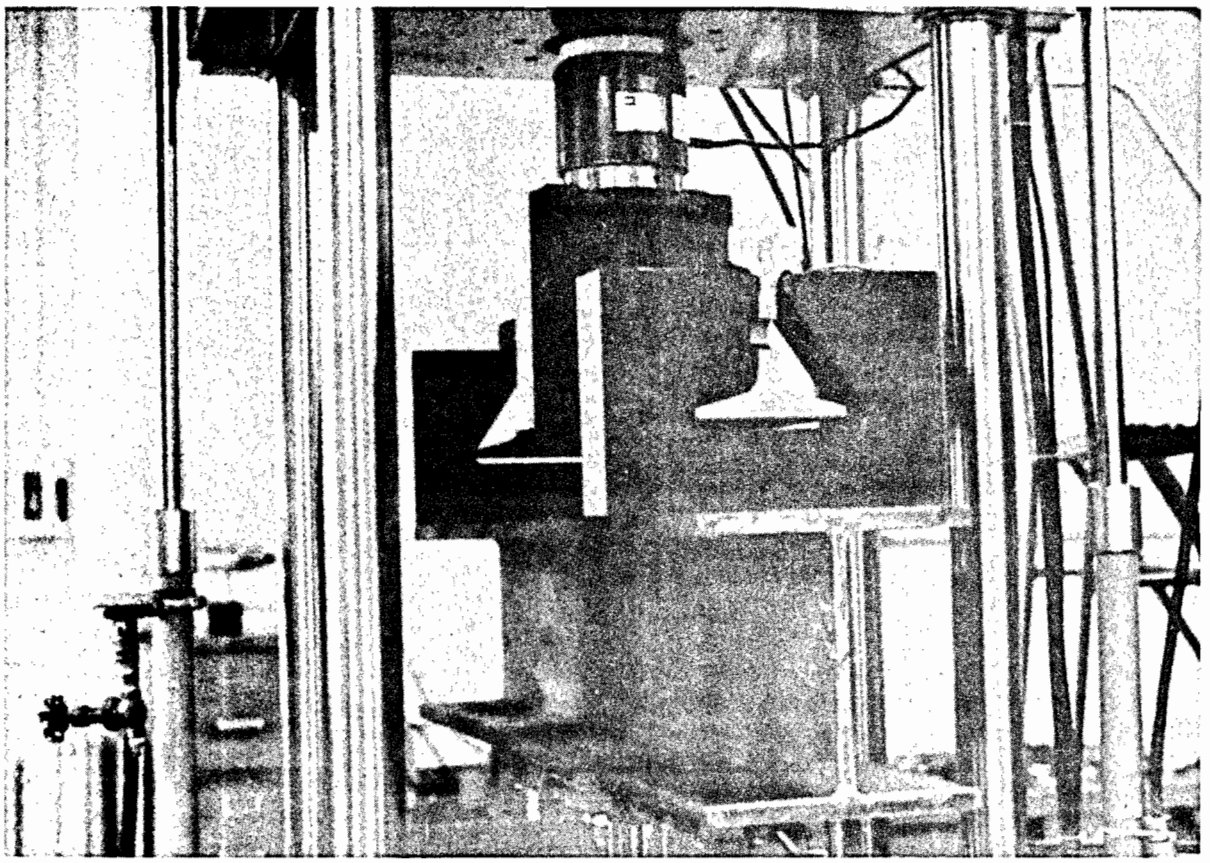

Figure 13: A photograph of the rail fixture and specimen used to generate crack growth data.

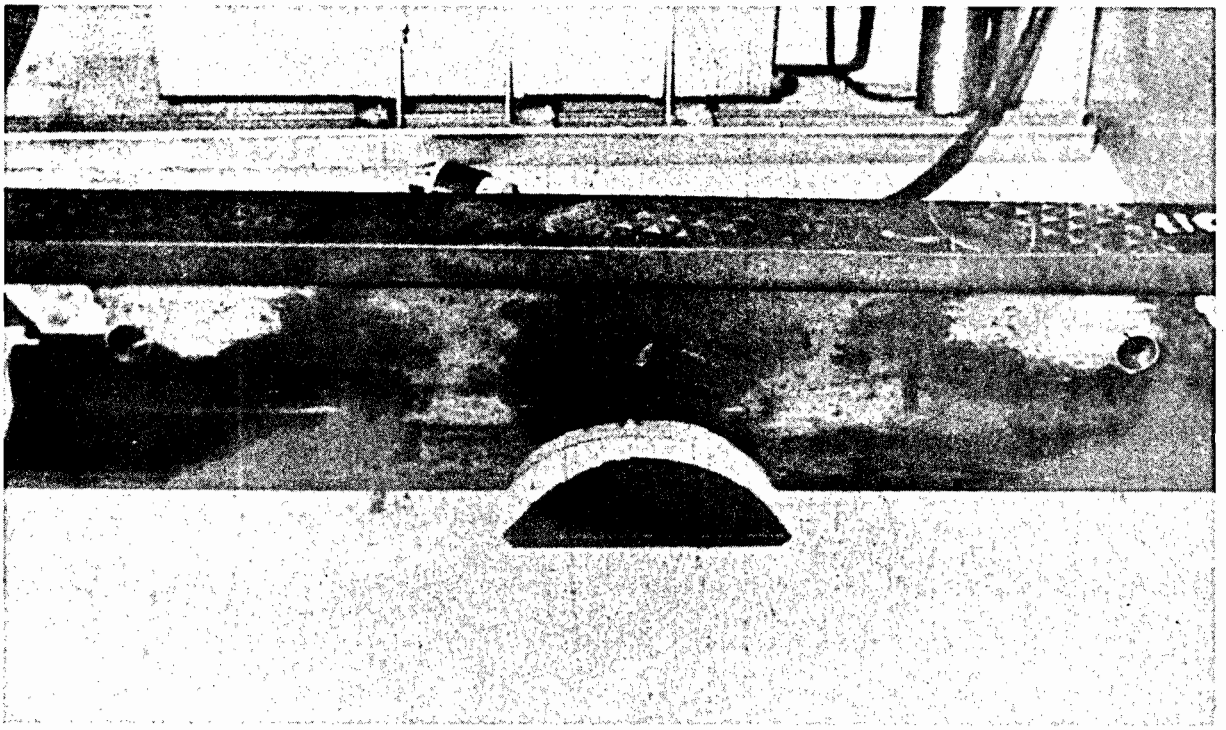

Figure 14: A photograph of the first rail specimen which broke at the base under the central load point.

in. from one side of the web to the other. A portable traveling microscope was used to make measurements of the horizontal extent of the crack length increments, and these were converted to absolute crack length increments by dividing by cos 45°. Crack length measurements were made every 10,000 - 15,000 cycles which resulted in horizontal crack growth increments of between 0.016 - 0.024 in. The angle of crack growth was measured after completion of the tests and was found to be almost exactly 45° for the entire crack.

The first rail specimen yielded less than 0.5 in. of crack growth data before fracture in the base under the center support occurred. The fatigue crack in the second specimen extended into the rail head, after which the test was terminated. Locating the crack tip optically at this point was difficult and crack growth on the surface decreased substantially. Photos of the fatigue crack after it was broken open are shown in Figures 15 and 15b. Figure 15b reveals that crack growth was considerably greater at the center of the crack as the crack extended into the rail head.

The crack length vs number of cycles data were converted to crack growth rates using the procedure recommended in ASTM E-647 [15], in which five consecutive data pairs are used to calculate the crack growth rate for the middle data pair. The growth rates were then converted to values of ΔK_I using equation (4) with $C = 11.7 \times 10^{-12}$ and $m = 4.04$ which correspond to data obtained from a compact tension specimen removed from the web of a different standard carbon rail [16]. The ΔK_I values were converted to values of K_I by dividing by (1-R). The values of K_I were then normalized by the calculated maximum shear stress for comparison to the infinite plate-in-shear model. The values of τ were obtained from the maximum value in Figure 9 and are equal to 8.2 ksi for the first rail specimen and 9.1 ksi for the second. The results are shown in Figure 16 in comparison to the predictions of the model results.

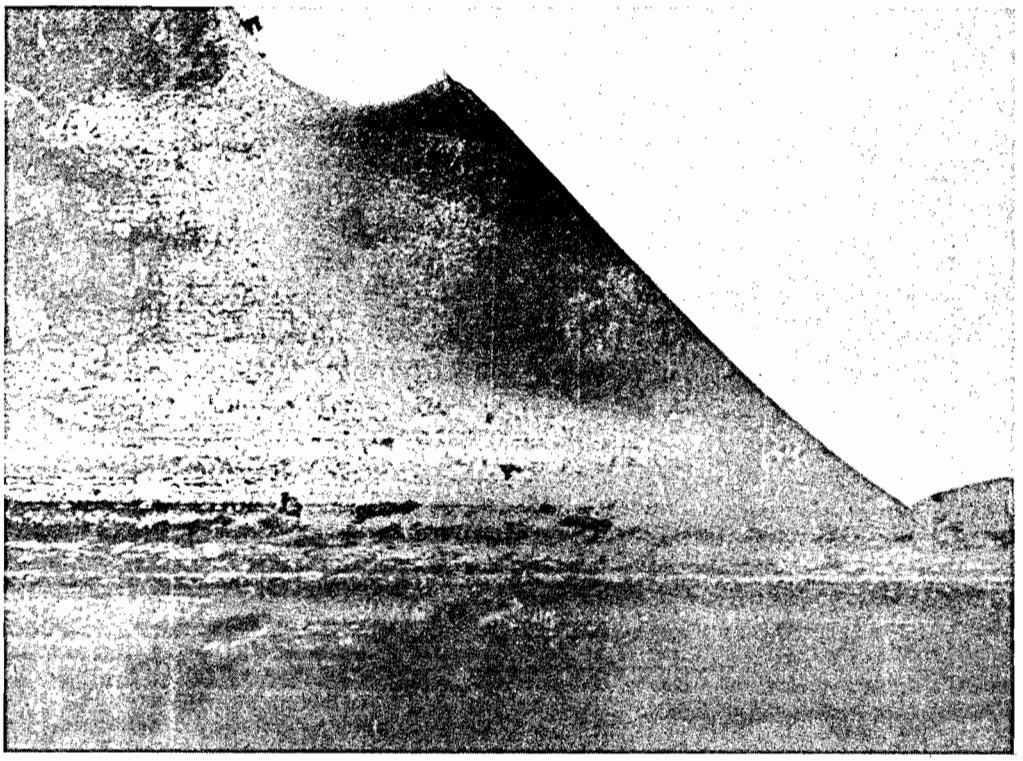

Figure 15a: A photograph of one of the bolt hole cracks from the second rail. The rail head is at the bottom of the photo.

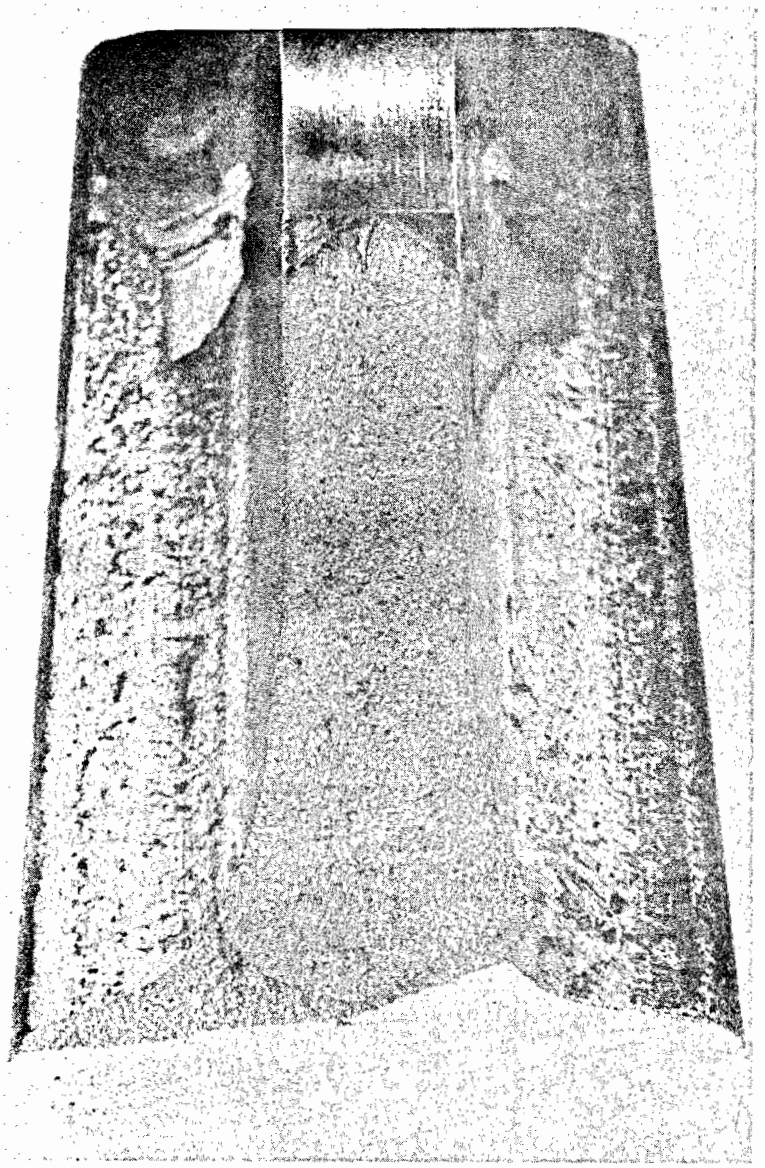

Figure 15b: A photograph of the fracture surface of one of the bolt hole cracks from the second rail specimen.

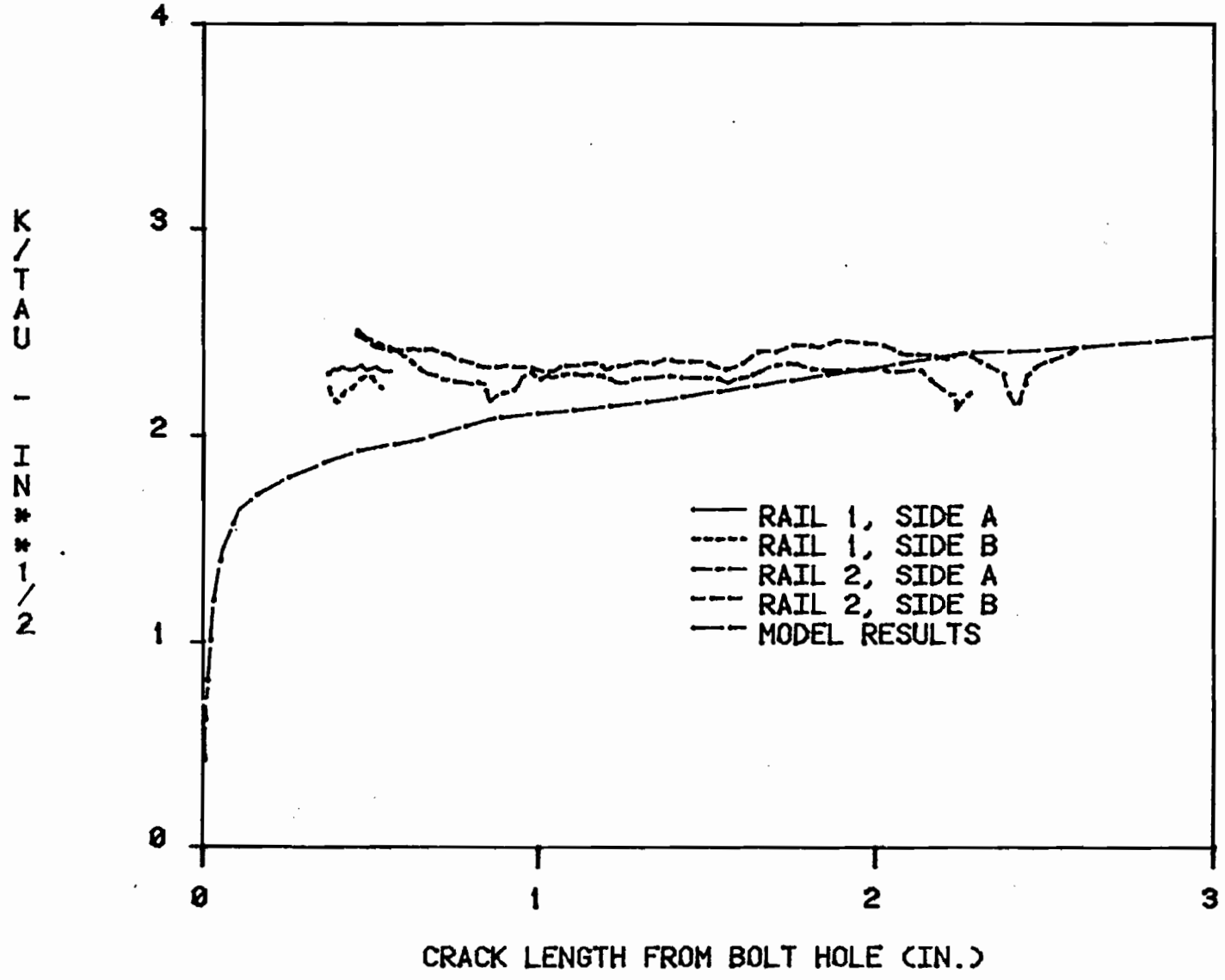

Figure 16: Derived K_I/τ values from the three-point bend rail tests in comparison to infinite plate-in-shear model predictions.

The experimental data demonstrate that the value of K_I, or K_I/τ, changes very little for the entire range of crack lengths studied. This is the same phenomenon observed in [6] for the double crack case. The value of K_I does appear to decrease for longer crack lengths as one would expect from the decreasing magnitude of shear stress for long cracks; that is, larger distances from the neutral axis. The observation that K_I does not decrease substantially with crack length suggests that the crack may have a considerable effect on the shear stress distribution. Data from the second specimen indicate that the highest value of K_I occurs at relatively small crack lengths and is greater than the predicted value by about 30%. The results from [6], shown in Figure 10, do not exhibit this effect even for very small crack lengths. There are not enough results to draw definite conclusions, but the results of the present investigation suggest that loading the rails under the head may provide a more severe environment in terms of fatigue crack growth than loading under the base. This is supported by the fact that the K_I/τ values of Figure 10 are about 30% lower than the values given in Figure 16 even though they should be greater because Figure 10 corresponds to a double crack; Figure 8 shows that K_I/τ for the double crack is greater than that for the single crack. Differences in derived K_I values of 30%, from which the above conclusions are drawn, must be considered with caution. A difference in K_I of 30% converts to a difference in crack growth rate of a factor of three. Such differences can occur from one specimen to another.

4. IN-SERVICE CRACK GROWTH ESTIMATION

One of the primary goals in conducting the present investigation is to be able to predict crack growth rates in service. This can be done by combining the results of the bolted joint mechanics with the crack growth rate results of the laboratory experiments. The procedure is to calculate the maximum value of shear force for the track-train conditions and bolt hole of interest using the procedure outlined in Section 2. The maximum value of shear stress is then obtained from a curve similar to that shown in Figure 9; for 136 lb/yd rail τ_{max}/V =

0.23. The value of K_I/τ_{max} for a given crack length could then be obtained from Figure 14, but considering the slight variability in K_I with crack length it seems practical to choose a single value. For 136 lb/yd rail a value of $K_I/\tau_{max} = 2.2$ is reasonable. Finally, the value of K_I so derived is used to obtain crack growth rate from equation (4). Since by this procedure growth rate is constant, it is a simple matter to calculate the tonnage required to grow a crack from one length to another. For example, assume,

$u = 3000\ lb/in^2$

$E = 30 \times 10^6\ lb/in^2$, $I_R = 94.9\ in^4$ (136/lb std. carbon rail)

$W = 33$ kips

$\alpha = 2.0$

$k = 0.6$ in.

$b = 12$ in.

$XSP = 66$ in.

Using the parameters just listed with the analysis of Section 2 gives $V = 49.5$ kips. Therefore, $\tau_{max} = 0.238 \times (49.5) = 11.4$ ksi and $\Delta K_I = K_{Imax} = 2.2\ (11.4) = 25.1\ ksi\sqrt{in}$ from which,

$$\frac{da}{dN} = 11.7 \times 10^{-12}\ (25.1)^{4.04} = 5.3 \times 10^{-6}\ \text{in/cycle.}$$

Each wheel passage provides one cycle but accounts for only one-half the total weight (tonnage) carried by the track. Therefore, the tonnage required to propagate the bolt hole crack 1 in. according to the methodology of this report is

$$\frac{2(33\times10^3\ lb/wheel)}{(5.3\times10^{-6}\ in/wheel)(2000\ lb/ton)} = 6.2\ \text{MGT/inch of crack growth.}$$

where MGT stands for million gross tons. To the authors' knowledge there are no data on crack growth rates for bolt hole cracks in service. However, it is possible to infer an average growth rate from a failure analysis made by the authors of a bolt hole crack from service [2]. For that particular bolt hole crack, which occurred in 132 lb/yd standard

carbon rail subjected to 33 kip static wheel loads, a series of ridges were observed on the fracture surface. The results of stress analysis and a special experiment strongly suggested that each of the ridges corresponded to one day of traffic. There were about 30 ridges/inch of crack growth, and it is known that the average daily tonnage was about 0.3 MGT/day. Therefore, the crack growth rate was approximately 9 MGT/inch of crack growth, which is reasonably close to the calculated growth rate made above. It has been assumed in this calculation that K_{Imin}/K_{Imax} (the R- ratio) = 0. In reality the R-ratio = -0.3, which results in some compression of the crack faces. It has been assumed here that only the tensile portion of the cyclic load is effective in the fatigue crack growth process.

5. DISCUSSION

One of the disconcerting aspects of the 36 in. rail specimen experiments is the observation that small bolt hole cracks--less then 0.5 in.--are at least as, if not more, dangerous than long cracks that have not penetrated very deeply into the rail head. Discussions with railroad personnel confirm that the majority of bolt hole fractures occur from small cracks. The implication is that inspection and removal of bolt hole defects increases safety by virtue of decreasing the probability of fracture rather than eliminating or decreasing substantially the number of defects which attain a critical size. In fact, the critical flaw size concept for the bolt hole crack should probably be replaced by a critical load concept; that is, the occurrence of a critical load as caused, for example, by a wheel flat, is what causes fracture as opposed to the attainment of a critical crack size. The magnitudes of K_I calculated in this investigation suggest that the dynamic amplification factor must exceed 2.8, with k = 0.6, for fracture to occur; this is based on a fracture toughness of 35 ksi$\sqrt{\text{in.}}$.

In order for inspection to be an effective means of removing potentially critical bolt hole defects, it appears that the inspection system must be capable of detecting bolt hole cracks on the order of 0.1

in. To achieve this, improvements in flaw inspection techniques are required. Alternatively, it might be possible to characterize the dynamic amplification-joint efficiency characteristics of a joint during inspection.

6. CONCLUSIONS AND RECOMMENDATIONS

The methodology to calculate fatigue crack growth rates for a particular kind of bolt hole crack has been developed. The crack geometry considered is a crack with length ranging from 0.5 - 3 in. propagating from the first bolt hole toward the rail head away from the rail end at 45° to the rail axis. This is the most common type of bolt hole crack observed in service. The first step in the methodology is to calculate the shear force at the bolt hole for the track-train conditions of interest using a computer program based on beam-on-elastic foundation equations. The part of this calculation most likely to cause substantial error is specifying appropriate values of the dynamic amplification and joint efficiency factors. Values of $\alpha = 2$ and $k = 0.6$ appear to be reasonable choices, based on a good comparison between calculated crack growth rates and inferred crack growth rates for a bolt hole crack from service. Comparisons of the model predictions for shear force variation are found to agree quite well with the variation of the derived shear stress from a strain gage mounted inside a bolt hole which experienced the passage of a train at 2.25 mph. The shear force calculated from the computer program is converted to a web shear stress using mechanics of materials. The web shear stress is then converted to a stress intensity factor using an experimentally derived factor and to growth rates from a Paris law equation for the rail steel in question.

The experiments performed to obtain the K_I/τ factor utilized 36 in. long rail specimens with a prenotched bolt hole in each end and loaded in three-point bending. The loading arrangement was designed to simulate the joint bar force system: the end loads were applied under

the rail head, and the center load was applied to the top of the base. The crack length was measured optically and the results from two specimens--four holes--showed that crack growth rate does not vary greatly for crack lengths from ≅ 0.5 - 3 in. Therefore, it appears that a single value of stress intensity factor or crack growth rate can be used for this range of crack lengths. The implication of this constancy in K_I and da/dN is that a critical load concept may have to be used to specify fracture conditions instead of a critical crack length concept, at least for the conditions and crack lengths studied here. For bolt hole cracks that have entered the rail head or have propagated along the head-web fillet, a critical crack size may still be appropriate.

Several tasks are recommended to support and supplement the present work. Most useful would be accurate and thorough field experiments under quasistatic and full-speed train conditions. Strain gage measurements should be made inside the bolt holes, on the rail web and in the joint bars. Some method should also be developed to determine the total dynamic wheel loads. The frequency and importance of load eccentricity and lateral loads should also be established from the field tests. It would also be useful to determine if there is some method by which the state of a rail joint--in terms of dynamic amplification and joint efficiency--can be determined in the field. Some theoretical work to determine the magnitudes of the joint efficiency factor and the moment arm of the joint bar forces would also be useful.

Acknowledgement

The authors would like to acknowledge the technical assistance of Oscar Orringer and James Morris of the Transportation Systems Center and the financial support of the Department of Transportation in the performance of this work. We would also like to acknowledge the use of the 100 kip servohydraulic testing machine at the Massachusetts Institute of Technology.

REFERENCES

1. Orringer, O., Morris, J.M. and Steele, R.K., "Applied Research on Rail Fatigue and Fracture in the United States", Fracture Mechanics Technology, 1, 1 (1984).

2. Mayville, R.A. and Hilton, P.D., "Fracture Mechanics Analysis of a Rail-End Bolt Hole Crack", Fracture Mechanics Technology, 1, 1 (1984).

3. "Stresses in Railroad Track - The Talbot Reports", reprinted reports of the Special Committee on Stresses in Railroad Track, 1918-1940, Prof. A.N. Talbot, Chairman, American Railway Engineering Association (1980) 1304 pages.

4. Wise, S., Lindsay, D. and Duncan, I.G.T., "The Strength of Rails with Particular Reference to Rail Joints", Proc. Instn. Mech. Engr., 174, 9 (1960) 371-407.

5. Jenkins, H.H., Stephenson, J.E., Clayton, G.A., Morland, G.W. and Lyon, D., "The Effect of Track and Vehicle Parameters on Wheel/Rail Vertical Dynamic Forces", Railway Engr. Journal (Jan. 1974) 2-26.

6. Allen, R.J. and Morland, G.W., "The Significance of Defects in B.S. 11 Rails; Bolt-Hole Failures and Taches Ovales", Iron and Steel Inst. Meeting on Rail Steels, 23 Nov. 1972.

7. Choros, J. and Gitlin, I., "Track Component - Property Tests. Vol. II - Rail, Ties, Jointbars and Fasteners", Report R-479, Amer. Railway Engr. Assoc. (June 1982) 81 pages. Assn. of Amer. Railroads Res. & Test Dept.

8. Johns, T.G., Sampath, S.G., Bell, J.C. and Davies, K.B., "Engineering Analysis of Stresses in Railroad Rails", Report FRA-ORD-81/51 (NTIS PB82129610) (March 1981).

9. Roark, R.J. and Young, W.C., Formulas for Stress and Strain (New York; McGraw-Hill) 1975, Fifth Ed. pg. 89).

10. Wells, A.A., Private Communication to Allen and Morland [6] in 1968.

11. Tada, H., Paris, P. and Irwin, G., "The Stress Analysis of Cracks Handbook", Del Research Corp. (1973) p. 19.2.

12. James, L.A. and Anderson, W.E., "A Simple Experimental Procedure for Stress Intensity Factor Calibration", Engr. Fract. Mech., 1 (1969) 565-568.

13. Allen, R.J., "The K-Calibration of Bolt-Hole Cracks in Rails", Tech. Note FM13, British Rail (Dec. 1972) 28 pages.

REFERENCES (continued)

14. Lindh, D.V., Taylor, R.Q. and Rose, D.M., "Sleeve Expansion of Bolt Holes in Railroad Rail", Vol. I, Report DOT-TSC-1048, Boeing Commercial Airplane Company (Dec. 1977) 67 pages.

15. E-647 Standard Test Method for Constant-Load-Amplitude Fatigue Crack Growth Rates above 10^{-8} m/cycle, Part 10 - Annual Book of ASTM Standards, (Philadelphia; American Soc. of Testing and Materials) 1981, pg. 765.

16. Mayville, R.A. and Hilton, P.D., "Laboratory Analysis of Rails Containing Detail Fractures", Arthur D. Little, Inc. Report 85662-01 to DOT (March 1983).

PART II

TABLE OF CONTENTS

PART II

LIST OF FIGURES

LIST OF FIGURES (Continued)

LIST OF FIGURES (Continued)

PART II

LIST OF TABLES

1. FATIGUE INITIATION AT RAIL END BOLT HOLES

1.1 Introduction

Methods of connecting the ends of railroad rails in track have changed considerably since iron rail came into use in the eighteenth century. Originally, rail ends were not connected at all, but set end-to-end on a common support, which was usually a stone. Next came the use of "chairs"; metal supports into which each end of the rail could be set and fastened. It was apparently after the Civil War that joint bars came into use. These first joint bars were simple plates, known as fish plates, that made no contact with the head and base of the rail. This geometry eventually evolved into the bolted joint currently found in about 50% of the railroad track in the United States and illustrated in Figure 1-1. Today, most new joints are welded to form what is called continuous welded rail (CWR). New bolted joints are still installed, but generally as insulated joints, in crossings and special connections, and in curves in which frequent rail replacement is anticipated.

One of the reasons CWR has come into such widespread use is the weakness associated with the bolted joint. The bolted joint is a significant discontinuity in both the rail running surface and the bending stiffness of the track structure. This results in excessive deformations and forces at the bolted joint which cause plastic deformation and spalling of the rail head, dynamic excitation of the rail vehicle, and rail end cracking. It is the cracking which occurs at the rail end bolt holes that is the topic of this report.

Bolt hole cracks are usually found to initiate at the first bolt hole of the rail end that receives the loaded trains. This indicates that the impact of the vehicle wheel on the rail end must play a significant role in the initiation process. Furthermore, bolt hole cracks almost always propagate initially at 45° to the rail axis, generally toward the rail head away from the rail end. Figure 1-2 is an example of the most common bolt hole crack. The fact that the cracks initiate

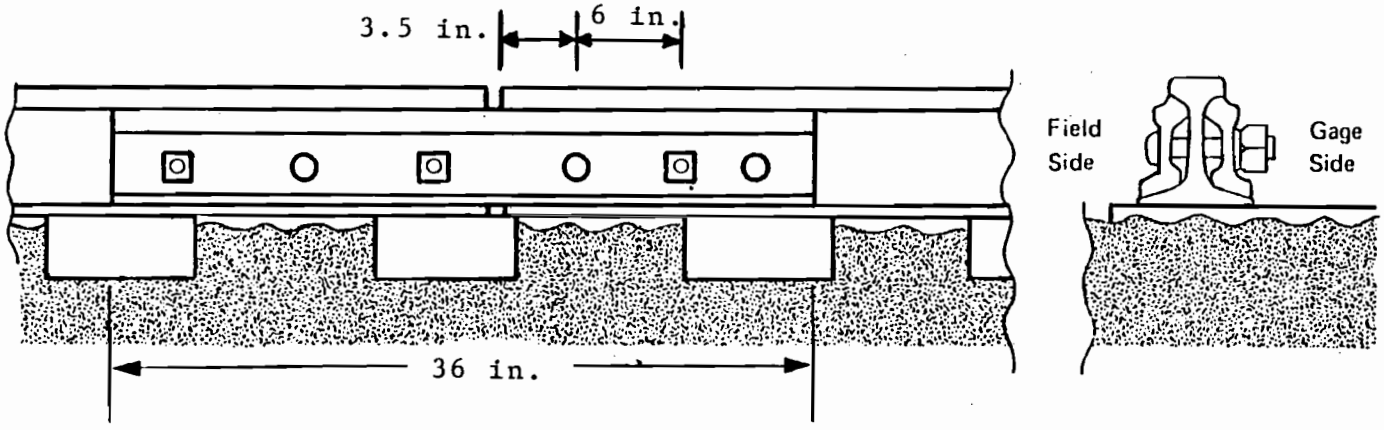

Figure 1-1: Geometry of a Bolted Joint

and propagate at 45° to the rail axis is explained by a state of stress in the rail web around the hole that is essentially pure shear. The common orientation of the crack with respect to the rail end--illustrated in Figure 1-2--can be explained by the mechanics of the rail joint which will be described in the next section.

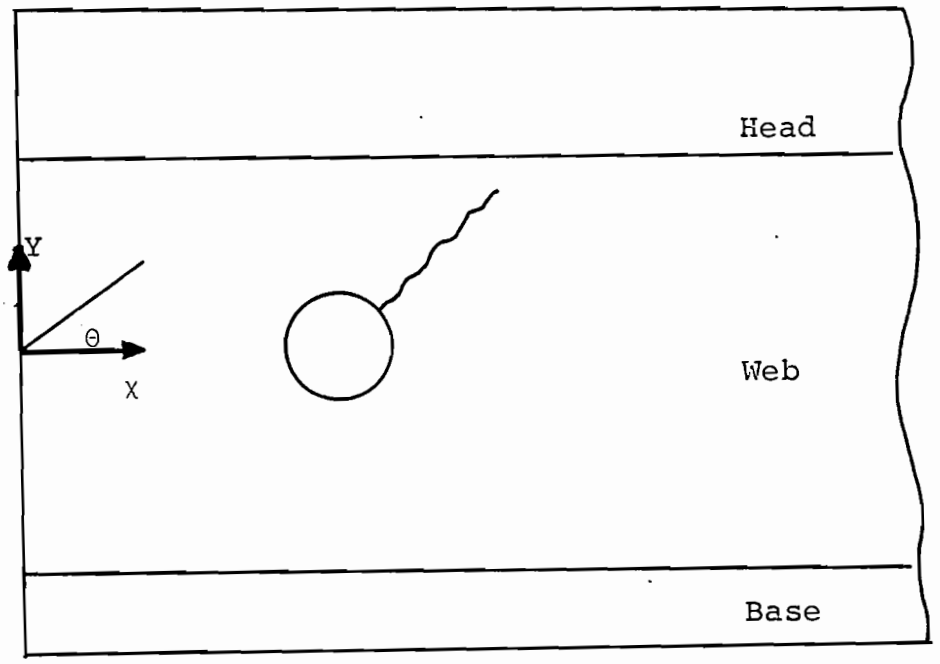

Figure 1-2: Common Bolt Hole Crack

Several studies have been conducted over the years to try to understand and solve the problem of fatigue crack initiation at rail end bolt holes. Many of these studies conclude that conditions must be severe for initiation to occur. Wise, Lindsay and Duncan [1] used electrical resistance strain gages applied to the inside of rail end bolt holes in service and compared these values to measured fatigue strength. They concluded that fatigue appeared to be possible only when very severe conditions of dynamic load and poorly maintained joints existed, producing high stresses, and the rail was badly corroded, contributing to low fatigue strength. The authors suggested work-hardening the bolt hole surfaces by forcing through the bolt hole a steel ball with diameter slightly greater than the hole diameter. A recent study by Lindh, Taylor and Rose [2] was carried out to establish the influence of a similar work-hardening procedure on the fatigue resistance of rail end bolt holes. These investigators used a cold-expansion technique that resulted in compressive surface stresses at the bolt hole. Their work, which included field tests, showed that the number of fatigue cracks could be reduced by about a factor of three if the cold-expanding procedure was carried out carefully.
Other solutions to the fatigue problem that have been suggested over the years are tapering the edges of the bolt holes and using elongated holes so that the bolt does not contact the hole surface and reduce the fatigue strength. Both of these suggestions have been examined at one time or another. The first does not provide a significant improvement in fatigue strength and the latter suggestion is impractical.

It is, in fact, the contact between the bolt and bolt hole and its potential detrimental effect on fatigue strength that motivated part of the present investigation. When joints are not perfectly assembled and in cold or hot weather when the rails contract or expand, the bolts make contact with the bolt hole surfaces. In the winter, this sometimes results in the fracturing of a rail end, even in the absence of trains. In any case, when contact does occur there is rubbing, or fretting,

action at the bolt/bolt hole interface. Such fretting is known to result in considerable reductions in fatigue strength in other structures. This poses the question of whether fretting is necessary for fatigue initiation to occur at rail end bolt holes, the main topic of this chapter.

The approach taken to answer this question is to establish the magnitudes of the mean and alternating stresses at the bolt holes using the mechanics of the bolted joint developed in a previous project and some further analysis to relate the forces in the joint to the stresses at the hole. These stresses are used to perform an elementary fatigue analysis to determine how low the fatigue strength must be for fatigue to occur. The fatigue strength so obtained is compared to fatigue strengths determined experimentally under conditions with and without fretting and corrosion to establish if fretting is necessary for fatigue to occur at rail end bolt holes. Included is a discussion on observations made on three bolt hole cracks removed from service.

1.2 Stress Analysis

An analysis of whether or not fatigue initiation can occur at the bolt hole requires a reasonably accurate knowledge of the stresses. This is a difficult task. The bolted rail joint represents a discontinuity in the track and consequently is a source of dynamic loads. In addition, the structural condition of the joint varies considerably according to such factors as bolt tightness and local foundation (ballast) stiffness and additional stresses arise as a result of lateral load, wheel eccentricity and longitudinal forces caused by thermal contraction and expansion.

Loads

The static wheel loads for train vehicles vary depending on the type of vehicle and the type of traffic. For loaded 100 ton hopper cars, the static wheel loads can be as high as 33×10^3 lbs. (33 kips). Locomotive static wheel loads are about 30 kips. Ahlbeck, Johnson, Harrison and Tuten [3] have measured the dynamic wheel loads

that arise in bolted joint rail. The measurements were made on tangent track in the Mojave Desert carrying loaded 100 ton hopper cars that had a static wheel load of 25 kips.

The variation of the wheel load as the wheel passes a joint has a form similar to that illustrated in Figure 1-3 [3,4] at least for "dipped" joints; that is, joints at which the rail ends meet at an oblique angle less than 180°. The first peak occurs about 2 in. beyond the rail gap, which is between the rail end and the first bolt hole. The second peak occurs about 10 in. from the rail end, which is close to the second bolt hole.

Figure 1-4 shows the variation of the mean peak and maximum loads at bolted joints as a function of train speed; mean peak load is the average of all of the peak loads and maximum load is the maximum of the peak loads. The maximum loads are considerably greater than the mean peak loads, reaching a value 2.6 times the static wheel load at 55 mph. The authors [3] report that they measured a load of 104 kips for a wheel flat.

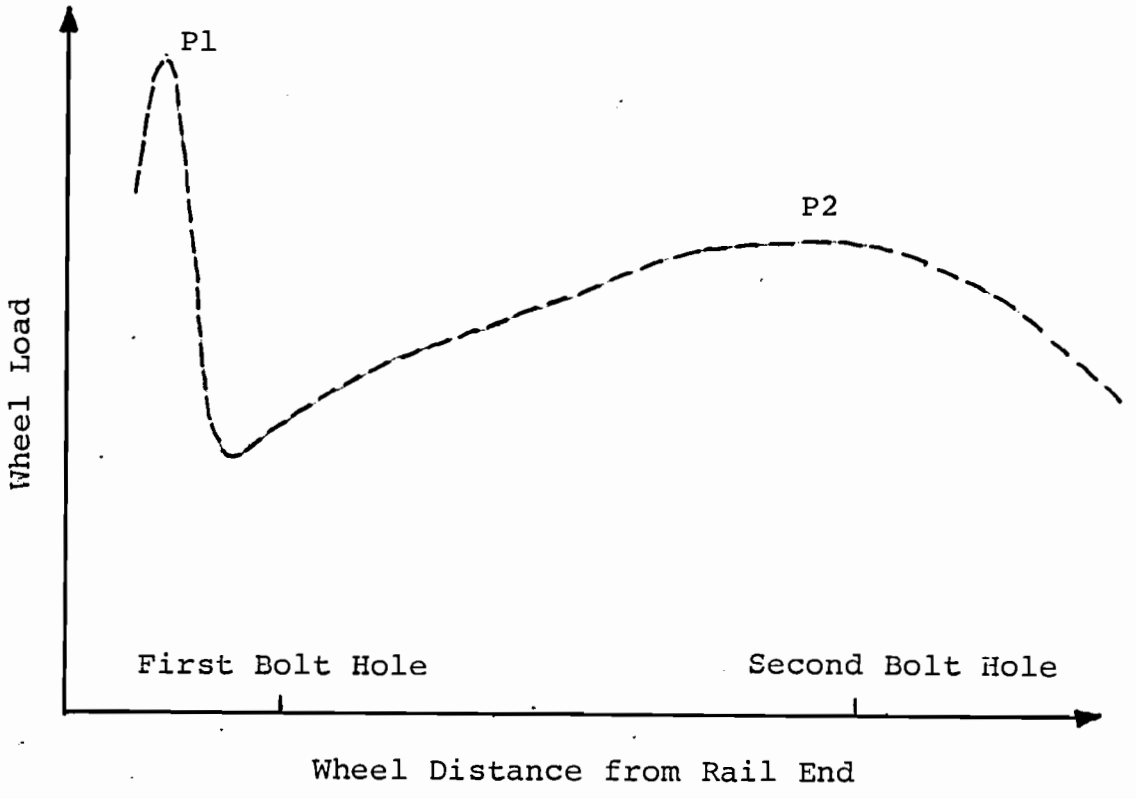

Figure 1-3: Variation of Wheel Load Across a Bolted Joint

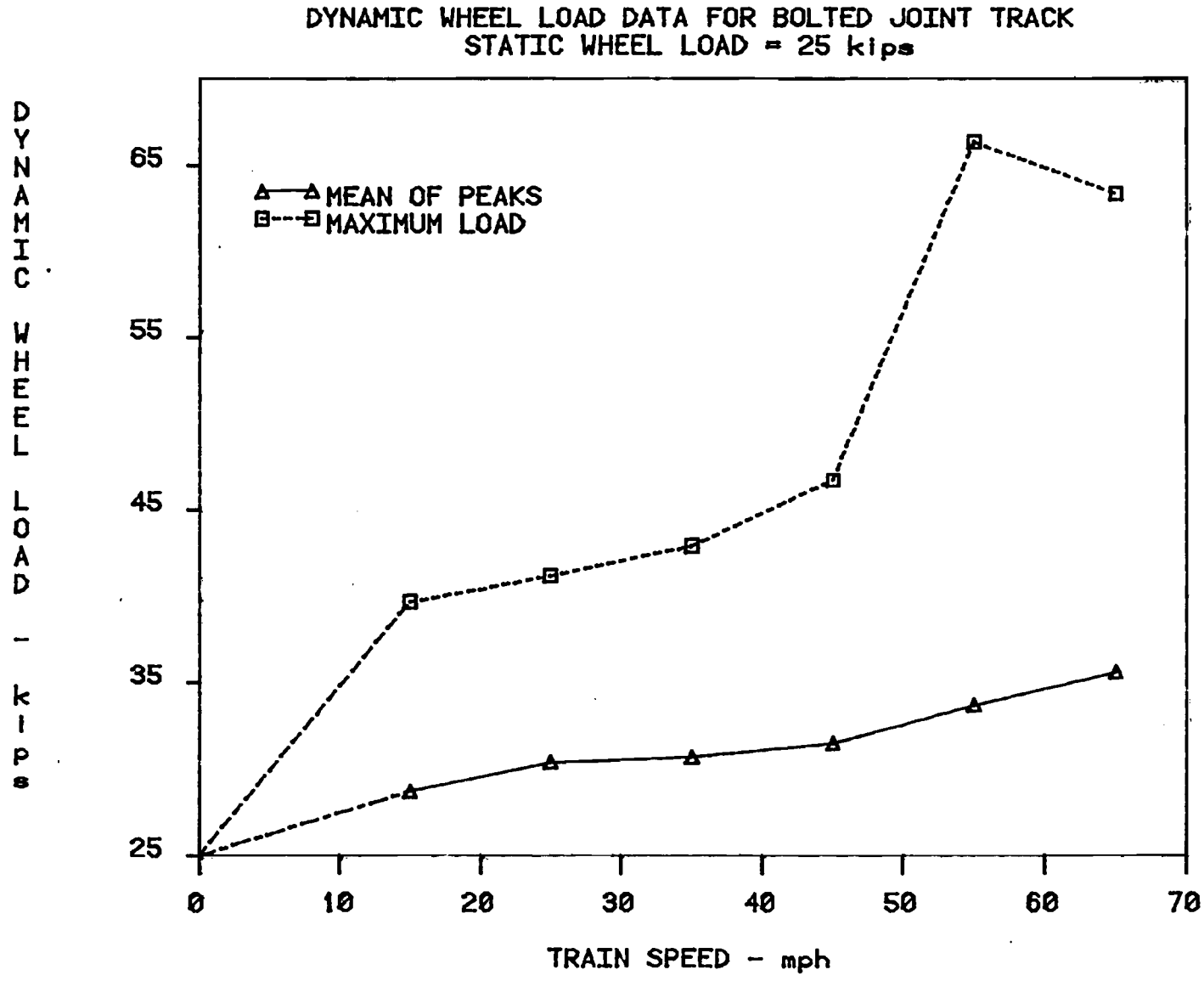

Figure 1-4: Variation of Mean Peak and Maximum Wheel Loads With Train Speed [3]

These data were obtained by analyzing load data that had been read digitally. The rate of this digital data acquisition was slow in comparison to the transient time of the first peak illustrated in Figure 1-3 as P1, so that most of the peak load data corresponds to the second peak, P2. It is probable, on the other hand, that the maximum loads in Figure 1-4 correspond to the peak, P1.

Based on this data alone it appears that the impact load on the rail end can be up to two and one-half times the static wheel load as the wheel crosses the joint gap. The second peak in the wheel load, which occurs after the wheel has passed the first bolt hole, is usually no greater than 1.5 times the static wheel load. This is further illustrated in Table 1-1 which lists the data in Figure 1-4, normalized by the static wheel load.

Table 1-1: Wheel Load Data for 100 Ton Hopper Cars on Tangent Bolted Joint Rail [3]; Static Wheel Load is $W = 25 \times 10^3$ lb

Train Speed (mph)	Mean of Peaks W_p (kips)	W_p/W	Max Load Recorded W_M (kips)	W_M/W
15	28.7	1.15	39.7	1.59
25	30.4	1.22	41.2	1.65
35	30.7	1.23	42.9	1.72
45	31.5	1.26	46.7	1.87
55	33.7	1.35	66.3	2.65
65	35.6	1.42	63.3	2.53

Joint Forces

Some progress has been made in calculating the type and magnitude of the forces at a bolted joint produced by the wheel loads [5]. The analysis assumes that the joint bars transfer a certain amount--usually 50 to 75%--of the bending moment and shear force which would exist at the joint if it were continuous rail and behaved like a beam on an elastic foundation. The joint bars transfer load to the rail ends through four-point bending loads, the magnitudes of which are determined from equilibrium with the moment and shear force at the joint center. Added to these loads are any wheel loads which may be on the rail. The primary force considered to cause cracking in the bolt hole is the shear force at the bolt hole in question obtained by solving the problem of a semi-infinite beam on elastic foundation loaded by the joint bar forces and any wheel loads on that rail. Figure 1-5 shows the results of calculations made with the joint mechanics methodology. The modeled conditions are quasistatic--corresponding to a very slow train--and compare in form quite favorably to a strain trace taken from inside a bolt hole for a track in service with a slowly moving train. The assumption here is that the bolt hole surface strain is proportional to the bolt hole shear force. The two model curves in Figure 1-5 correspond to two different joint efficiency factors; the joint efficiency is the fraction of the moment and shear for a continuous rail carried by the joint [5].

A closer examination of the shear force variation at the bolt hole is useful to explain some of the observations made on rail end bolt hole cracks. Expanded variations for two wheels passing the bolted joint are shown in Figure 1-6. The solid line corresponds to the same conditions as in Figure 1-5 with joint efficiency $k = 0.5$. The broken line corresponds to the type of shear force variation that is expected from a fast moving train. Shear forces greater than zero (load acting upward at the end of the rail) correspond to maximum circumferential tensile stresses at the locations along the bolt hole $\theta = \pi/4$ and $5\pi/4$ and maximum circumferential compressive stresses at the

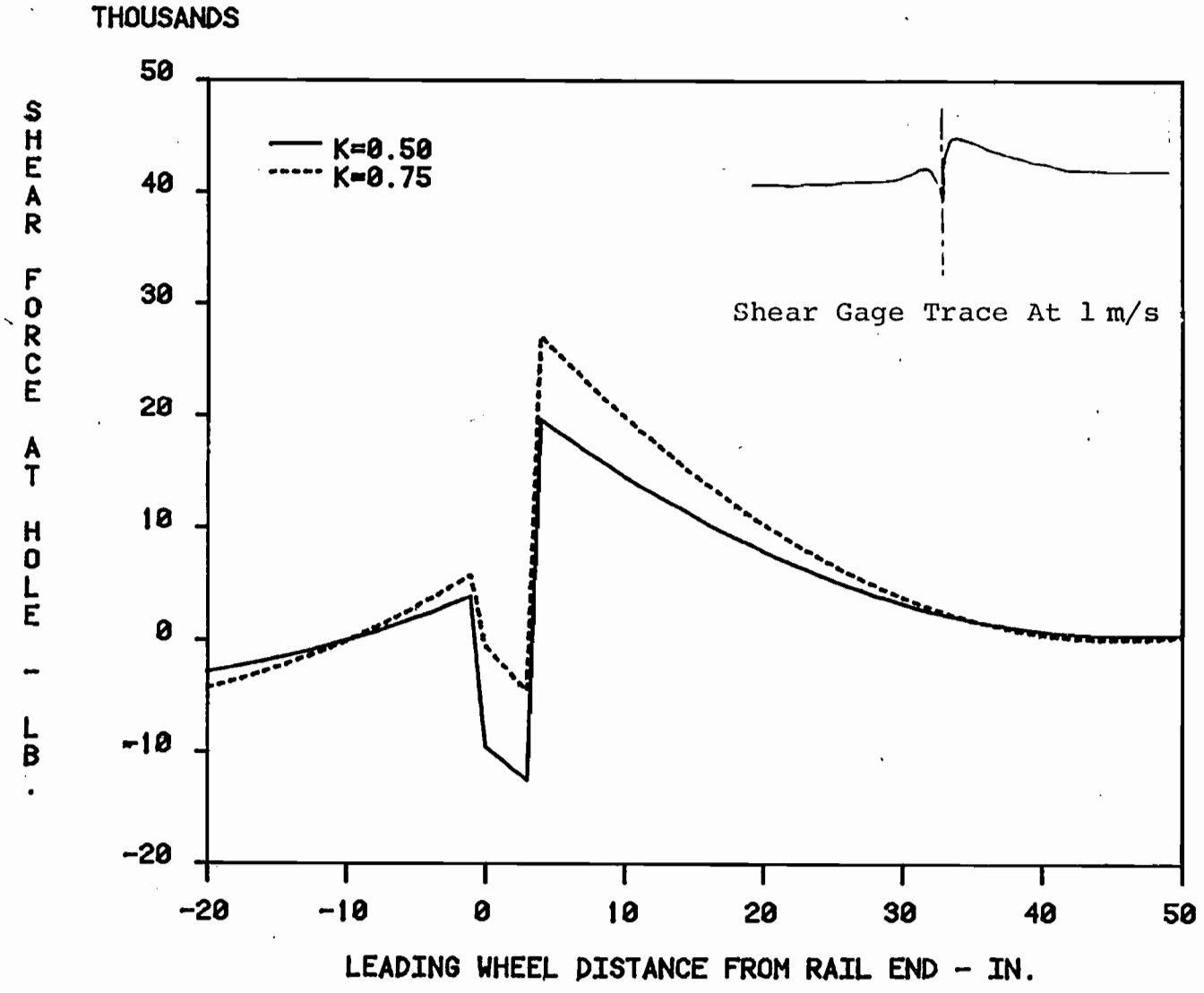

Figure 1-5: Predictions of Bolted Joint Force Model in Comparison to Field Measurement from [1]

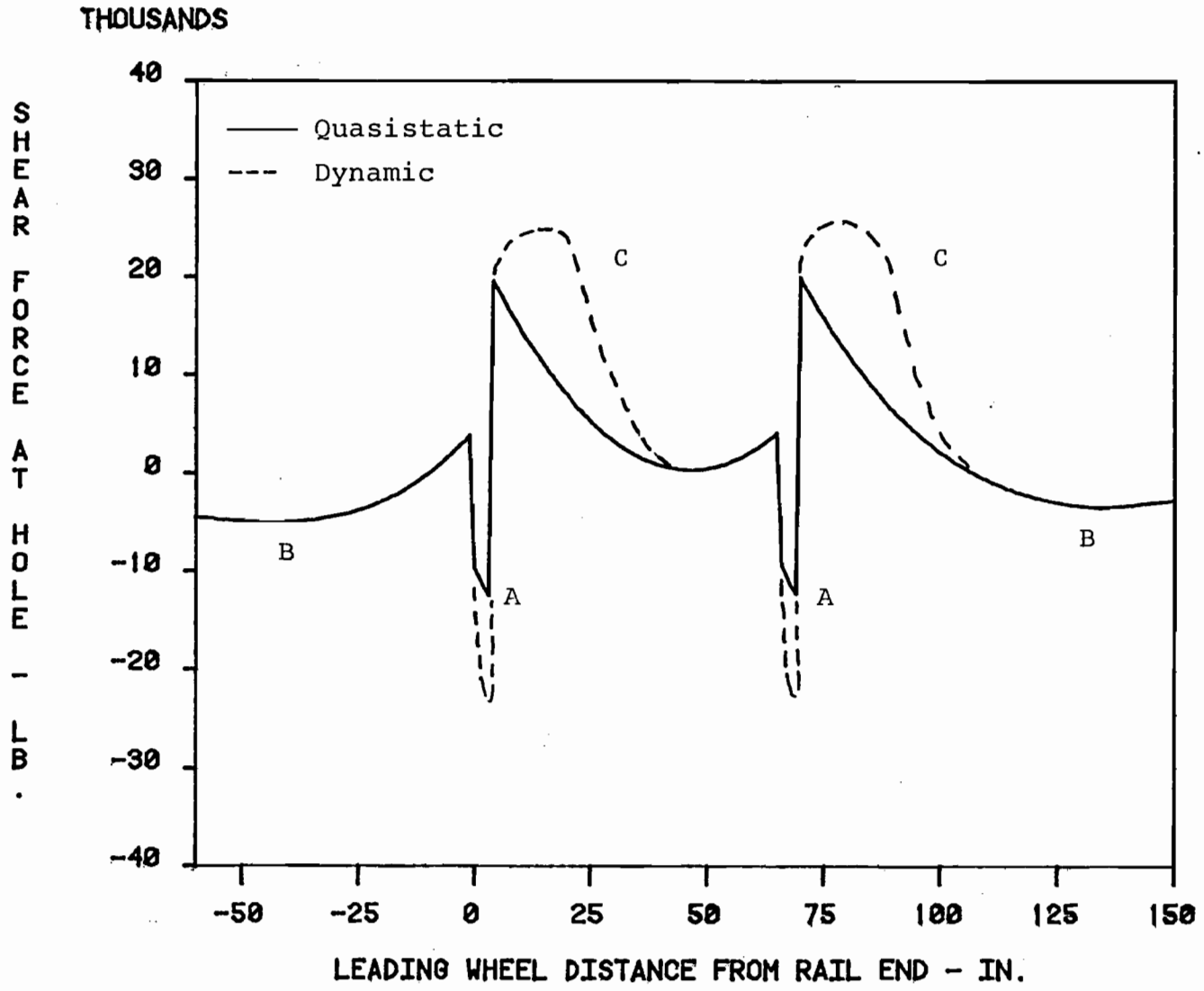

Figure 1-6: Variation of the Shear Force at the First Bolt Hole: solid-line-model; dashed line-expected variation

locations $\theta = 3\pi/4$ and $7\pi/4$; θ is measured counterclockwise from the rail axis, pointing away from the rail end (see Figure 1-2). The parts of the curve below V=0 cause the locations of maximum tension and compression to switch. Figure 1-6 shows that, unless the magnitude of the shear forces at points A or B are very high, fatigue crack initiation and propagation are favored at $\theta = \pi/4$ and $5\pi/4$ in agreement with observations.

The negative peaks indicated by points A in Figure 1-6 correspond to the instant that the wheel crosses the joint. The data presented in the last section demonstrated that this force can be almost three times the static wheel load. Some investigators have reported impact loads as great as five times the static wheel load [4], especially for dipped and battered rail ends. The magnitude of the negative peaks at A is also determined by the joint efficiency as shown in Figure 1-5. In the absence of joints, the shear force at the bolt hole would always be negative or zero, except for some slight reversed bending. The parts of the curve marked B in Figure 1-6 correspond to reversed bending of the rail. The maximum value of the negative shear force resulting from this reversed bending is generally equal to -0.3 times the maximum positive shear force for quasistatic conditions. Thus, under conditions of high impact load and poor joint efficiency, cracks are more likely to occur at $\theta = 3\pi/4$ and $7\pi/4$. Such cracks do, of course, occur. In some cases, cracks are found to initiate at all four locations: $\theta = \pi/4$, $3\pi/4$, $5\pi/4$ and $7\pi/4$.

Bolt Hole Stresses

The close similarity between the calculated shear force variation and the measured strain on the inside of a bolt hole demonstrated in Figure 1-5 indicates that the shear force and bolt hole surface stress are proportional. The simplest model to calculate the constant of proportionality is the model of an infinite plate-in-shear containing a circular hole, which is shown in Figure 1-7a. In this case,

$$\sigma_{max} = 4\ \tau \qquad (1.1)$$

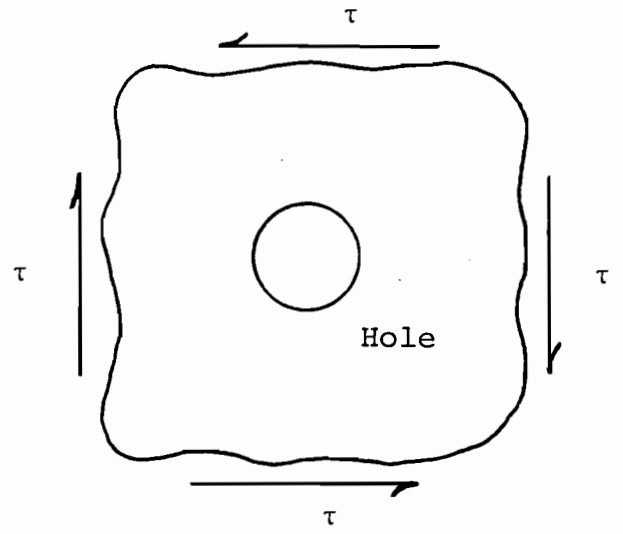

(a)

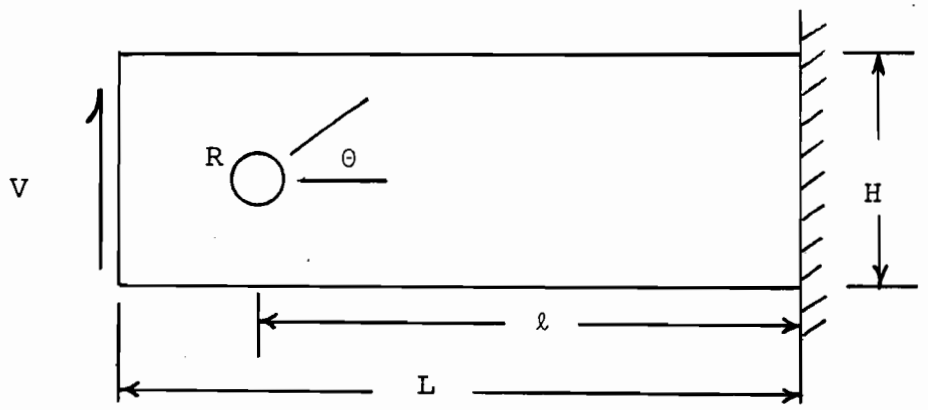

(b)

Figure 1-7: Models Used to Calculate Bolt Hole Stress: (a) Infinite Plate-In-Shear; (b) Cantilever Beam

and occurs at 45° to the rail axis. When the shear force at the rail end acts upward, the stress is tensile for $\theta = \pi/4$ and $5\pi/4$ and compressive for $\theta = 3\pi/4$ and $7\pi/4$ (see Figure 1-2).

The difficulty with using this model is the choice of τ. The shear stress varies parabolically through the rail section, reaching a maximum at the neutral axis. Choice of the theoretical maximum shear stress for use in equation (1.1) would appear to predict stresses that are conservative but perhaps much too high.

A better model for the rail end is a cantilever beam containing a circular hole located at the neutral axis loaded at its end by a shear force. This model is shown in Figure 1-7b. The stress on the inside of the hole is given by Savin [6] as

$$\sigma = \frac{V}{I} \{R(L-\ell)[\sin\theta - \sin 3\theta] + [(\frac{1}{2} H^2 - R^2)\sin 2\theta + R^2 \sin 4\theta]\} \quad (1.2)$$

where

V = shear force

I = moment of inertia of the rectangular section

R = radius of the hole

L = length of beam

ℓ = distance of the hole center from the fixed end of the beam

H = height of the rectangular section.

The stress magnitude is a maximum at the four locations 45° to the rail axis. At $\theta = \pi/4$, which is where most bolt hole cracks occur in service, .

$$\sigma = \frac{V}{I} (\frac{1}{2} H^2 - R^2). \quad (1.3)$$

In order to apply this equation to the rail cross section--equation (1.2) was derived for a rectangular section--some equivalent values for I and H must be determined.

A method suggested by Johns, Sampath, Bell and Davies [7], is to calculate a value of H which gives the rectangular section of unit thickness the same moment of inertia as the rail. For 132 lb/yd rail, $I = 88.2\ in^4$, and the equivalent H is equal to 10.2 in. Substituting this into equation (1.3) with R = 0.56 in. gives

$$\sigma_{max}/V = 0.586.$$

For 132 lb/yd rail, $\tau_{max}/V = 0.25$[5] and this implies that $\sigma_{max} = 2.34\ \tau_{max}$, which is considerably less than what would be predicted from the infinite plate in shear model with the maximum shear stress, equation (1.1). The physical justification for using an equivalent H based on equal moments of inertia is not clear. However, as will be shown presently, this procedure seems to yield surprisingly accurate predictions for the rail cross-sectional geometry.

Finite element analyses have been conducted [7] to simulate a section of 132 lb/yd rail built-in on one end and loaded by various concentrated loads along its length. The rail model contained a single bolt hole located 3.5 in from the free end. In one example, which was run to test the analysis of Savin [6], the rail was loaded by a single concentrated load at the free end, as illustrated in Figure 1-8a. The maximum calculated stress in the bolt hole, which occurred at $\pi/4$ and $5\pi/4$, was $\sigma_{max} \cong 6$ ksi for V = 10 kips therefore,

$$\sigma_{max}/V = 0.6,$$

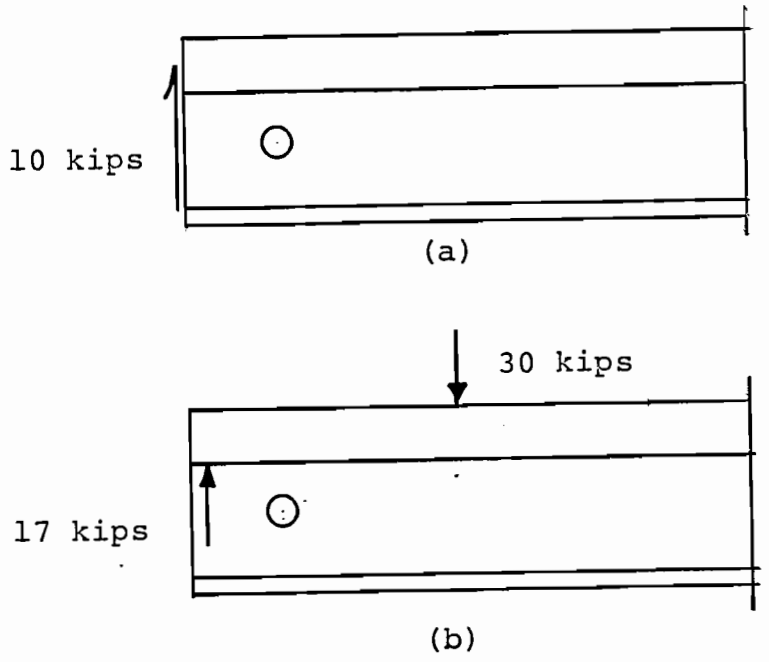

Figure 1-8: Loading Configurations Used in Finite Element Analyses in [7].

which is very close to the value predicted from the Savin analysis using the geometry equivalence based on equal moments of inertia. In another example, which was designed to simulate the forces which occur in an actual bolted joint, the rail model was loaded under the rail head at the rail end and on the running surface at a distance of 8 in. from the free end. This example is illustrated in Figure 1-8b. The shear force at the rail end was V = 17.4 kips and the calculated maximum stress on the bolt hole surface was σ_{max} = 10.5 ksi, giving

$$\sigma_{max}/V = 0.603.$$

Wise, Lindsay and Duncan [1] report strain measurements made on the inside of a bolt hole in a 109 lb/yd rail in service exposed to the loads of a slowly moving train. These are the same results shown in the upper part of Figure 1-5. The results can be used to test the Savin analysis. The total stress range as the train wheel passes the bolt hole location is, from [1], approximately 18 ksi. The shear force range as the wheel passes the bolt hole must be equal to the wheel load, which in this case was approximately 26 kips. Therefore,

$$\sigma_{max}/V = 0.692 \text{ (experiment)}.$$

The moment of inertia for 109 lb/yd rail is $I = 55.9$ in^4 which gives an equivalent $H = 8.75$ in. The radius of this bolt hole was $R = 0.59$in. From equation (1.3)

$$\sigma_{max}/V = 0.679 \text{ (theory)}.$$

Based on these results it is concluded that the Savin analysis can be used to calculate bolt hole stresses when used with a value of H which gives the rectangular cross section of unit thickness the same moment of inertia as the rail cross section. It may be fortuitous that the equivalent geometry accounts for the fact that the force at the end of the rail is concentrated instead of being distributed over the rail end as is apparently assumed in the Savin analysis. One expects that the load distribution at the rail end has an effect on the stresses at the bolt hole, because the bolt hole is only 3.5 in. from the rail end in comparison to a rail height equal to 7 in.

The stresses caused by the train wheels are undoubtedly the primary stresses causing fatigue. But there are additional stresses which contribute to the fatigue process. One source associated with the wheel loads but not considered in the previous discussion is wheel eccentricity with respect to the rail head and lateral loads, both of which

result in out-of-plane bending stresses in the web. These effects have not been considered in detail in the present investigation, but some general observations can be made. The first observation is that the web bending stresses resulting from eccentric and lateral loads are on the order of 5 ksi [7], at least for tangent track. Secondly, this stress is spread over a distance along the rail which is larger than the distance over which the stress reversal caused by the primary wheel load is spread [8]. This latter observation implies that the web bending stresses caused by eccentric and lateral wheel loads has the effect of changing the mean stress at the bolt hole more than changing the alternating stress, an implication which is important in the fatigue analysis.

Other sources of bolt hole stresses are the stresses caused by joint bolt tension and longitudinal stresses that arise when the rails contract or expand. Bolt tension causes a stress in the same direction as eccentric and lateral wheel loads: perpendicular to the rail axis and in the plane of the web. Estimating the magnitude of the stresses caused by bolt tension is almost impossible because the stresses depend on the bolt tension and the uniformity of contact between the bolts and the joint bars and the joint bars and the rail, both of which are found to vary with traffic. In fact, the bolt tension and the associated web stresses vary as a wheel passes the joint because the joint bar tends to lose contact with the rail base at its center and with the rail head at its ends.

The longitudinal stresses caused by temperature variations are most severe when it is cold and the rails contract, placing the rails in tension. The load is transferred to the rail through bearing pressure between the bolt and the bolt hole surface. The magnitude of the resulting bolt hole stresses depends on many factors, including the temperature change, the original clearance between the bolts and the bolt holes, the distribution of the total longitudinal load between the different bolts of the joint and the load transferred to the foundation

through the fasteners. It is known that the resulting forces can sometimes be sufficient to fracture the end of a rail, but estimating the associated bolt hole stresses during regular service has, to the author's knowledge not been accomplished.

The previous discussion highlights the difficulties in calculating the bolt hole stresses that result from the secondary effects of eccentric and lateral loads, joint bar bolt tension and longitudinal stresses caused by rail thermal contraction or expansion.

Extremes in one or more of these effects may be the explanation for fatigue in some cases. For example, a joint that is subjected to eccentric wheel loading on the passage of each wheel, due to, say, a gage that is too large, would make fatigue initiation more likely. In reality, all of the secondary effects probably occur in a random manner, adding to the fatigue process but in no systematic way. Inclusion of these effects in a fatigue analysis would require a reasonable knowledge of their probability distribution. In any case, more work is required to calculate the stresses that result from these effects.

Examples

We are now in a position to calculate maximum and minimum bolt hole stresses for actual track-train conditions. All of the calculations in this section are performed for the following conditions:

W	=	33 kips	static wheel load for loaded 100 ton hopper car
XSP	=	66 in.	wheel spacing
I	=	88.2 in^4	moment of inertia for 132 lb/yd rail
E	=	30 x 10^6 psi	Young's modulus for steel
z	=	3.5 in.	distance of first bolt hole center from rail end
b	=	12 in.	distance between outer four-point bend forces at the rail end
k	=	0.5	joint efficiency factor
u	=	3000 psi	foundation modulus

Table 1-2 lists the results of calculations for different values of the wheel load dynamic amplification factor α corresponding to the range of load conditions listed in Table 1-1. The results important for the fatigue analysis of the next section are the maximum and minimum stresses. The review of load data given previously indicated the wheel load could be as great as 2.5 times the static wheel load as the wheel just crosses the joint and for high train speeds. This corresponds to point A in Figure 1-6 and results in a compressive stress at $\theta=\pi/4$ and $5\pi/4$. The second peak in load, which occurs just after the wheel passes the first bolt hole, was generally only 1.5 times the static wheel load. This corresponds to points C in Figure 1-6 and results in tension at $\theta = \pi/4$ and $5\pi/4$. Under these conditions one obtains,

$$\sigma_{min} = -16.5 \text{ ksi} \; ; \quad \alpha = 2.5$$

$$\sigma_{max} = +19.0 \text{ ksi} \; ; \quad \alpha = 1.5$$

Under the assumptions of the analysis in this report, if the first load peak, P1, is greater than 3 times the static wheel load, and the second peak is less than 1.5 times the wheel load, fatigue initiation is favored at $\theta = 3\pi/4$ and $7\pi/4$, since it has been assumed that the magnitude of the stresses is the same at $\theta = \pi/4$, $3\pi/4$, $5\pi/4$ and $7\pi/4$.

Table 1-2 also shows that the minimum stress caused by reversed bending is constant. This reflects an aspect of the model which does not include dynamic amplification when the wheels are relatively far from the joint [5].

Table 1-2: Maximum and Minimum Stresses at the Bolt Hole for Various Dynamic Load Amplification Factors (see text for values of other parameters used in the calculations)

α	αW kips	V_{minA} kips	V_{minB} kips	V_{max} kips	σ^*_{min} ksi	σ^*_{max} ksi
1.00	33.0	-12.9	-5.0	20.1	-7.7	12.1
1.25	41.2	-15.4	-5.0	25.8	-9.2	15.5
1.50	49.5	-17.9	-5.0	31.6	-10.7	19.0
2.00	66.0	-22.8	-5.0	43.2	-13.7	25.9
2.50	82.5	-27.5	-5.0	54.7	-16.5	32.8
3.00	99.0	-32.5	-5.0	66.5	-19.5	39.9
4.00	132.0	-42.3	-5.0	89.7	25.4	53.8

*σ = 0.6V; stresses at $\theta = 3\pi/4, 7\pi/4$

1.3 Fatigue Analysis

The analysis for fatigue crack initiation in the rail end bolt hole requires a knowledge of the mean and alternating stresses, a fatigue initiation criterion and fatigue data for the rail steel. Bolt hole stresses were presented in the previous section. The objective of the fatigue analysis in the present work is to determine if fretting conditions must prevail in order for high cycle fatigue initiation to occur at rail end bolt holes. Considering the uncertainty of most of the

track/train parameters this analysis need only be approximate. Therefore, the following assumptions are made:

- Fatigue initiation occurs if the Goodman diagram equation is satisfied;

$$\frac{\sigma_a}{\sigma_e} + \frac{\sigma_m}{\sigma_u} = 1 \qquad (1.4)$$

where

$\sigma_a = (\sigma_{max} - \sigma_{min})/2$, the alternating stress,

$\sigma_m = (\sigma_{max} + \sigma_{min})/2$, the mean stress

σ_e = endurance strength and

σ_u = tensile strength.

- Every wheel in every train causes the same σ_a and σ_m at the bolt hole. In other words, variable amplitude loading is not considered.

- There are no effects of eccentric and lateral wheel loads, bolt tension and longitudinal thermal stresses.

The approach is to use the stresses calculated in the section on stress analysis to obtain values for σ_a and σ_m; estimate the endurance strength, σ_e, for rail steel that is not exposed to fretting conditions; and then perform a calculation to determine if fatigue initiation is possible without fretting conditions.

Several sources were reviewed for data on the fatigue strength of rail steels. Jensen [9], performed flexure fatigue tests on specimens removed from the rail web of standard carbon 112 lb/yd rail. The yield and ultimate strengths of the material were almost identical for the longitudinal and transverse orientations and were equal to σ_o = 78 ksi

and σ_u = 136 ksi. The reduction in area and elongation were 16% and 10% respectively. These tensile properties are typical of most standard carbon rail. Jensen's results for fatigue under ambient conditions are plotted in Figure 1-9. The solid line in Figure 1-9 corresponds to the Goodman Diagram--the equality of equation (1.4)--and agrees well with the data when σ_e = 34 ksi. Jensen also performed a few tests under corrosive conditions, using contaminated tap water as a medium, and found that $\sigma_e \cong 26$ ksi.

Table 1-3 lists values of σ_e obtained from the literature for specimens removed from the rail web and head; specimens from the head have a longitudinal orientation.

Table 1-3: Values of Endurance Strength, σ_e, for Standard Carbon Rail

Reference	Loading	Location	σ_o (ksi)	σ_u (ksi)	σ_e^* (ksi)
[9]	Flexure	Web	78	137	34
[10]	Push-pull	Web	68	130	35
[11]	Push-pull	Head	72	135	48
[12]	Flexure	Head	-	140	46
[13]	Rotating Beam	Head	71	130	50

*at 10^6 cycles.

The data in Table 1-3 indicate that the endurance strength for specimens removed from the web is lower than for specimens removed from the head, even though the yield and tensile strengths are comparable.

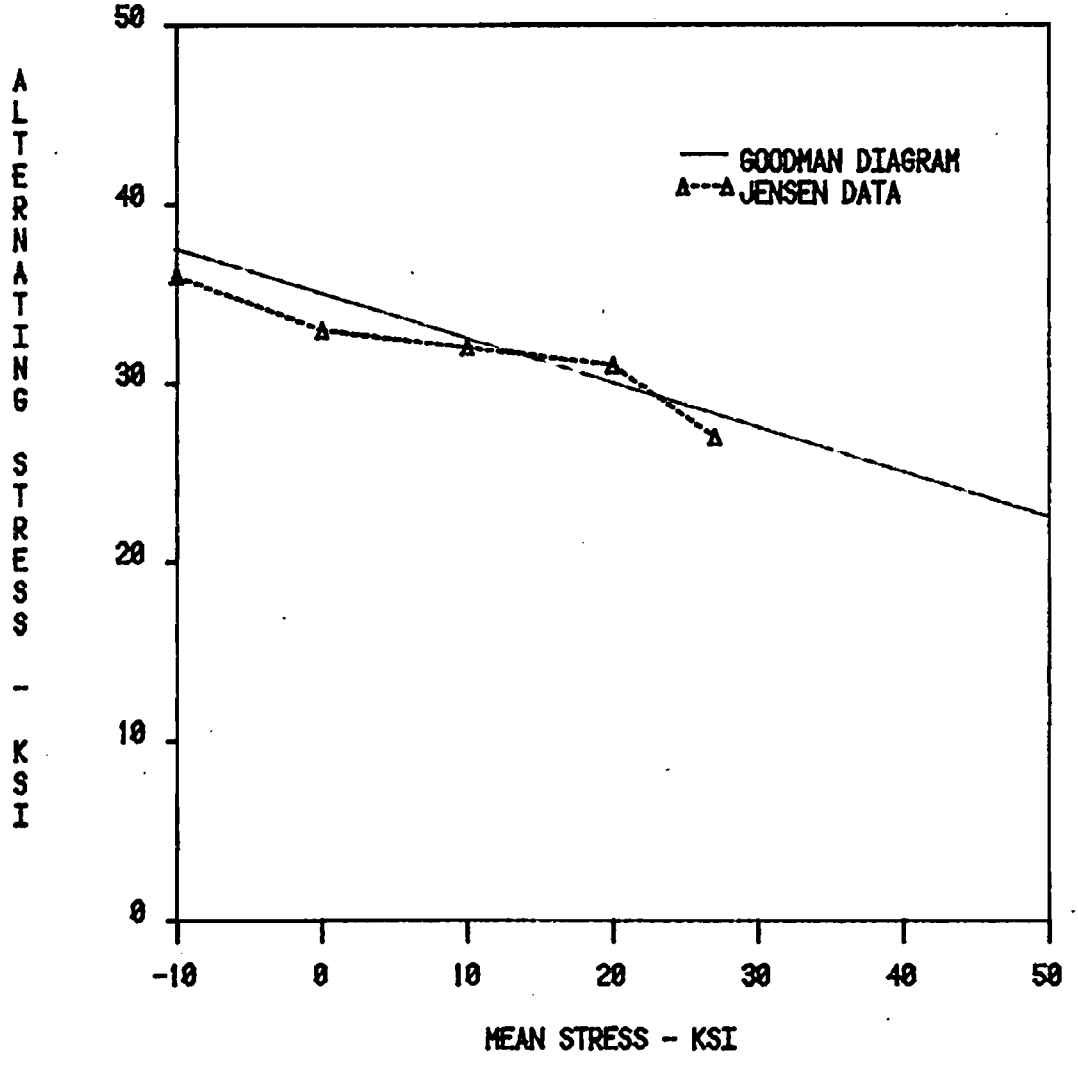

Figure 1-9: High Cycle Fatigue Data for Standard Carbon Rail Web Steel [9]

The conclusion from this data is that, for standard carbon web steel under ambient conditions,

$$\sigma_e = 35 \text{ ksi}$$

This value of σ_e can be used in equation (1-4) with $\sigma_u = 140$ ksi. The mean and alternating stresses are calculated from values in Table 1-2, discussed at the end of the section on bolt hole stresses. In particular,

$$\sigma_m = \tfrac{1}{2}[(19.0) + (-16.5)] \text{ ksi} \cong 1.2 \text{ ksi}$$

$$\sigma_a = \tfrac{1}{2}[(19.0) - (-16.5)] \text{ ksi} \cong 17.8 \text{ ksi}.$$

Using these values, the left side of equation (1.4) is equal to 0.52 which is considerably less than the value of 1.0 needed to satisfy the fatigue criterion; this explains why most bolt holes do not crack. In order for fatigue to occur under the assumed track/train conditions and with our force-stress model, a reduction in the fatigue strength with respect to the value measured in the laboratory is necessary. Alternatively, or in addition, stresses induced by secondary effects, such as eccentric loading, must be extreme.

The fatigue strength would have to be reduced to $\sigma_e \cong 18$ ksi in order to account for the occurrence of fatigue without secondary stress effects; this corresponds to a factor of 1.9 times lower than the fatigue strength measured under ambient laboratory conditions. Jensen's fatigue tests [9] under corrosive conditions demonstrated that the fatigue strength could be reduced to $\sigma_e = 26$ ksi, but this was for continuous corrosion conditions--conditions that might be found in a tunnel or at a crossing but probably not on regular track.

Thus, it appears that fretting may be necessary to account for fatigue initiation at bolt holes. There is still some contention about the mechanism by which fretting causes a reduction in fatigue strength. There may be a combination of mechanisms which may differ for different

situations. Some investigations have shown that fretting causes mechanical and corrosive damage to the surface. Others have shown that the increase in local stress caused by the contacting bodies is sufficient to raise the stresses above the normal fatigue strength of the material.

There are two ways in which the rail joint bolts can contact and exert pressure on the bolt hole surface. In cold weather, when the rails contract, the bolts will bear against the part of the bolt hole surface closest to the rail end. However, some vertical movement or misalignment is required for the bolt to make contact near the 45° locations, which is where most bolt hole cracks occur. In any case, contact on the upper, opposite side of the bolt hole surface, which is where most bolt hole cracks apparently initiate, is not likely under these conditions, although the stress at this location would certainly be increased. The other way in which contact occurs is through the combined action of joint bar movement relative to the rail and variations in clearance between the bolt and the hole surface caused by misalignment and thermal expansion or contraction. The joint bar movement may be accentuated if the bolt tension is low. Under these conditions contact can occur in several locations around the bolt hole surface.

The observations made on actual bolt hole cracks removed from service, and described in Appendix A, indicate that there is always contact associated with fatigue. In fact, the location of crack initiation is usually on the edge of the contact zone, which is characteristic of fretting; the local tensile contact stresses are greatest at this point. This may be coincidental because the edge of the contact zone usually ends at the 45° location along the bolt hole surface. Nevertheless, on a few of the observed bolt holes that cracked a reddish powder characteristic of fretting of steel surfaces was observed.

Fatigue strength can easily be reduced by a factor of two or three in the presence of fretting (cf.[14]). Lindh, Taylor and Rose [2]

appear to be the only investigators who have conducted fretting tests on rail steel. Both fretting and nonfretting tests were performed with actual rail specimens that contained bolt holes. Their single fatigue stress was very high and resulted in fatigue failures in 10^5 cycles for fretted and nonfretted specimens; that is, the presence of fretting did not result in a significant reduction in fatigue life. This behavior is observed in most fretting fatigue experiments [14] and is explained by the greater role of crack propagation instead of initiation for lives of 10^5 cycles or less.

Fretting data were reported by Waterhouse [15] for a 0.7%C, normalized steel with σ_u = 136 ksi, which is similar to rail steel. The fatigue strength at 10^7 cycles was 31 ksi, which is also comparable to the fatigue strength of rail web steel, and the fretting fatigue strength at 10^7 cycles was 22 ksi. These values may not apply to rail steel, but they do approach the reduced fatigue strength, σ_e = 18 ksi, needed to explain the occurrence of fatigue in bolt holes according to the assumptions of this investigation.

An increase in the mean or alternating stress caused by secondary effects could also account for the occurrence of fatigue, but this is doubtful. Suppose the combined effect of wheel eccentricity and lateral load was to cause the bolt hole stress to increase by an additional σ_A with the passage of each wheel. In other words, $\sigma_a = 17.8 + \sigma_A/2$ and $\sigma_m = 1.2 + \sigma_A/2$. Then σ_A must exceed 27 ksi for fatigue to occur with σ_e = 35 ksi, σ_u = 140 ksi.

Summary

The analysis of this and the previous section indicate that certain characteristics must be associated with the rail joint in order for fatigue crack initiation to occur. The rail ends must have a geometry that induces relatively large dynamic forces. This geometry could be a large rail end gap or dipping and batter. The joint must be somewhat loose; that is, the joint efficiency must be about 0.5 or lower. This results in a significant contribution of the first load peak, P1, to the

fatigue process. Finally, the fatigue strength must be reduced substantially from the laboratory-determined value. This can be caused by corrosion, as in tunnels or at road crossings, and by fretting or a combination of fretting and corrosion in normal track.

The analysis and results of this investigation are not detailed enough to conclude that fretting is necessary to cause fatigue. In particular, there are uncertainties in the following aspects of the analysis:

- the loads at a bolted joint
- the occurrence and magnitude of eccentric and lateral wheel loads
- the bolt hole stresses caused by eccentric and lateral wheel loads
- the relationship between bolt hole stress concentration and shear load at the bolt hole
- the effect of variable amplitude fatigue loading and
- the reduction in fatigue strength in rail web steel caused by fretting.

2. FATIGUE CRACK GROWTH OF CORNER CRACKS IN RAIL END BOLT HOLES

2.1 Introduction

Because of variations in stress through the web thickness, a fatigue crack will tend to initiate as a corner crack on the field or gage side of the bolt hole. It thus becomes important to predict the fatigue crack growth rates for corner cracks at bolt holes, and one must be able to calculate the stress intensity factor along the crack front in terms of the crack and rail geometry and the loading conditions. The bolt hole region is dominated by a shear stress field resulting from rail bending. As a result, cracks tend to initiate and grow at the 45^{o} locations on the bolt holes (see Figure 1-2), which correspond to the maximum value of the circumferential stress component. We plan in this chapter to use the solution of an appropriate boundary value problem to quantify crack growth rates at these locations.

The two-dimensional problem of a remotely sheared plate with a through crack emanating from a hole is dealt with by Tada et.al. [16]. The corresponding three-dimensional problem with a corner crack emanating from a hole has not, to our knowledge, been solved. Newman and Raju, however, have analyzed the corner crack emanating from a hole in a plate subjected to remote tensile loading [17]. Both these three-dimensional problems are represented schematically in Figure 2-1. Even if a solution were available to the remote shearing problem in Figure 2-1a, however, the stress concentration of 4 that prevails in the uncracked body is not appropriate for the rail, as discussed in Section 1.2 of this report. For this reason, we will choose to implement the Newman-Raju solution [17] directly, by scaling down the remote tensile loading to reflect a lower stress concentration at the rail bolt hole. The Newman-Raju work is particularly amenable to use for fatigue crack growth predictions because the results are presented in the form of analytic expressions for the variations of the stress intensity factor along the crack front. These expressions were obtained by curve fitting of finite element results with polynomial series.

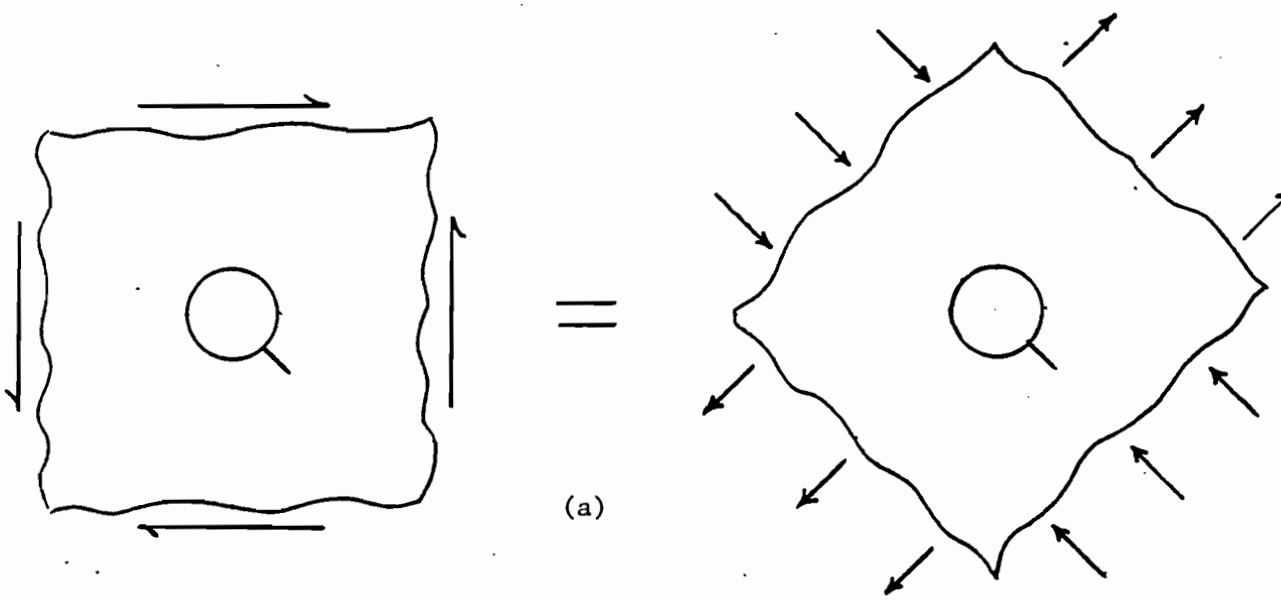

(a)

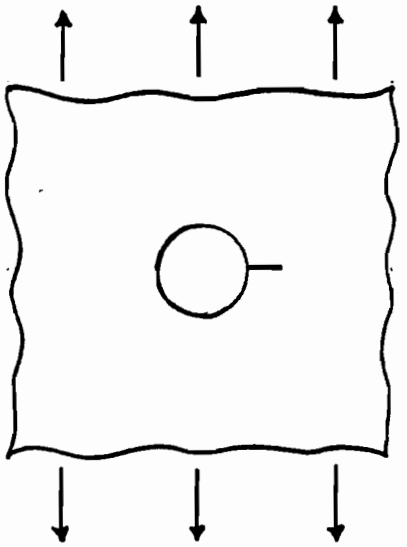

(b)

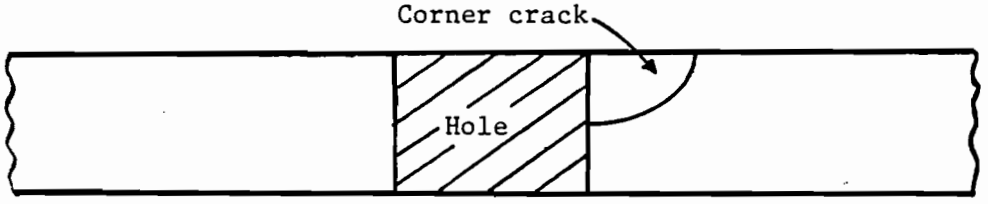

(c)

Figure 2-1. Model corner crack configurations: (a) Remote shear = biaxial tension/compression. (b) Remote tension, considered in [17]. (c) Cross sectional view of crack.

Historically, the earliest work on corner cracks emanating from holes was photoelastic [18] or approximation-based using simple idealizations [19]; Kobayashi et al. [20] used the alternating method to calculate the stress intensity factor for quarter-elliptical corner cracks. Subsequently, three dimensional finite element procedures were applied to the surface crack problem enabling the treatment of boundary effects, such as the influence of plate thickness and hole radius. The earliest finite element analysis of a surface crack was by Tracey [21] who considered circular, semi-circular, and quarter circular cracks in a large diameter cylindrical (or partially cylindrical) body. Atluri and his coworkers have performed finite element analyses of numerous surface crack problems for pressure vessel components; reference [22] is one example. Newman and Raju have carried out extensive finite element analysis for surface cracks in plates [23]; their latest work involving cracks emanating from holes is most appropriate here.

We have chosen to make use of the Newman-Raju formulae for the stress intensity factors in a corner crack on the periphery of a cylindrical hole in a plate subjected to remote tensile loading. The remote tensile stress to be applied is determined as follows. For a static wheel load of 33 kips, the corresponding dynamic load near the bolt hole should not exceed 50 kips, based on the 1.5 amplification factor discussed in connection with Table 1-1. The maximum shear force at the bolt hole corresponding to the static load is 29 kips (see Figure 1-5), so the corresponding dynamic shear force is 44 kips. The maximum tangential stress in the bolt hole, according to Section 1.2, is approximately (0.6)(44)= 26.4 ksi. For an uncracked plate with a hole, a remote tension of 8.8 ksi would produce this same maximum tangential stress. Both for convenience and conservatism, a remote stress of 10 ksi was applied here in conjunction with the Newman-Raju solution to obtain upper bounds to the actual crack growth rates from the rail bolt hole.

We expect that this upper bound solution will lead to good estimates for fatigue crack growth rates when the crack size is small in comparison

with the hole radius, particularly when the maximum radial extent of the crack is much smaller than the hole radius R.

2.2 Analysis

According to the Newman-Raju formula for the corner crack emanating from a hole in a tensile stress field, the equation for the stress intensity factor along the crack front is

$$K_I = S\sqrt{\pi a/Q}\ F_{ch}\ (a/c,\ a/t,\ R/t,\ \phi)$$

where the geometric parameters a,c,t,R and ϕ are defined in Figure 2-2, and S is the applied stress.

Also,

$$F_{ch} = [M_1 + M_2\ (a/t)^2 + M_3\ (a/t)^4]g_1g_2g_3f_\phi h$$

$$h = \sqrt{(4/\pi + ac/2tr)/(4/\pi + ac/tR)}$$

$$\lambda = 1/(1 + c/R\ \cos(0.85\phi))$$

$$g_2 = (1 + 0.358\lambda + 1.425\lambda^2 - 1.578\lambda^3 + 2.156\lambda^4)/(1 + 0.13\lambda^2)$$

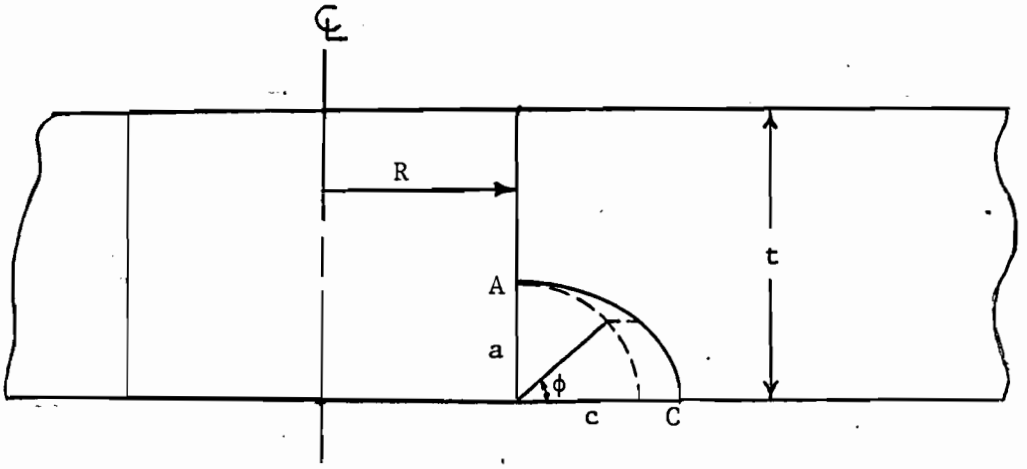

Figure 2-2. Schematic showing corner crack geometry parameters.

and for $a/c \leq 1$

$$Q = 1 + 1.464\ (a/c)^{1.65}$$

$$M_1 = 1.13 - 0.09\ (a/c)$$

$$M_2 = -0.54 + 0.89/(0.2 + a/c)$$

$$M_3 = 0.5 - 1/(0.65 + a/c) + 14(1 - a/c)^{24}$$

$$g_1 = 1 + [0.1 + 0.35(a/t)^2](1 - \sin\phi)^2$$

$$g_3 = (1 + 0.04\ a/c)[1 + 0.1(1 - \cos\phi)^2]\ [0.85 + 0.15\ (a/t)^{1/4}]$$

$$f_\phi = [((a/c)^2\cos^2\phi + \sin^2\phi)^{1/4}]$$

while for $a/c > 1$

$$Q = 1 + 1.464\ (c/a)^{1.65}$$

$$M_1 = c/a(1 + 0.04\ c/a)$$

$$M_2 = 0.2\ (c/a)^4$$

$$M_3 = -0.11\ (c/a)^4$$

$$g_1 = 1 + [0.1 + 0.35\ (c/a)(a/t)^2](1-\sin\phi)^2$$

$$g_3 = (1.13 - 0.09\ c/a)[1 + 0.1(1 - \cos\phi)^2]\ [0.85 + 0.15\ (a/t)^{1/4}]$$

$$f_\phi = ((c/a)^2 \sin^2\phi + \cos^2\phi)^{1/4}$$

The fatigue crack growth rate estimate at points along the crack front is based on the Paris Law $da/dn = \alpha\ (\Delta K)^m$ where m, α are chosen to fit the equation to the fatigue crack growth data for the material under consideration. Representative values for m and α for rail steels are m = 4.33, $\alpha = 5.12 \times 10^{-12}$ [24] where ΔK is measured in ksi/$\sqrt{\text{in}}$ and a is measured in inches.

Hole radius and web thickness at the hole for typical rails (132 lb/yd. rail) are R=0.5625 inch and t=0.675 inch, respectively. In Table 2-1 growth rates are given at each crack end for an appropriate range of crack geometry.

In Table 2-1, note that because the growth rate is proportional to K_1 to the 4.33 power, changes in K_1 lead to amplified changes in growth rate. The stress intensity factors at locations A and C in Figure 2-2 depend linearly on the applied stress, but the dependence on crack size is more complex.

The stress intensity factors are also very sensitive to crack shape. For example, if a>>c then $K_1(C) > K_1(A)$. This information is used with the initial crack shape and the crack growth law to predict the evolution of the crack geometry with number of load cycles. The results shown in Table 2-1 indicate that as the relative dimension (a/c) of the crack increases the ratio of stress intensity factors $K_1(A)/K_1(C)$ decreases. This suggests that the crack will grow by fatigue to a natural shape (as modeled here by the ratio of a to c) for which the stress intensity factor is approximately constant along the

Table 2-1

Crack Growth Estimates for Corner Crack at Rail End Bolt Hole

Stress (ksi)	Crack Dimensions (inches)		Stress Intensity Factors (ksi$\sqrt{in}$)		Crack Growth Rates (inch/cycle)	
	a	c	$K_1(A)$	$K_1(C)$	da/dn	dc/dn
10.00	0.10	0.10	11.06	9.16	1.69×10^{-7}	7.49×10^{-8}
10.00	0.20	0.10	10.48	12.37	1.34×10^{-7}	2.75×10^{-7}
10.00	0.20	0.20	14.86	11.29	6.09×10^{-7}	1.85×10^{-7}
10.00	0.30	0.20	14.56	13.73	5.57×10^{-7}	4.32×10^{-7}
10.00	0.30	0.30	17.29	12.82	1.17×10^{-6}	3.21×10^{-7}
10.00	0.40	0.20	13.84	15.27	4.48×10^{-7}	6.85×10^{-7}
10.00	0.40	0.40	18.99	14.31	1.76×10^{-6}	5.17×10^{-7}
10.00	0.50	0.10	7.85	14.95	3.84×10^{-8}	6.25×10^{-7}
10.00	0.50	0.30	16.34	16.26	9.17×10^{-7}	8.97×10^{-7}
10.00	0.50	0.50	20.22	15.90	2.31×10^{-6}	8.16×10^{-7}
10.00	0.60	0.20	12.33	17.11	2.71×10^{-7}	1.12×10^{-6}
10.00	0.60	0.40	17.90	17.35	1.36×10^{-6}	1.19×10^{-6}
10.00	0.60	0.60	21.04	17.58	2.74×10^{-6}	1.26×10^{-6}

crack front. Similar observations have been made by other authors, e.g. Newman [23], with respect to interior elliptical cracks and semielliptical surface cracks. For the case of a corner crack at the periphery of a hole analyzed here, the "natural" growth is such that a>c, presumably because the stress field (for the uncracked plate) associated with the hole is nonuniform and of larger amplitude at A than at C. The predictions of more rapid growth at A than at C contained in Table 2-1 are consistent with experimental observations for corner crack growth from aircraft fastener holes [19].

To relate these predictions directly to the condition of crack growth from a rail end bolt hole, it is helpful to convert crack growth rates from inches/cycle to inches/gross ton of traffic. For 33 kip wheel loads, 30.3 load cycles correspond to 10^3 gross tons of traffic. An abbreviated table of crack growth rates in terms of gross tonnage of traffic is given below.

Table 2-2

Crack Growth Rates as Function of Traffic - Summary Table

Crack Dimensions (inches)		Crack Growth Rates (inches/10^6 tons = MGT)	
a	c	da	dc
0.20	0.20	0.18	0.06
0.40	0.20	0.14	0.21
0.40	0.40	0.55	0.16
0.60	0.20	0.08	0.33
0.60	0.40	0.42	0.36
0.60	0.60	0.82	0.39

As a representative example of crack growth from a corner crack at a hole, we consider an initially quarter circular crack of radius 0.2 inch from a cylindrical hole in a plate (t=0.675 inch, R=0.5625 inches) subject to remote tensile loading of magnitude 10 ksi. Using the crack growth law described earlier, $da/dn = 5.12 \times 10^{-12} (\Delta K)^{4.33}$, we predict crack growth resulting in increases of dimensions a and c as shown in Figure 2-3. Crack front geometries at representative points during the fatigue crack growth are shown in Figure 2-4.

To relate the fatigue crack growth rates given in Tables 2-1 and 2-2 and crack sizes shown in Figure 2-3 and 2-4 to actual service conditions, imagine a track which is used for coal transport. Suppose 25 loaded unit trains of 100 cars each traverse the track daily. This corresponds to 10,000 load cycles per day. For that condition, it would require on the order of one month of service* to grow a corner crack of 0.2 inch radius to a through crack at the bolt hole.

The crack shape predictions shown in Figures 2-3 and 2-4 result from the use of the Newman-Raju solution for a crack in a tensile field, and they do neglect the influence of the compressive stress component parallel to the crack direction. The stress field as one moves away from the bolt hole is known to decay more rapidly for the biaxial tension/compression loading case than for the uniaxial tension case. Therefore, we expect that the crack shape will also be influenced by the compressive stress component parallel to the crack direction, and that the actual shape will have larger a/c ratios than predicted here. This effect will become more pronounced as the crack size (relative to the hole radius) increases.

The above analysis was based on the assumption that the wheel load was vertical and concentric with respect to the rail cross section. In actual service conditions, some wheel load eccentricity can be expected and a lateral component of wheel load is likely, particularly on curved track. Preliminary estimates of these effects follow.

---

*One should be cautioned that because of the uncertainties in the actual stress level and the approximation in the calculation of the stress intensity factor, crack growth rates could easily be in error by as much as a factor of 4.

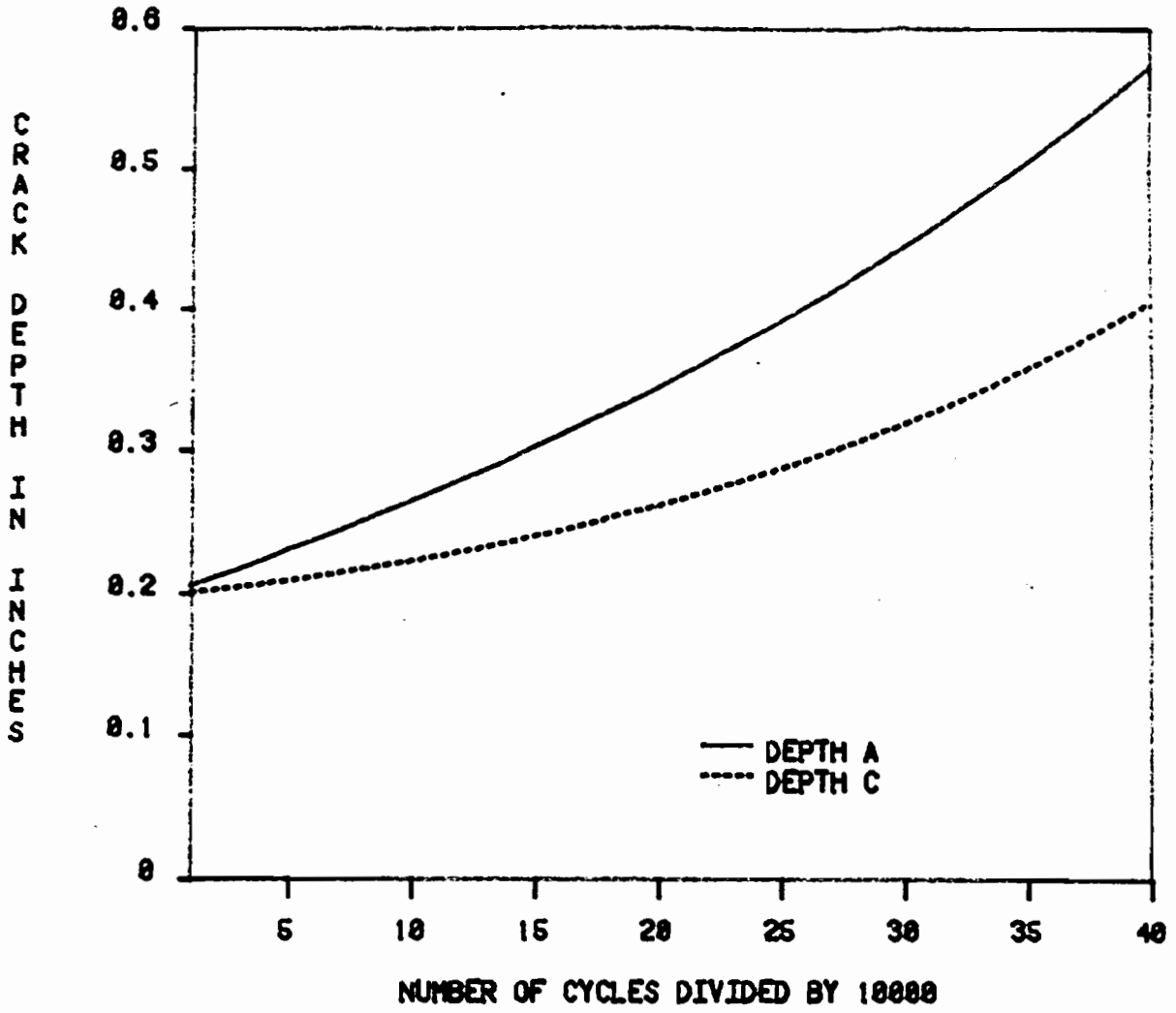

Figure 2-3. Fatigue crack growth of a corner crack with initial dimensions a = 0.2", c = 0.2".

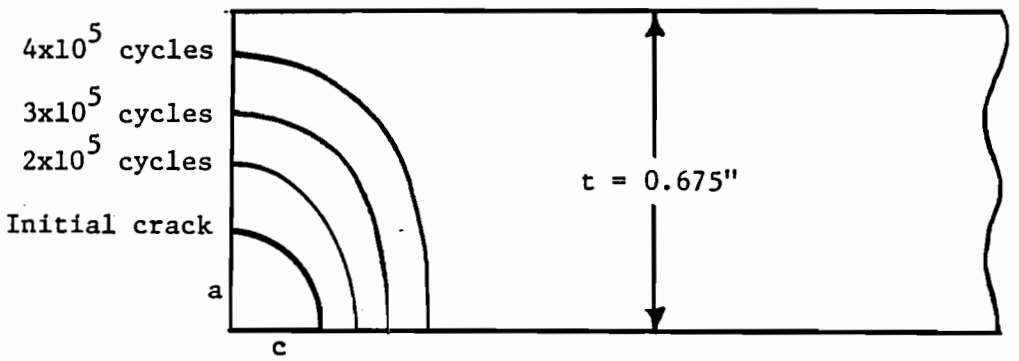

Figure 2-4. Contours showing growth stages of corner crack with initial dimensions a = 0.2", c = 0.2".

2.3 Preliminary Analysis of Lateral and Eccentric Loading Effects

To determine the influence of lateral loads and vertical load eccentricity on corner crack propagation at bolt holes it is necessary to determine the magnitudes and eccentricities of the loads, to analyze the relationship between the applied lateral and eccentric loads and the web stress distribution, and to calculate the variation of the stress intensity factor along the crack front in terms of the stress distribution. We use available information to make estimates for each of these three steps and to predict the level of influence of load eccentricity and lateral forces on crack growth.

Typical wheel load eccentricities are in the range of 0.5 to 1.0 inch for 132 lb/yd rail. Lateral loads can vary over a wide range. A 10 kip lateral load for a 30 kip vertical load is representative of more severe conditions.

Timoshenko and Langer [8] provide analysis methodology and experimental results relating vertical stresses in the rail web to vertical load eccentricity and lateral load magnitude. For 130 lb/yd. rail (similar in cross section to 132 lb/yd. rail), the maximum vertical (bending) stress at the mid-height of the web due to a 10 kip lateral load is approximately 5 ksi. This stress level is significant when compared with the web shear stress (roughly 10 ksi for a 33 kip wheel load on 132 lb/yd. rail) which is believed to drive the bolt hole crack. The maximum vertical bending stress at the center of the web associated with a 30 kip load applied one inch from the symmetry axis is approximately 8 ksi.

To estimate the effect of lateral loads and vertical load eccentricity on the magnitude and direction of the maximum principal stress in the center of the rail web, consider the case where the maximum vertical bending stress is equal to the shear stress of, say, 10 ksi. When comparing this condition to that of central vertical loading only (pure shear at the center of the web), note that the principal stress is increased by a factor of $\left(\frac{1+\sqrt{5}}{2}\right) = 1.62$ and its direction is changed by about 13° as shown in the Mohr circle below:

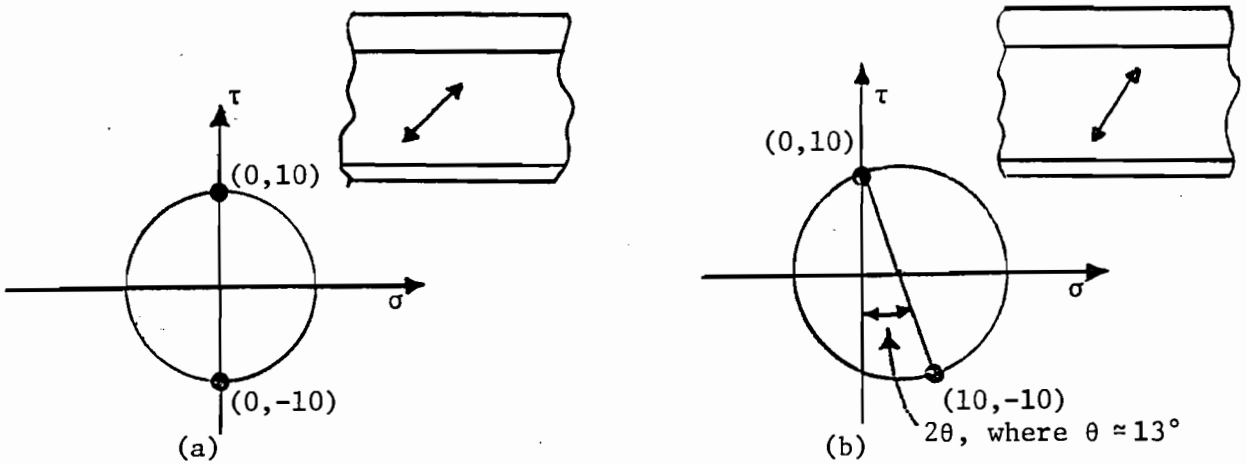

Figure 2-5. Mohr's circle: (a) Pure shear in web. (b) Shear plus bending in web. The orientation of the maximum principal stress is indicated in the insets.

On the opposite side of the web (field or gauge) the vertical bending stress will have the opposite sign and, as a result, the magnitude of the maximum principal stress will be decreased rather than increased, and its direction will be changed in the opposite direction.

These results suggest that crack initiation at a bolt hole is more likely to occur in the presence of transverse bending stresses associated with asymmetric wheel loading, and that it will occur at the intersection of the cylindrical surface of the hole with the planar surface of the web in the form of a corner crack. Presuming that eccentric vertical loading occurs most commonly on the gage side of the rail head, we would expect this corner crack to initiate on the field side of the web.

Finite element stress analysis of rail ends subjected to eccentricity and lateral loading, performed by Battelle [7], yields qualitatively similar results. These analyses include the bolt hole explicitly and results for principal stress along the bolt hole periphery are reported. One inch eccentricity of the vertical load on a 132 lb/yd. rail is found to increase the maximum principal stress at the bolt hole by approximately 60%. Similarly, the application of 10 kips lateral load also causes a 60% increase in maximum principal stress over that due to shear from a 30 kip vertical load. The Timoshenko and Langer paper and the Battelle report are consistent in their predictions for the increase in local bolt hole maximum principal stress due to lateral loads or vertical load eccentricity. In the event that the eccentric vertical and lateral loads occur simultaneously on the same side of the rail head, these stresses tend to cancel each other, whereas they would superpose if the asymmetric loads were on opposite sides of the rail head.

Given that a corner crack may initiate at a bolt hole due to asymmetric wheel loads, we next wish to determine the influence of lateral and eccentric loads on the growth rate and changing crack geometry. To do this we require a solution for the variation of the stress intensity factor for a corner crack at a hole in a plate subjected to combined tensile and bending stresses. The bending loads are applied in such a way that they give rise to a through thickness transition from tension to compression. Kobayashi and Enetanya [20] have presented solutions for corner cracks subjected to tensile and bending loads but not including the influence of the bolt hole. The results are reproduced here in Figures 2-6 and 2-7. We use the Kobayashi and Enetanya solutions to estimate the influence of bending on the variation of the stress intensity factor by comparing tension and bending solutions (recognizing that the absolute values will be in error). For example, assume a corner crack with a=c and a/t = .3 in a remote stress field where the bending stress component increases the maximum stress by 60% as shown below in Figure 2-8. We can then

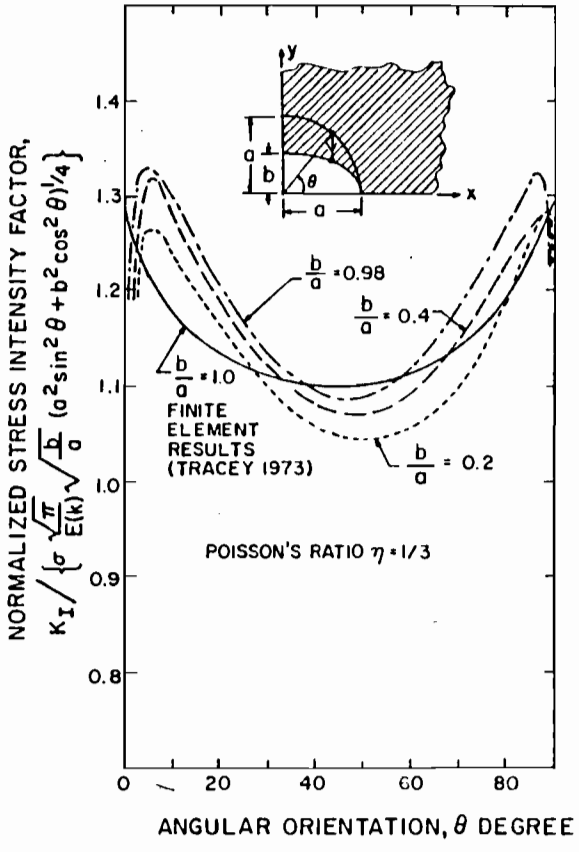

Figure 2-6. Stress Intensity Factors for a Corner Flaw in a Quarter Infinite Solid Subject to Uniaxial Tension σ, from [20].

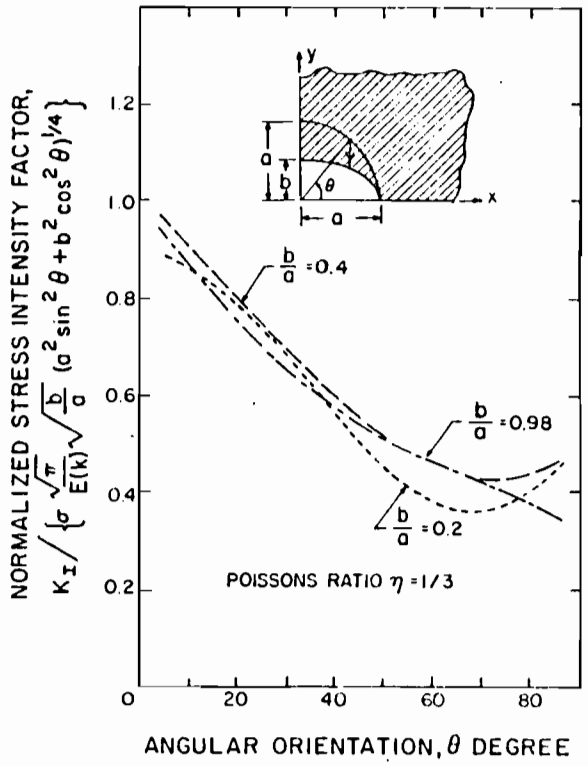

Figure 2-7. Stress Intensity Factors for a Corner Flaw in a Quarter Infinite Solid Subject to Linear Loading = (1-y/b)σ, from [20].

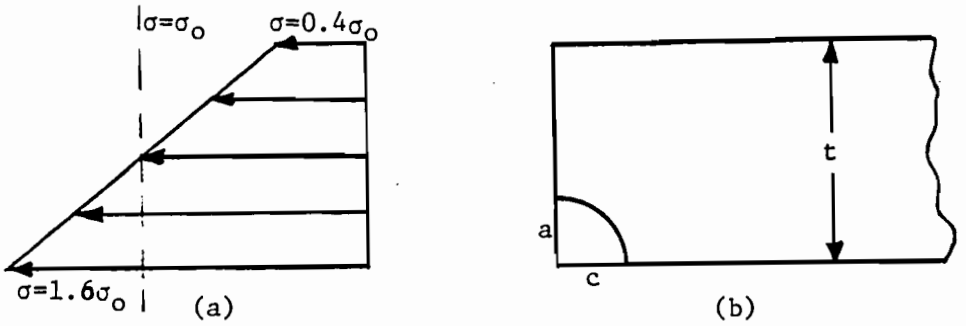

Figure 2-8. Model for combined tension and bending in rail web. (a) Remote tension distribution. (b) Corner crack geometry.

estimate the variation of the stress intensity factor by superposing the results in Figures 2-6 and 2-7 to correspond to Figure 2-8(a):

$$\frac{k}{k_{nom}} = 1.24 + 0.36\ k_b/k_{nom}$$

where k_{nom} is the stress intensity factor associated with the tensile stress solution and k_b is that for the bending case. The resulting variation of the stress intensity factor is indicated in Figure 2-9.

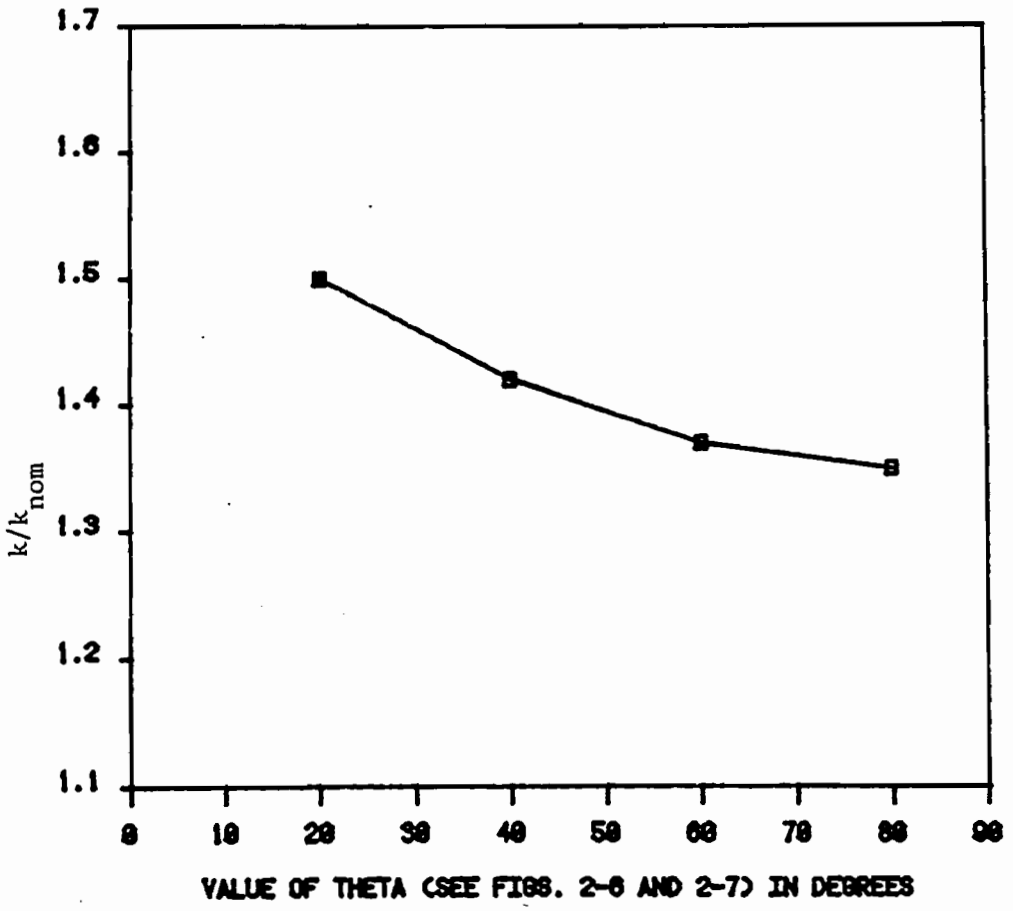

Figure 2-9. Variation of stress intensity factor for combined tension and bending of a corner crack.

These results indicate that the added bending stress increases the stress intensity factor at all points along the periphery of the corner crack considered and that the increase varies mildly along the crack front with a maximum at the plate surface. Based on these results, we would expect earlier crack initiation and more rapid growth of corner cracks at bolt holes as a result of asymmetric wheel loads. This effect will be mitigated as the crack grows deeper through the rail web thickness, away from the high bending stresses due to asymmetric loading.

3. ENGINEERING ANALYSES FOR RAIL END BOLT HOLE CRACKS

3.0 Review of Earlier Report

Our previous study [5] focused on fatigue crack growth of through-thickness bolt-hole cracks. The theory of a beam on an elastic foundation was used to determine the shear stress prevailing in the rail web near the bolt hole, and this stress was in turn used to calculate the Mode I stress intensity factor at the tip of a bolt hole crack, oriented as in Figure 1-2, as a function of crack length. While increasing crack length tends to increase the stress intensity factor, the reduction in shear stress away from the neutral axis and proximity of a longer crack to the rail head lead one to conclude that the stress intensity factor at the tip of a bolt hole crack may either be constant or decrease slightly with length.

An experimental program was also undertaken to assess fatigue crack growth rates from rail end bolt holes. Symmetrical three-point bending was applied to 36 in. sections of 136 lb/yd. rail in which bolt holes had been drilled and prenotched. Growth rates were converted to stress intensity factors, which were found to be virtually constant for crack lengths ranging from ½ to 2½ inches. From these data, the gross tonnage required to grow a crack one inch was determined to be 6.2 MGT (million gross tons), based on wheel loads of 33 kips. Because of the apparent constancy of stress intensity factors over a wide range of crack lengths, it was concluded that a critical crack size would not precipitate a fracture so much as a critical load, perhaps from a wheel flat. If the crack extends well into the rail head, however, the analysis to be presented in Section 3.4 will indicate that rail fracture is imminent under ordinary loadings.

The experiments performed in [5] also serve as a guide to design of a loading fixture to determine the breaking strength of rails containing defects. This design is discussed in Appendix B of the present report.

3.1 Introduction

The previous chapters have focused on bolt hole crack initiation and the early stages of growth. For these analyses, the assumption that the bolt hole is essentially acted upon by a uniform shear field is reasonable since the flaw sizes considered are much less than the hole diameter. For longer cracks, however, the crack tip extends beyond the local bolt hole region; stresses and crack driving forces may be drastically affected by the change in cross section associated with the rail head.

The studies of Johns, Sampath, Bell, and Davies [7] have addressed the issue of longer cracks by applying two-dimensional finite element analyses to several configurations of bolt hole cracks with lengths up to and exceeding three inches. The emphasis in this chapter is on solutions for stress intensity factors of bolt hole cracks which extend upwards from the bolt hole away from the rail end. Part of the methodology needed to accomplish this is discussed in Section 3.3 where the shear stress distribution over the entire rail cross section is obtained for a particular loading. This solution is available for use in the analyses of Section 3.4, which examines bolt hole cracks that extend up to the head and then proceed to grow along it or into it. Section 3.5 presents a three-dimentional finite element analysis of a bolt hole crack which extends up to the head-web interface.

First, however, Section 3.2 addresses the influence on cracking of bolt bearing on the bolt hole, which gives rise to a stress field that is primarily longitudinal tension, in contrast to the bending and shear loadings which are the focus of most of the rest of this chapter.

3.2 The Effects of Bolt Bearing

Completely apart from the severe static and dynamic loads which a train may impose on a bolted joint, temperature variations can set up high axial stresses in railroad rails. In the case of jointed track, contraction of the rails in cold weather frequently causes the bolts

which secure the joint bars to bear on the rail end side of the rail bolt holes, and tensile stresses arise in the rail. High stresses local to the bolt hole are also present, as reported in [25]. This section aims to provide a conservative approach to deriving stress intensity factors for bolt hole cracks when bolt bearing is important. We focus on the most frequently observed crack orientation, viz. that which leads away from the rail end toward the head at roughly 45° from horizontal. The results in reference [26] suggest that when the bearing bolts set up tensile stresses, cracks growing toward the rail end are less favored than those which grow away from it.

The stress intensity factors here are obtained by direct application of the numerical solution in [26] for a load applied via cosine bearing to a row of three fastener holes, the middle of which is cracked. The geometry from which solutions are actually taken is shown in Figure 3-1. Since free boundaries are closer to the hole in Figure 3-1 than they are in the actual rail, it is expected that the solution from [26] leads to conservative (high) values of the stress intensity factor. Results here are only given for three crack lengths, but comparison to other geometries for which more results are furnished in [26] indicates that the range of K values in Table 3-1 is representative, and that variations in K are relatively smooth.

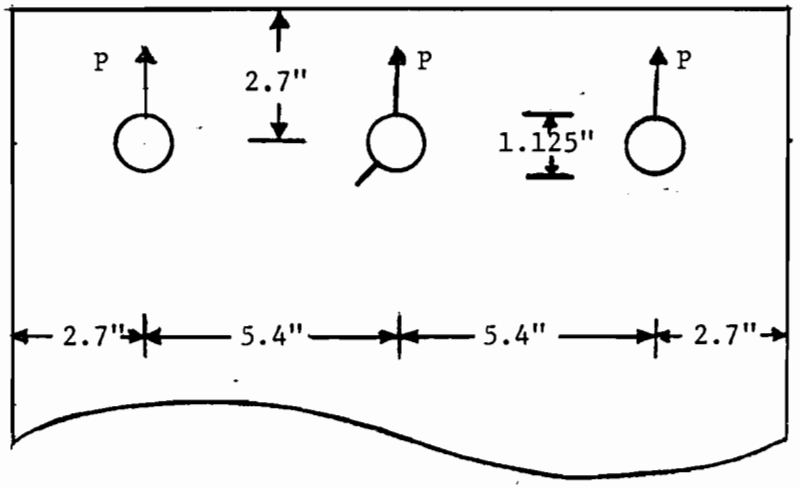

Figure 3-1. Model Configuration Used to Analyze the Effect of Bolt Bearing

Table 3-1. Stress Intensity Factors in ksi $\sqrt{in}$ for Figure 3-1 with P = 52 kips

Crack Length in Inches:	0.09	0.36	0.63
K_I	13.8	15.8	14.8
K_{II}	7.6	17.9	13.5

Table 3-1 shows values of K_I and K_{II}, derived from [26], for a web thickness of 0.75 inches and a hole diameter of 1.125 inches when the axial load in the rail due to bolt bearing is 52 kips. This load figure is determined as follows. Assume a worst case temperature change of $\Delta T = -100°F$. The corresponding stress in the rail is $\sigma = E(\varepsilon - \alpha\Delta T)$, where ε is the (negative) strain that the rail can accommodate without any stress. Young's modulus is denoted by E and the coefficient of thermal expansion by α. Assuming a gap of 0.0625 inches between bolt and bolt hole when no loads are present, and accounting for this space at both ends of a rail 468 inches long, we find $\varepsilon = -2.67 \times 10^{-4}$. For rail steel, $\alpha = 6.50 \times 10^{-6}/°F$, so that $\varepsilon - \alpha\Delta T = 3.83 \times 10^{-4}$. For $E = 3 \times 10^7$ psi, $\sigma = 11.5$ ksi. In a 136 lb/yd rail, this corresponds to a load of 154 kips. Joint tests in tension [25] indicate that from 70 to 85 percent of this load is carried by the two bolt holes farthest from the rail end, but we choose to assume that one-third of this load is borne by the first bolt hole in a worst case scenario. Thus the load used in arriving at the stress intensity factors in Table 3-1 is 52 kips.

The main effect contributing to stress intensity factors locally greater than these is the appreciable nonuniformity of bolt bearing through the web thickness. It is felt, however, that the above analysis is still conservative. We have assumed infinitely stiff bolts and joint bars, but in reality these give a little, reducing tensile stresses in the rail. Also, to the extent that the ties and ballast resist contraction of the rail, the stresses will be diminished further. These adjustments, together with the infrequency of extreme cold as compared to train passages, suggest that while the

stress intensity factors shown in Table 3-1 are certainly comparable to those in Table 2-1, they probably do not contribute a significant number of severe load cycles.

3.3 Shear Stresses in the Rail Cross Section

In an earlier report [5], the vertical shear stress distribution arising from the beam theory shear force was calculated as a function of distance from the neutral axis. The calculated distribution is expected to apply along the rail centerline, but the geometry of the rail cross section leads to a more complex shear stress field away from the centerline, particularly near the head-web and web-base fillets. The stress state in the region of the head-web fillet is of special importance in the present study as it is expected to affect the tendency of long bolt hole cracks to grow outward to the edges of the head.

The work of Johns, Sampath, Bell and Davies [7] includes three-dimensional finite element analyses of a section of rail symmetric about a concentrated wheel load. While their results furnish important information on longitudinal stress variations due to local load effects, the shear stress components which they calculate do not appear to satisfy traction-free boundary conditions in the region of the head-web fillet. The aim of the work described in this section is to provide an accurate analysis of shear stresses through the rail cross section for a particular load configuration. While the stresses obtained are rigorously valid only for a resultant shear force that is constant along the rail length, they do provide insight as to the precise nature of the shear stress field over the rail cross section, especially to the extent that this field is affected by the sinuous traction-free boundary.

The approach followed here derives from an analysis for bending of bars presented in Timoshenko and Goodier [27]. The problem for which an elasticity solution will be calculated is shown schematically in Figure 3-2. Note that the shear force is constant over the length of the beam. The shear stress field obtained is valid over the entire length shown provided that the concentrated loads are distributed in a

manner consistent with the solution. Although this is not expected to be true for wheel and joint bar loads on a rail, St. Venant's principle implies that the solution obtained will be accurate a reasonable distance away from the applied loads.

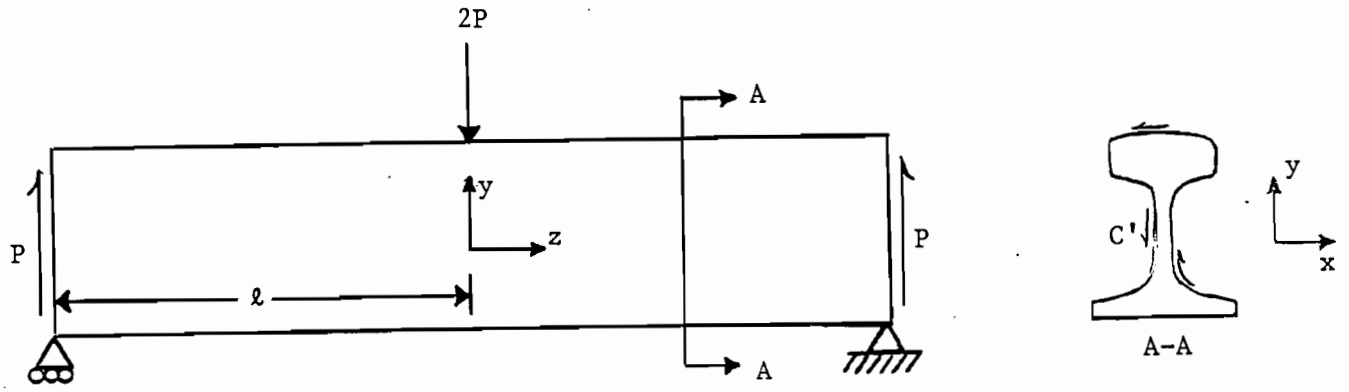

Figure 3-2. Model Problem Solved in Section 3.3

A semi-inverse method is employed to seek an elasticity solution for Figure 3-2. We hypothesize a solution which includes the following stresses:

$$\sigma_{xx} = \sigma_{yy} = \sigma_{xy} = 0 \tag{3.1a}$$

$$\sigma_{zz} = \frac{My}{I} = \frac{P(\ell - |z|)y}{I} \tag{3.1b}$$

Here M is the bending moment and I is the bar moment of inertia. The stress equilibrium equations (excluding body forces) in conjunction with (3.1) imply the following:

$$\frac{\partial \sigma_{xz}}{\partial z} = \frac{\partial \sigma_{yz}}{\partial z} = 0 \tag{3.2a}$$

$$\frac{\partial \sigma_{xz}}{\partial x} + \frac{\partial \sigma_{yz}}{\partial y} = \frac{Py}{I} \tag{3.2b}$$

Attention has been confined, without loss, to the portion of the bar $z > 0$. According to (3.2a), the nonzero shear stresses are, like the transverse shear force, independent of axial position. Since the intention is to solve directly for the variation of these stresses with respect to x and y, the equations of stress compatibility are needed. Only two of the six compatibility equations are nontrivial for the hypotheses (3.1). These two are

$$(1+\nu)\ \nabla^2 \sigma_{yz} + \frac{\partial^2 (\sigma_{xx} + \sigma_{yy} + \sigma_{zz})}{\partial y \partial z} = 0 \tag{3.3a}$$

$$(1+\nu)\ \nabla^2 \sigma_{xz} + \frac{\partial^2 (\sigma_{xx} + \sigma_{yy} + \sigma_{zz})}{\partial z \partial x} = 0, \tag{3.3b}$$

which imply

$$\nabla^2 \sigma_{yz} = \frac{P}{I(1+\nu)} \tag{3.4a}$$

$$\nabla^2 \sigma_{xz} = 0. \tag{3.4b}$$

The only nontrivial boundary condition is

$$\sigma_{xz}\, n_x + \sigma_{yz}\, n_y = 0 \tag{3.5}$$

which applies over the entire lateral surface area of the bar; i.e., all the surface area for which $n_z = 0$. The vector $\underset{\sim}{n}$ is the outward unit normal to the bar surface. The boundary value problem may now be stated

as follows: Equations (3.2) and (3.4) need to be solved over the section A-A in Figure 3-2, subject to (3.5) on the contour C'.

If we introduce a stress function ϕ such that

$$\sigma_{xz} = \frac{\partial \phi}{\partial y} \tag{3.6a}$$

$$\sigma_{yz} = -\frac{\partial \phi}{\partial x} + \frac{Py^2}{2I} + f(x), \tag{3.6b}$$

equation (3.2b) is satisfied identically. The function $f(x)$ is arbitrary at this point. Insertion of (3.6) into (3.4) implies

$$\frac{\partial}{\partial y}(\nabla^2 \phi) = 0 \tag{3.7a}$$

$$\frac{\partial}{\partial x}(\nabla^2 \phi) = \frac{P\nu}{I(1+\nu)} + f''(x) \tag{3.7b}$$

We now make the choice $f(x) = -P\nu x^2/(2I(1+\nu))$ which implies $\nabla^2 \phi =$ constant. For cross sections like the rail, which are symmetrical about the y-axis, this constant can be shown to vanish; it is related to an average value of rotation in the x-y plane, which is clearly zero for the symmetrical loading considered here.

The boundary conditions (3.5) become, in terms of ϕ,

$$\frac{d\phi}{ds} = \left[\frac{Py^2}{2I} - \frac{P\nu x^2}{2I(1+\nu)}\right]\frac{\partial x}{\partial s} \quad \text{on } C' \tag{3.8}$$

where we have used $n_x = \partial y/\partial s$ and $n_y = -\partial x/\partial s$, and s denotes arc length along C'. Equation (3.8) may be rewritten

$$d\phi = \frac{Py^2}{2I}\,dx - d\left(\frac{P\nu x^3}{6I(1+\nu)}\right), \tag{3.9}$$

from which we find $\int_{C'} d\phi = (P/2I)\int_{C'} y^2 dx$. But $\int_{C'} y^2 dx = -\int_{C'} y^2 n_y ds = -\int_{C'} 2ydxdy = -\int_{C'} ydA = 0$ when y is measured from the neutral axis of the cross section. Therefore ϕ is single-valued on the boundary. Equation (3.9) allows for an arbitrary constant in ϕ, which does not affect the stresses (3.6). We therefore choose $\phi = 0$ on $x = 0$, and note that this makes ϕ an odd function of y. We now have reduced the boundary value problem to

$$\nabla^2\phi = 0 \text{ in R subject to} \tag{3.10a}$$

$$\phi(s) = \frac{P}{2I}\int_o^s y^2 dx - \frac{P\nu x^3}{6I(1+\nu)} \quad \text{on C,} \tag{3.10b}$$

where R and C are shown schematically in Figure 3-3.

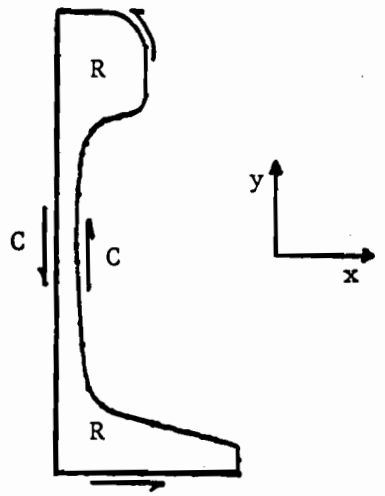

Figure 3-3. Region R and contour C for the boundary value problem (3.10).

The system (3.10) is solved here by a finite element method derived as follows. The functional

$$J = \frac{1}{2} \int_R \left[\left(\frac{\partial \phi}{\partial x} \right)^2 + \left(\frac{\partial \phi}{\partial y} \right)^2 \right] dA \qquad (3.11)$$

is minimized subject to the essential boundary conditions (3.10b) by making use of the variational principle $\delta J = 0$. This principle implies

$$\int_R \left[\frac{\partial \phi}{\partial x} \frac{\partial \delta \phi}{\partial x} + \frac{\partial \phi}{\partial y} \frac{\partial \delta \phi}{\partial y} \right] dA = 0. \qquad (3.12)$$

from which finite element stiffness equations are derived in the usual fashion. The actual finite element grid, which consists of 52 nine-node isoparametric quadrilaterals and 201 degrees of freedom, models only half the rail due to symmetry considerations along the rail centerline. When the mesh is reflected through this centerline, it appears as in Figure 3-4.

The boundary conditions (3.10b) must be evaluated to obtain values of ϕ at the boundary nodal points before the stiffness equations arising from (3.12) can be solved. Each element side on the boundary connects three nodes. The integral $\int y^2 dx$ must be evaluated from the first node to the second, and from the second node to the third. The coordinates along such a boundary segment are expressed in terms of shape functions as

$$x = \sum_1^3 x_i N_i(s), \quad y = \sum_1^3 y_i N_i(s) \qquad (3.13)$$

where x_i and y_i for $i = 1,2,3$ represent Cartesian coordinates of the three boundary nodes in question. The shape functions are given by

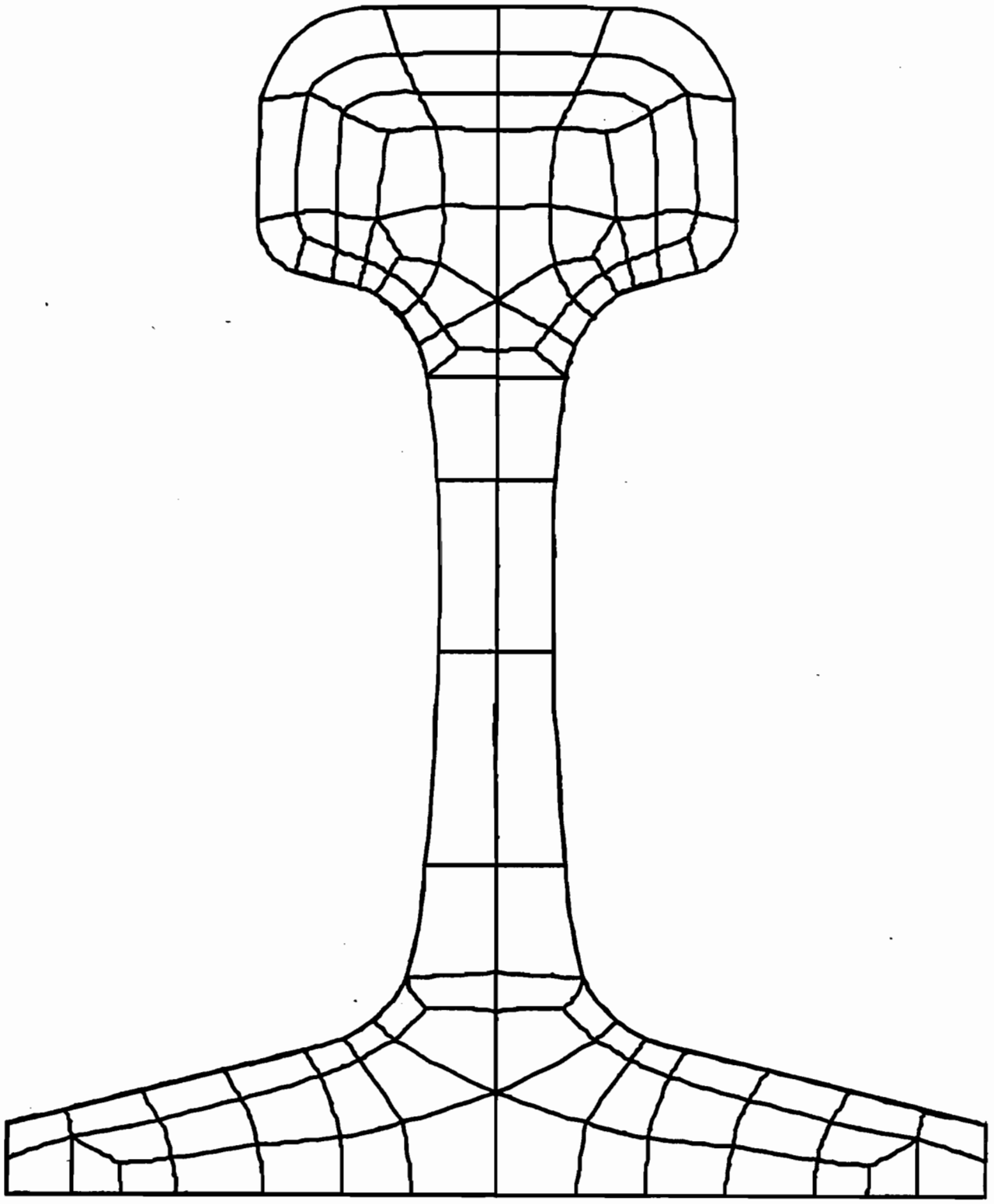

Figure 3-4. Finite element mesh used for modeling (3.10).

$$N_1 = \frac{1}{2}\, s(s-1), \quad N_2 = (1-s^2), \quad N_3 = \frac{1}{2}\, s(s+1). \tag{3.14}$$

Thus the integrals to be evaluated are

$$\int_{\text{First node}}^{\text{Second node}} y^2 dx = \int_{-1}^{0} \left(\sum_{1}^{3} y_i N_i \right)^2 \left(\sum_{1}^{3} x_i N_i' \right) ds \tag{3.15a}$$

$$\int_{\text{Second node}}^{\text{Third node}} y^2 dx = \int_{0}^{1} \left(\sum_{1}^{3} y_i N_i \right)^2 \left(\sum_{1}^{3} x_i N_i' \right) ds \tag{3.15b}$$

These integrals over the variable s were evaluated analytically; the value of (3.10b) was then obtained at each boundary node in terms of boundary node coordinates. The finite element equations were then solved in the usual fashion using a skyline matrix solver.

Since the finite element solution gives only the stress function ϕ, a small amount of postprocessing is required to obtain the shear stresses based on (3.6). Derivatives of ϕ are most accurate at the quadrature points (nine in each element) used in integrating (3.12) over R. Stresses were first obtained at these quadrature points, and then a projection method based on the work of Chavez [28] was used to calculate stresses at the nodes. These nodal values were used to produce contour plots of σ_{xz} and σ_{yz} which are furnished in Figures 3-5 and 3-6. The contour levels give stresses in ksi for a P value of 31.7 kips, the constant shear force in the bar. This value of shear force is typical of that which prevails at the first bolt hole immediately after a wheel

CONTOUR VALUES

1 ---	-2.000
2 ---	-1.500
3 ---	-1.000
4 ---	-0.500
5 ---	0.000
6 ---	0.500
7 ---	1.000
8 ---	1.500
9 ---	2.000
10 --	2.500

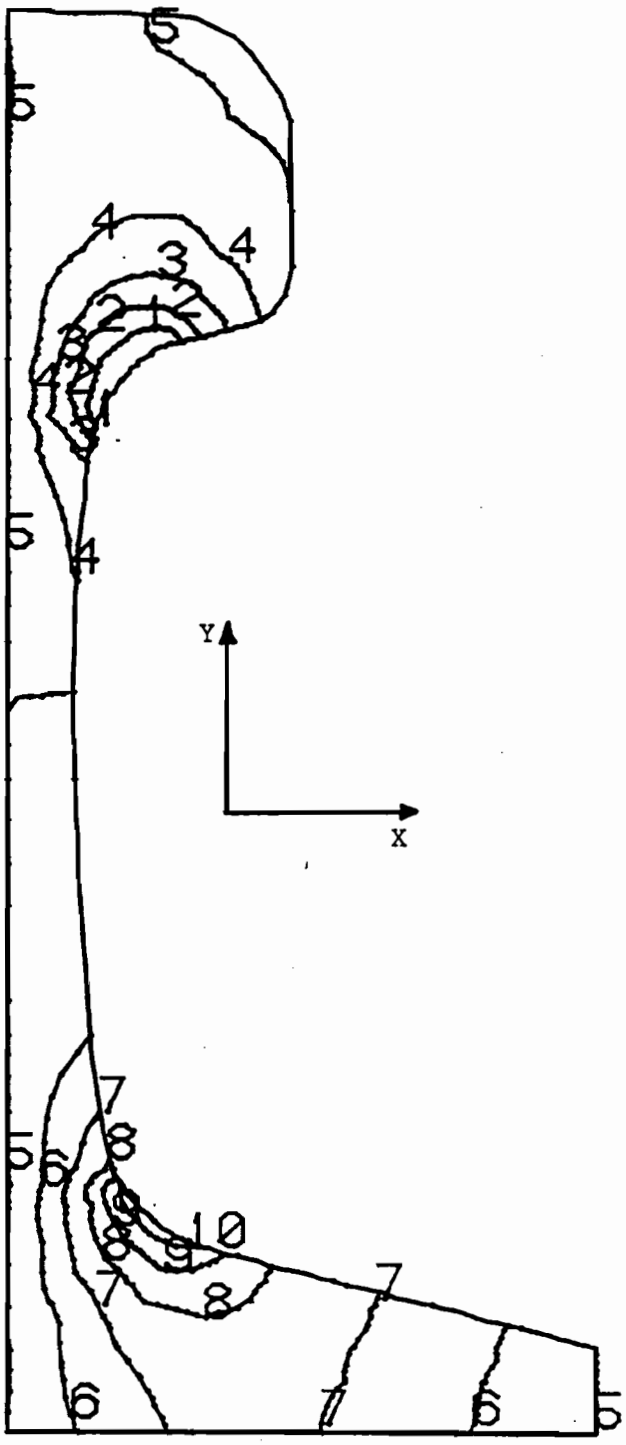

Figure 3-5. Contour levels of σ_{xz} when P = 31.7 kips.

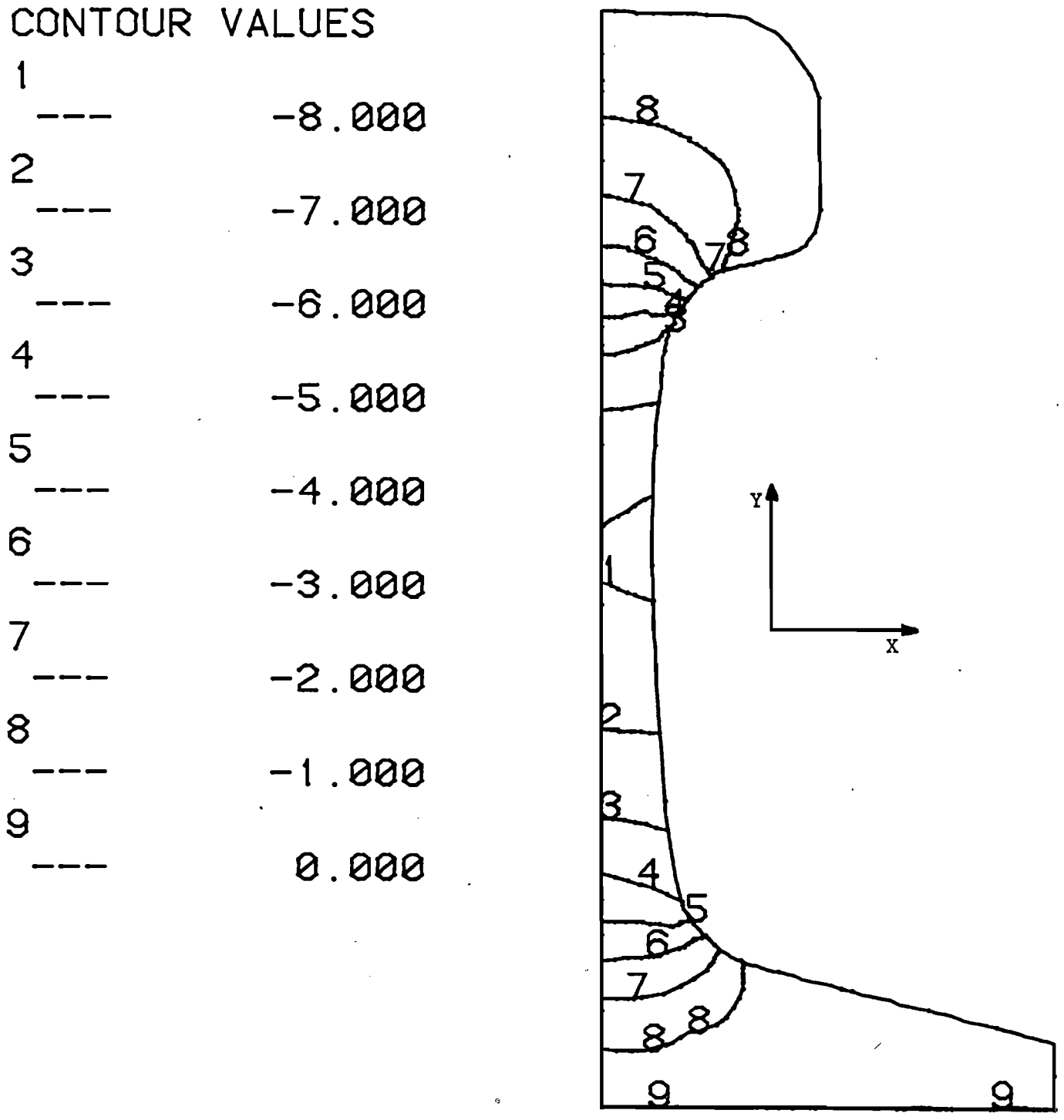

Figure 3-6. Contour levels of σ_{yz} when P = 31.7 kips.

has passed. Shear stresses at other levels of shear force may readily be obtained by scaling Figures 3-5 and 3-6 accordingly.

Figure 3-5 shows that σ_{xz} nearly vanishes over much of the cross section except at the head-web and web-base fillets. Both σ_{xz} and σ_{yz} are quite small in the outer portions of the head and base so it is expected that the most important stresses in these portions of the rail are axial stresses due to bending and residual stress effects. Figure 3-6 shows that the vertical shear stress is highest in the web as beam theory predicts. Figure 3-7 shows a favorable comparison of vertical shear stress along the rail centerline as computed here and by simple beam theory in reference [5]. Clearly, the important deviations from beam theory occur away from the centerline of the rail.

It is worth noting that Figures 3-5 and 3-6 are precisely consistent with traction-free boundaries around the periphery of the rail cross section. Since such a great portion of the rail cross section is so close to a free boundary, the shear distributions in Figures 3-5 and 3-6 are expected to be nearly correct for portions of an actual rail which are far enough away from the effects of concentrated wheel loads. The magnitude of the shear stresses is governed by the shear force at the particular cross section.

The results in this section will prove helpful in what follows for assessing the tendency of long bolt hole cracks to grow outward through the rail head.

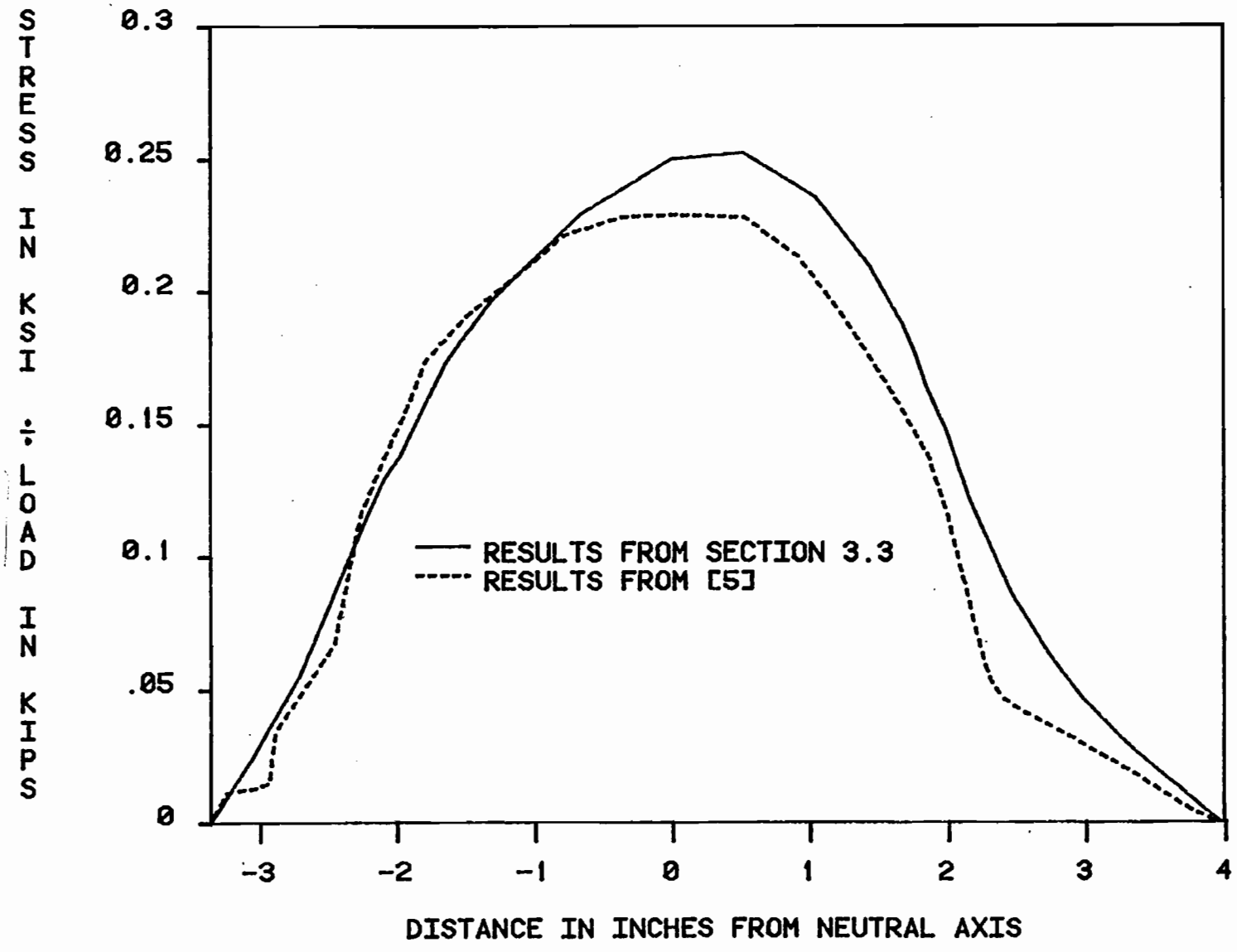

Figure 3-7. Vertical shear stress, normalized by load, along the rail centerline.

3.4 Cracks Extending Into the Rail Head

In Section 2.2, the rail web was idealized as an infinite plate in order to assess crack behavior local to the bolt hole. As bolt hole cracks grow longer than one or two hole diameters, however, the idealization of the web as an infinite plane becomes less appropriate. The presence of the head can significantly reduce stress intensity factors, by virtue of changes in both cross-sectional geometry and stress distribution. If and as growth proceeds into the rail head, the higher axial tension, due to residual stresses and head-on-web effects, may provide renewed driving force to the crack in question.

To address these issues, we will first consider the calculation of stress states in the rail apart from the presence of cracks. These stress fields include global rail stresses due to bending, shear, and residual stress. Local to the rail head, additional bending and shear from head-on-web influences are important, and the complex stress state near the head-web fillet will be considered as well. These stress distributions will then be used in conjunction with fracture mechanics analysis to determine the stress intensity factors for a variety of crack configurations, including a crack along the head-web interface, a 45° crack growing into the head, and a crack which kinks from its 45° orientation in the web to grow vertically through the head. These idealizations, which treat the crack as having uniform length through the rail thickness, are depicted in Figure 3-8. Also shown in Figure 3-8 is a projection of the rail cross section which indicates a more plausible crack shape. This idealization will be used with the fillet stress calculations of Section 3.3 to approximate stress intensity factors away from the central part of the web, as opposed to the other idealizations, which correspond more closely to the situation at the deepest point of the crack.

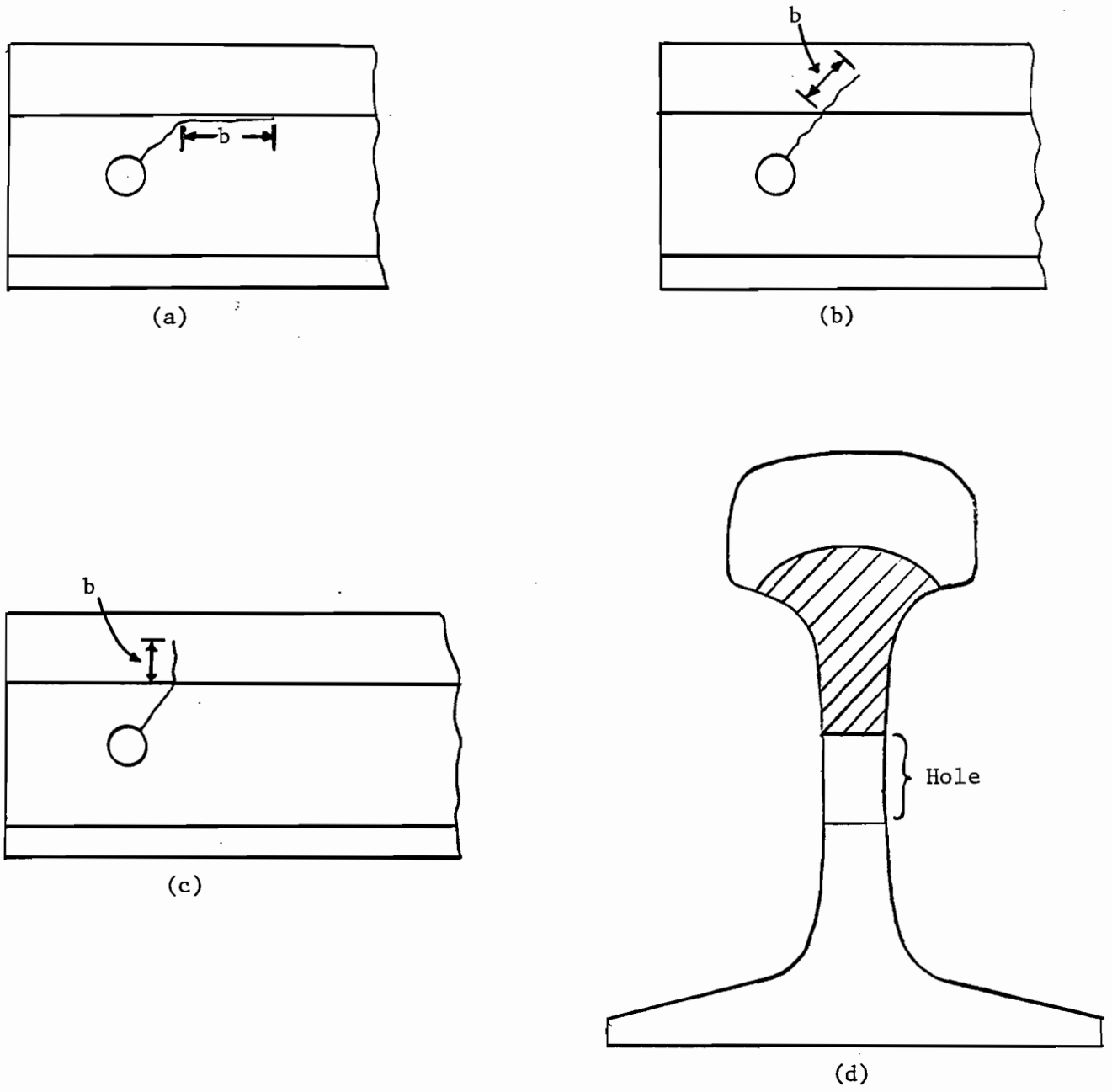

Figure 3-8. Schematics showing geometries of long bolt hole cracks.

Stresses in the Rail

Using the idealization of a semi-infinite beam on an elastic foundation, one may calculate moment and shear force for the rail end. Shear force calculations which include joint bar reactions [5] indicate that, for a joint having 75% efficiency, the maximum shear force seen at the first bolt hole is slightly less than W, the wheel load. This maximum shear occurs when the wheel is over the joint, and decays as the wheel travels farther from the rail end. Thus a conservative value for use as a shear force is W per wheel.

The bending moment in the rail gives rise to longitudinal stresses. The value of bending moment used here will consist of contributions from joint bar reactions and wheel load, W. The arrangement of these loads is shown in Figure 3-9. For a 75% efficient joint, a typical joint bar reaction force is 0.75W. These two reaction forces give a positive bending moment in the bolt hole region which does not exceed $W/8\beta$, where $\beta = (u/4EI)^{1/4}$ is calculated from the foundation stiffness u, Young's modulus E, and rail moment of inertia I. The wheel load itself would give rise to a maximum moment of $W/4\beta$ in an infinite rail, but this contribution is reduced considerably in a semi-infinite rail due to the free end, where the bolt holes are located. In fact, for a typical rail, the moment due to the wheel alone will not exceed $W/16\beta$ in the bolt hole region. Thus a bending moment value of $(W/8\beta + W/16\beta) = 3W/16\beta$ provides a conservative value for the fracture mechanics analysis.

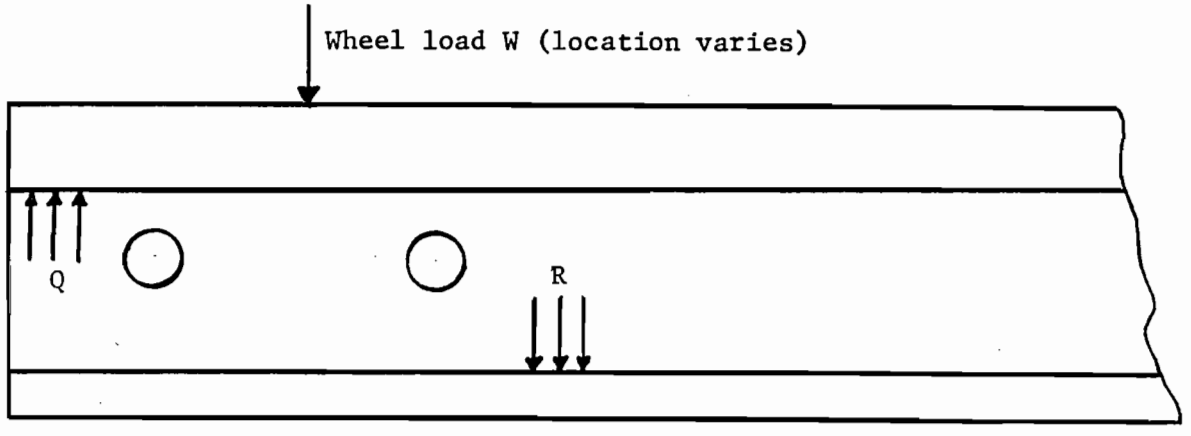

Figure 3-9. Loading system at rail end, including wheel load and joint bar forces.

In addition to global bending and shear, local bending and shear stresses are induced under the wheel due to the head-on-web effect, discussed in [8]. The web is taken to provide an elastic foundation $u_w = Et/d$ to the head, where t is the web thickness and d is the web height. Because the web foundation is much stiffer (relative to the moment of inertia of what it supports) than the ballast and the foundation, the free end does not significantly reduce the maximum head-on-web bending moment from its value for a continuous infinite rail head. Thus the head-on-web axial stresses may be obtained from a bending moment of $W/4\beta_w$, where

$$\beta w = 4 \sqrt{\frac{t}{4 I_H d}}$$

and I_H is an appropriate moment of inertia for the rail head. The actual axial stresses may be somewhat lower due to the high axial stiffness of the web, but this effect is neglected here. The shear stresses in head-on-web bending can be idealized by the parabolic distribution that prevails in a rectangular cross section. The magnitude of the maximum shear force in the head is thus W/2; the sign depends on whether or not the wheel has passed the point in question.

Also of interest is the complex stress state that exists at the head-web fillet. This stress state was calculated, for the case of constant shear along the rail, in Section 3.3. These results were taken to be a reasonable approximation to the distribution of shear stresses through the rail cross section in the problem at hand.

Parameters employed in order to make use of the above analysis will be as follows:

W = 33 kips
u = 2000 psi
I = 94.9 in^4 (136 lb/yd rail)
E = 30 x 10^6 psi

For head-on-web effects, we use the following, also based on 136 lb/yd. rail. Web height is taken as 4.19 inches, and web thickness (an average value) is taken as 0.8 inches. Thus u_w = 5728 ksi. The moment of inertia I_H, based on a head thickness of 2.94 inches and an average head height of 1.56 inches, is I_H = 0.93 in. Thus β_w = 0.476 reciprocal inches, and $\beta_w > 20\beta$, as suggested earlier.

Fracture Mechanics Analyses

The analyses described here for the crack geometries shown in Figure 3-8 are based on solutions to a variety of finite crack problems. Since attention is focused on the end of the crack near or in the rail head, the bolt hole from which the cracks originate will be idealized as the opposite end of a finite crack of appropriate length. This opens a wider range of stress intensity factor solutions for application to the rail. To find an equivalent length for the crack emanating from the hole, we focus on a crack which extends up to the head-web boundary. This crack has a length outside the hole of $(2.03\sqrt{2} - 0.5) = 2.37$ in. Under a remote shear stress field, the stress intensity factor at the end of this crack has the same stress intensity factor as a flat crack of length ℓ = 3.2 inches [16]. (See the comparison in Figure 3-10). This crack length will be used subsequently as the the effective length of the portion of the crack that has not entered the head.

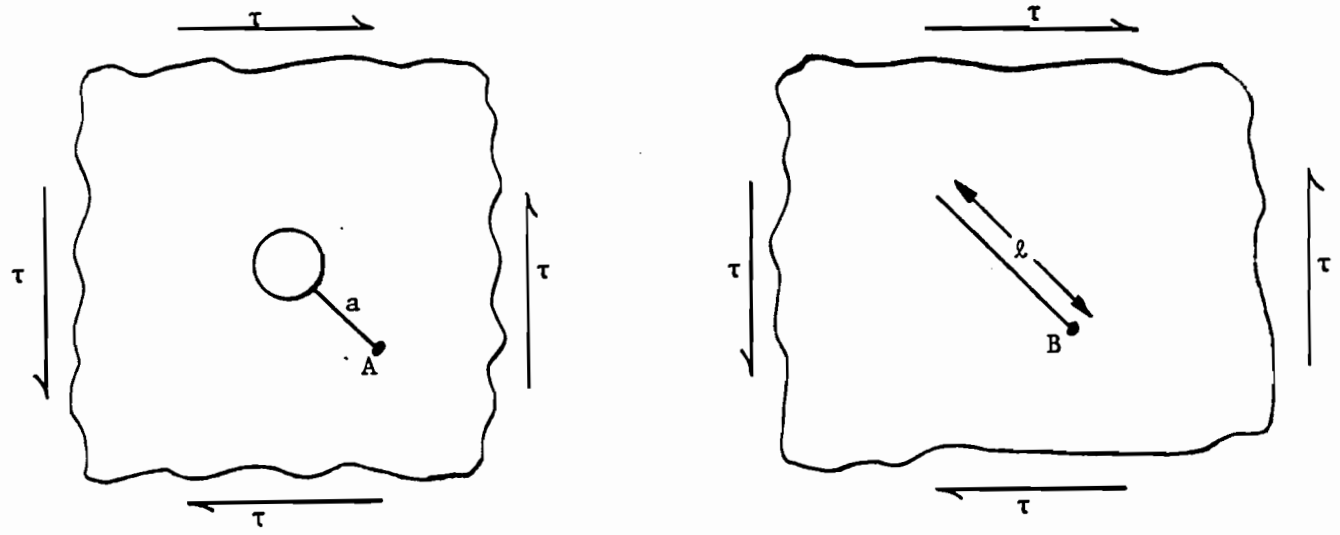

Figure 3-10. Sketch of methodology for assigning equivalent crack length ℓ to crack of length a emanating from bolt hole.

The stress intensity factors K_I and K_{II} are now calculated for various kink lengths b in Figure 3-8(a). With b=0, and before the crack has actually kinked, the shear force in the rail, W, gives rise to shear stresses tending to open the crack in Mode I, provided the wheel is past the bolt hole. Figure 3-7 has shown the rapid decrease of this shear stress away from the rail neutral axis. For the purposes of calculating a stress intensity factor, a shear stress value of W x 0.2 in^{-2}, or 6.6 ksi, is chosen. This is 20% less than the maximum shear stress, but greater than that which applies near the head; see Figure 3-6. The axial stresses from the bending moment are obtained from the usual beam theory formula applied to the moment $3W/16\beta$. With the distance from the crack tip to the neutral axis taken to be 2.0 inches, the maximum axial stress is $3W/8\beta I$ = 6.5 ksi. Superposing the solutions for a slant crack (with length ℓ = 3.2 inches) in an infinite plate and a flat crack under remote shear [16], one may obtain K_I and K_{II} for b = 0. These solutions are modified, however, for the proximity of the thicker head. The reducing factor F = 0.8 is obtained from the work of Yang et. al. [29] who measured fatigue crack growth in a plate with an abrupt change in thickness. The stress intensity factors for b = 0, then, are

$$K_I = (0.8)\ [6.6\sqrt{\pi(1.6)} + 6.5\ \sin^2(\pi/4)\sqrt{\pi(1.6)}] = 17.7\ \text{ksi}\sqrt{\text{in}},$$

$$K_{II} = (0.8)\ [6.5\ (\sin\pi/4)\ (\cos\pi/4)\sqrt{\pi(1.6)}] = 5.8\ \text{ksi}\sqrt{\text{in.}}$$

As soon as the crack kinks, the stress intensity factors change abruptly. With b still effectively equal to 0, the immediate effect of a 45° branch (along the head-web boundary) is to produce

$$K_I = (.79)(17.7) + (.98)(5.8) = 19.7\ \text{ksi}\sqrt{\text{in.}}$$

$$K_{II} = (-.33)(17.7) + (.52)(5.8) = -2.8\ \text{ksi}\sqrt{\text{in.}}$$

These adjustments are obtained from Suresh [30], who references Rice and Cotterell [31], and they are included in Table 3-2.

Table 3-2. Stress Intensity Factors for the Crack in Figure 3-8(a).

b(inches)	K_I(ksi$\sqrt{in}$)	K_{II}(ksi$\sqrt{in}$)	K (ksi$\sqrt{in}$)
0-	17.7	5.8	18.6
0+	19.7	-2.8	19.9
.32	7.8	-6.2	10.0
.64	7.6	-7.2	10.5
1.28	7.7	-8.1	11.2
1.92	8.0	-8.9	12.0
2.56	8.4	-9.4	12.6
3.20	8.8	-9.9	13.2
4.80	9.8	-10.9	14.7
6.40	10.5	-11.6	15.6

As b grows larger, we expect the significance of the axial stress field to decrease. Since the kink solutions used in the previous paragraph [31] are exact only as $b \to 0$, it is difficult to quantify how rapidly this decrease occurs. The results of Kitagawa et al [32] on bent cracks are used to derive stress intensity factors for various positive values of b, with the axial stress field neglected. The stress intensity factors $K_I(b)$ and $K_{II}(b)$ are obtained by multiplying the factors F_{1B} and F_{2B} from [32] by the quantity $(0.8)\ \sigma\sqrt{\pi(\ell+b\cos\theta)/2}$. Here θ is the kink angle, the 0.8 factor remains due to the presence of the head, ℓ is 3.2 inches as before, and σ is 6.6 ksi from the shear stress field. The results are shown in Table 3-2.

We turn next to the crack configurations of Figures 3-8(b) and 3-8(c). Because these cracks penetrate the head, a methodology different from that used for Figure 3-8(a) is needed. Since much more material resides in the rail head than in the web, the local stress field in the head is assumed to produce the primary contribution to the stress intensity factors there. This state of affairs is modeled by assuming the local head stresses to act as pressure and/or shear loading on the portion of the crack faces within the head. Justification for this model arises from the fact that stress intensity factors due to crack face tractions are equivalent to those derived from that remote loading which would produce equal and opposite crack face tractions in an equivalent uncracked body.

To obtain these local stresses, we draw from the earlier discussion relating to head-on-web effects. The head-on-web shear stresses in the head are assumed to follow a parabolic distribution which integrates to W/2. Thus the maximum shear stress in the head is $3W/(4(2.94)(1.56)) = 0.16W$, based on the same head height and thickness used to calculate I_H earlier. The global shear stress distribution also adds a contribution to the shear stress in the head, which Figure 3-7 has shown to be quite small. A sum of the global shear stress distribution and the parabolic head-on-web distribution shows that for the lower portion of the head, a shear stress of 0.20W is not exceeded. The shear stress is much less near the top of the head, and it actually vanishes at the running surface. For application here, 0.20 W = 6.6 ksi, the same level of stress as taken to act in the web.

The axial stress level is not as readily estimated, since residual stresses as high as 15 or 20 ksi may exist in the rail. Postponing consideration of these for the moment, we calculate the axial stresses that arise both from head-on-web bending and global bending. For head-on-web bending, the axial stress varies linearly from $(W/4\beta_w I_H)\ (\frac{1.94}{2}) = 18.0$ ksi to -18.0 ksi. The global bending stress varies linearly from $-(3W/16\beta I)\ (2.03) = -6.7$ ksi to $-(3W/16\beta I)(3.97) = -12.9$ ksi, where the head's distance from the neutral axis is taken to vary from 2.03 inches at its bottom to 3.97 inches at its top. (The head height used here is the maximum head height rather than the average used to obtain I_H). Thus the linear variation of axial stress in the head, exclusive of residual stress, is from 11.3 ksi to -30.9 ksi. This presumed variation in axial stress is plotted together with the presumed shear stress variation in Figure 3-11. For cracks part way through the head, a value of axial stress based on the above discussion will be averaged over the crack length. For example, a crack extending one inch into the head sees an average axial stress $(11.3 + (-10.5))/2 = 0.4$ ksi.

The stress distributions pictured in Figure 3-11 are not identical to the finite element results from [7], but they show mostly similar trends. The axial stresses used here, however, show a considerable tension at the base of the rail head that was not predicted in [7]. Residual stresses tend to be greatest in the core of the rail head [33], and it is thus probable that axial tension does exist through the lower portion of the rail head. This tension is accounted for here by performing calculations which assume additional tensions in the rail head of 0, 10, and 20 ksi. While these tensions may not in reality prevail through the entire head, the calculations will show their effect on stress intensity factors.

Another possible contribution to longitudinal tension in the head is reversed bending. Reversed bending occurs in continuous rail well away from a concentrated wheel load, but it also occurs when a wheel crosses an inefficient rail joint. We have performed some preliminary calculations, not reproduced here, which indicate that even for the most

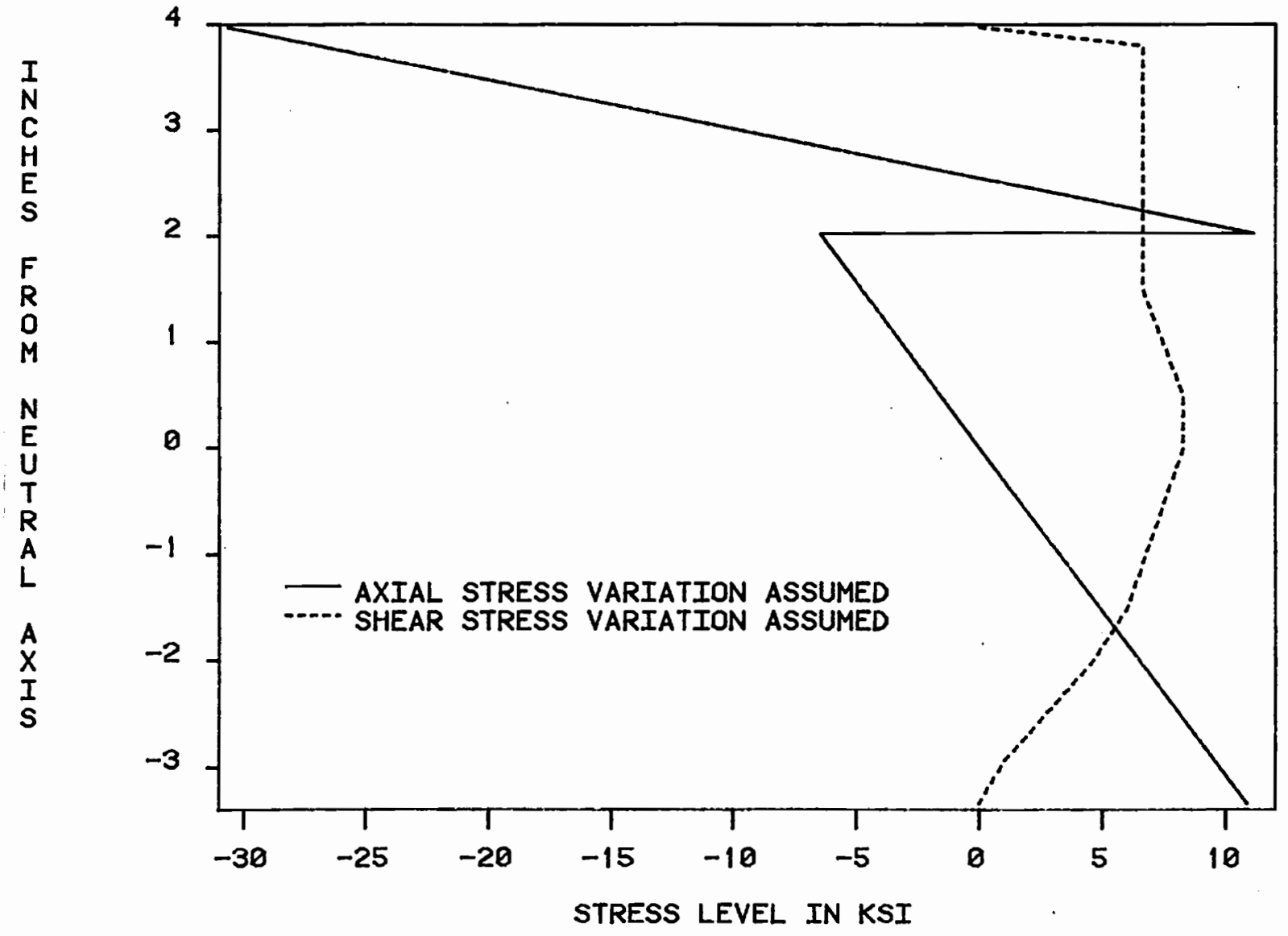

Figure 3-11. Stress variations in rail based on inclusion of head-on-web effect. The variations within the rail head are used for the fracture mechanics analyses.

severe case of a completely inefficient rail joint, tensile stresses due to reversed bending in the head near the bolt holes are well under 10 ksi. Nevertheless, especially in combination with residual stresses, reversed bending could provide the driving force for a crack to overcome compression at the running surface and to propagate entirely through the rail head. The subsequent calculations with residual stress levels of 10 and 20 ksi can also be thought of as including cases where reversed bending is especially severe.

The stress intensity factor calculations are based on handbook results [16] for flat cracks with pressure and shear tractions, p and q respectively, over a portion of the crack faces. A correction for proximity of the crack tip to the top of the head is included from Tada [16]. The actual idealizations of Figures 3-8(b) and 3-8(c) are shown in Figures 3-12(a) and 3-12(b) respectively. The results for the three residual stress levels and various crack lengths b are listed in Tables 3-3 and 3-4 along with the p and q values from which they were obtained. The results are also plotted in Figures 3-13 through 3-16. The Tables show a severe rise in stress intensity magnitude, $(K_I^2 + K_{II}^2)^{\frac{1}{2}}$, as the cracks grow deeper into the head. When $K_I < 0$, the stress intensity magnitude is taken to be that of K_{II} alone. Comparison of the results for growth in the head to those for growth along the head-web boundary (Table 3-2) suggests that fatigue crack growth may reasonably occur over long distances just underneath the head, but catastrophic propagation is quite likely shortly after the crack enters the rail head. Even at moderate crack depths, stress intensity factors approaching K_{IC} (about 35 ksi $\sqrt{\text{in}}$) exist, especially in the presence of tensile residual stress.

Finally, we consider the configuration depicted in Figure 3-8(d), and focus on the region where the crack front emerges into the head-web fillet. By calculating stress intensity factors here, we can make some judgments as to the relative propensity of a crack to grow outward through the sides of the rail head as well as upward through the center of the head.

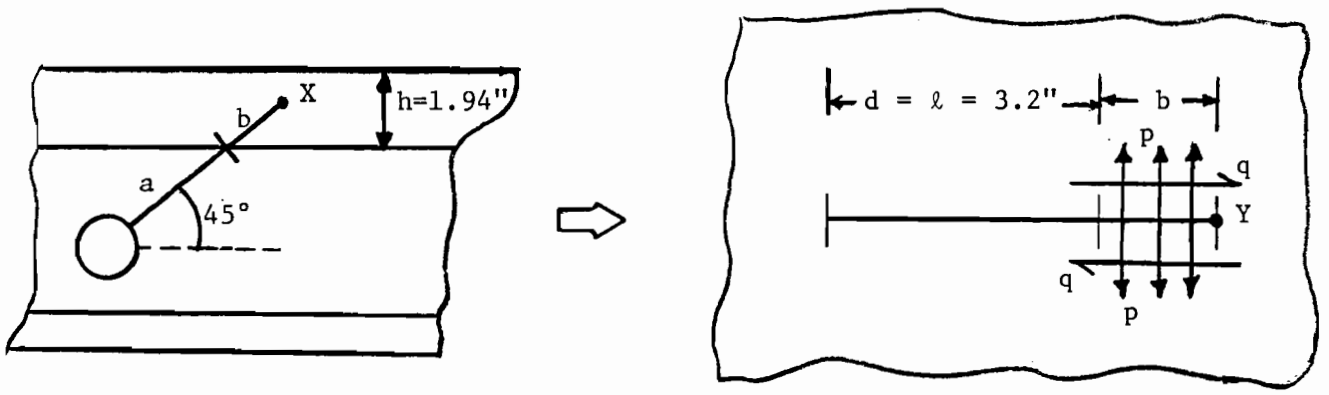

$$K_{I,II}(X) = K_{I,II}(Y)F(b(\cos 45°)/h)$$

$$K_{\{I,II\}}(Y) = \{p,q\}\left[\sqrt{\frac{d+b}{2\pi}}\left(\frac{\pi}{2} - \sin^{-1}\left(\frac{d+b}{d-b}\right) + \sqrt{1 - \left(\frac{d-b}{d+b}\right)^2}\right)\right]$$

$$F(r) = \sqrt{\frac{2}{\pi}\tan\frac{\pi r}{2}}\left(\frac{0.752 + 2.02r + 0.37(1 - \sin(\pi r/2))^3}{\cos(\pi r/2)}\right)$$

$$p = \tau + \sigma/\sqrt{2},\ q = \sigma/\sqrt{2}$$

(a)

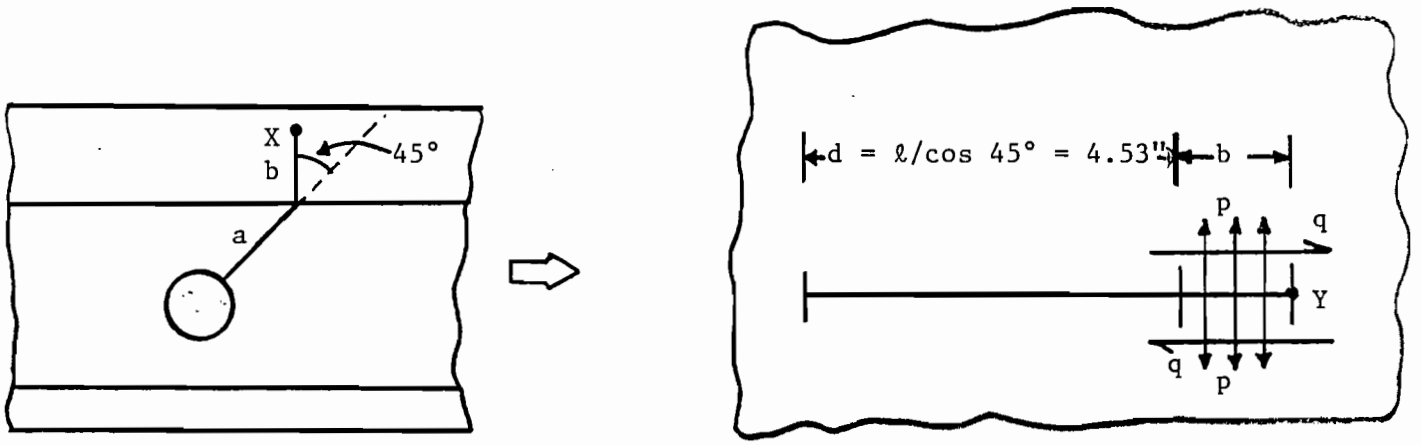

$$K_{I,II}(X) = K_{I,II}(Y)F(b/h)$$

$K_{I,II}(Y)$ and $F(r)$ as in (a)

$$p = \sigma,\ q = \tau$$

(b)

Figure 3-12. Idealizations used to obtain stress intensity factors for Figures 3-8(b) and 3-8(c). Axial stress is denoted by σ and shear stress is denoted by τ.

Table 3-3. Stress Intensity Factors for Figure 3-12(a)

b(inches)	Residual Stress (ksi)	Total Axial Stress (ksi)	Shear Stress (ksi)	p(ksi)	q(ksi)	K_I (ksi$\sqrt{in}$)	K_{II} (ksi$\sqrt{in}$)	$\|K\|$ (ksi$\sqrt{in}$)
0.1	0	10.5	6.6	14.0	7.4	8.4	4.5	9.5
	10	20.5	6.6	21.1	14.5	12.7	8.7	15.4
	20	30.5	6.6	28.2	21.6	17.0	13.0	21.4
0.2	0	9.8	6.6	13.5	6.9	12.2	6.2	13.7
	10	19.8	6.6	20.6	14.0	18.6	12.7	22.5
	20	29.8	6.6	27.7	21.1	25.1	19.1	31.5
0.3	0	9.0	6.6	13.0	6.4	15.3	7.5	17.1
	10	19.0	6.6	20.0	13.4	23.6	15.8	28.4
	20	29.0	6.6	27.1	20.5	31.9	24.2	40.0
0.4	0	8.2	6.6	12.4	5.8	18.0	8.4	19.8
	10	18.2	6.6	19.5	12.9	28.2	18.7	33.9
	20	28.2	6.6	26.5	19.9	38.4	28.8	48.0
0.6	0	6.7	6.6	11.3	4.7	22.8	9.5	24.7
	10	16.7	6.6	18.4	11.8	37.2	23.8	44.2
	20	26.7	6.6	25.5	18.9	51.5	38.2	64.1
0.8	0	5.1	6.6	10.2	3.6	27.3	9.6	29.0
	10	15.1	6.6	17.3	10.7	46.3	28.6	54.4
	20	25.1	6.6	24.3	17.7	65.0	47.4	80.5
1.0	0	3.6	6.6	9.1	2.5	31.6	8.7	32.8
	10	13.6	6.6	16.2	9.6	56.3	33.4	65.4
	20	23.6	6.6	23.3	16.7	81.0	58.0	99.6
1.2	0	2.1	6.6	8.1	1.5	36.4	6.7	37.0
	10	12.1	6.6	15.2	8.6	68.4	38.7	78.6
	20	22.1	6.6	22.2	15.6	99.8	70.2	122.0
1.4	0	.5	6.6	7.0	.4	41.2	2.4	41.2
	10	10.5	6.6	14.0	7.4	82.3	43.5	93.1
	20	20.5	6.6	21.1	14.5	124.1	85.2	150.5
1.6	0	-1.0	6.6	5.9	-0.7	46.4	-5.5	46.8
	10	9.0	6.6	13.0	6.4	102.3	50.4	114.0
	20	19.0	6.6	20.0	13.4	157.4	105.5	189.5

Table 3-4. Stress Intensity Factors for Figure 3-12(b)

b(inches)	Residual Stress (ksi)	Total Axial Stress (ksi)	Shear Stress (ksi)	p(ksi)	q(ksi)	K_I (ksi$\sqrt{in}$)	K_{II} (ksi$\sqrt{in}$)	$\|K\|$ (ksi$\sqrt{in}$)
0.1	0	10.2	6.6	10.2	6.6	6.3	4.1	7.5
	10	20.2	6.6	20.2	6.6	12.5	4.1	13.2
	20	30.2	6.6	30.2	6.6	18.7	4.1	19.1
0.2	0	9.1	6.6	9.1	6.6	8.7	6.3	10.8
	10	19.1	6.6	19.1	6.6	18.3	6.3	19.4
	20	29.1	6.6	29.1	6.6	27.9	6.3	28.6
0.3	0	8.0	6.6	8.0	6.6	10.3	8.5	13.3
	10	18.0	6.6	18.0	6.6	23.2	8.5	24.7
	20	28.0	6.6	28.0	6.6	36.0	8.5	37.0
0.4	0	6.9	6.6	6.9	6.6	11.3	10.8	15.6
	10	16.9	6.6	16.9	6.6	27.6	10.8	29.6
	20	26.9	6.6	26.9	6.6	43.9	10.8	45.2
0.6	0	4.8	6.6	4.8	6.6	11.7	16.1	19.9
	10	14.8	6.6	14.8	6.6	36.1	16.1	39.6
	20	24.8	6.6	24.8	6.6	60.5	16.1	62.6
0.8	0	2.6	6.6	2.6	6.6	9.2	23.3	25.1
	10	12.6	6.6	12.6	6.6	44.5	23.3	50.2
	20	22.6	6.6	22.6	6.6	79.8	23.3	83.2
1.0	0	0.4	6.6	0.4	6.6	2.1	34.1	34.1
	10	10.4	6.6	10.4	6.6	53.7	34.1	63.6
	20	20.4	6.6	20.4	6.6	105.3	34.1	110.7
1.2	0	-1.8	6.6	-1.8	6.6	-14.3	52.4	52.4
	10	8.2	6.6	8.2	6.6	65.1	52.4	83.5
	20	18.2	6.6	18.2	6.6	144.4	52.4	153.6
1.4	0	-3.9	6.6	-3.9	6.6	-52.8	89.4	89.4
	10	6.1	6.6	6.1	6.6	82.6	89.4	121.7
	20	16.1	6.6	16.1	6.6	218.0	89.4	235.6

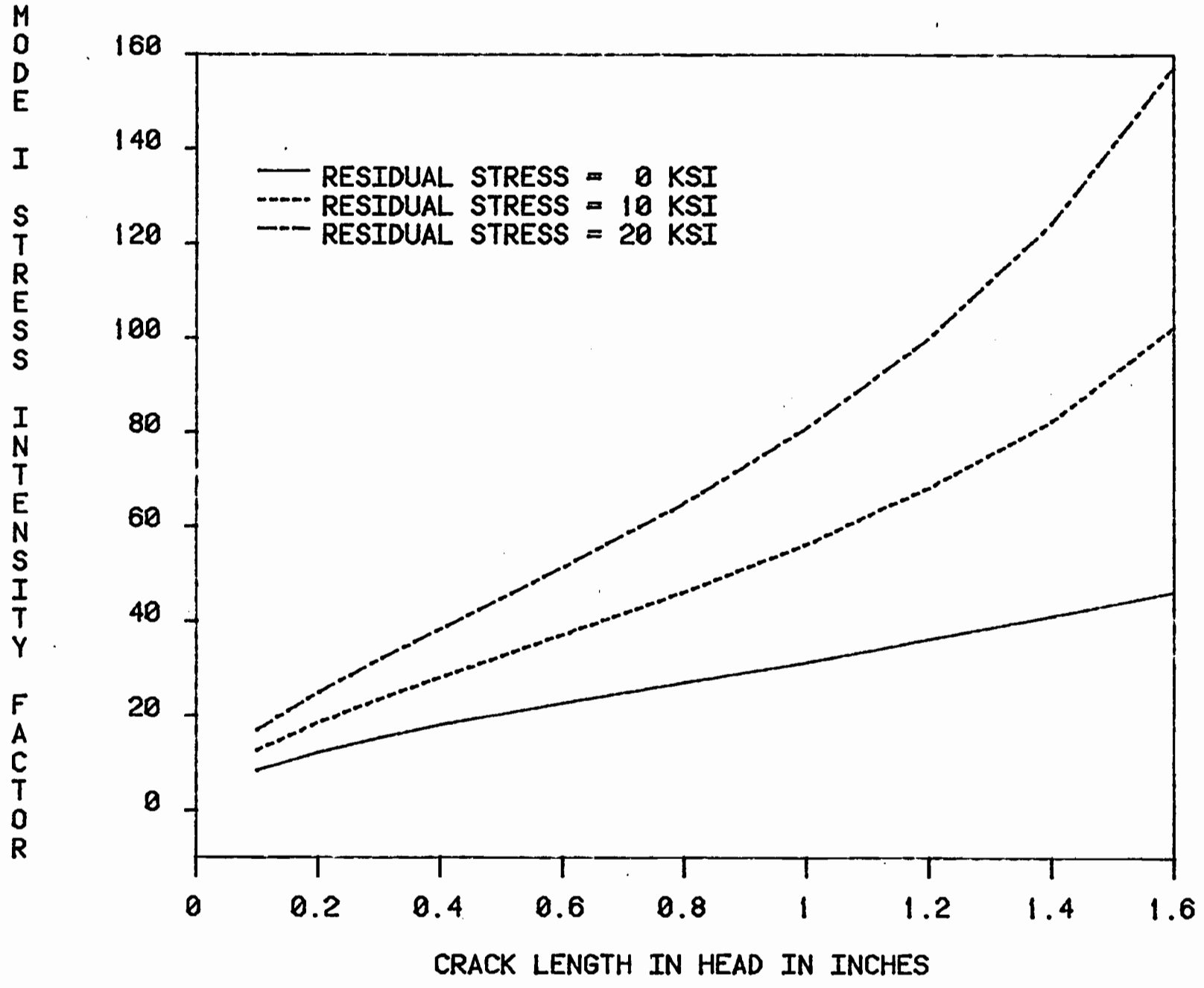

Figure 3-13. Plots of K_I from Table 3-3.

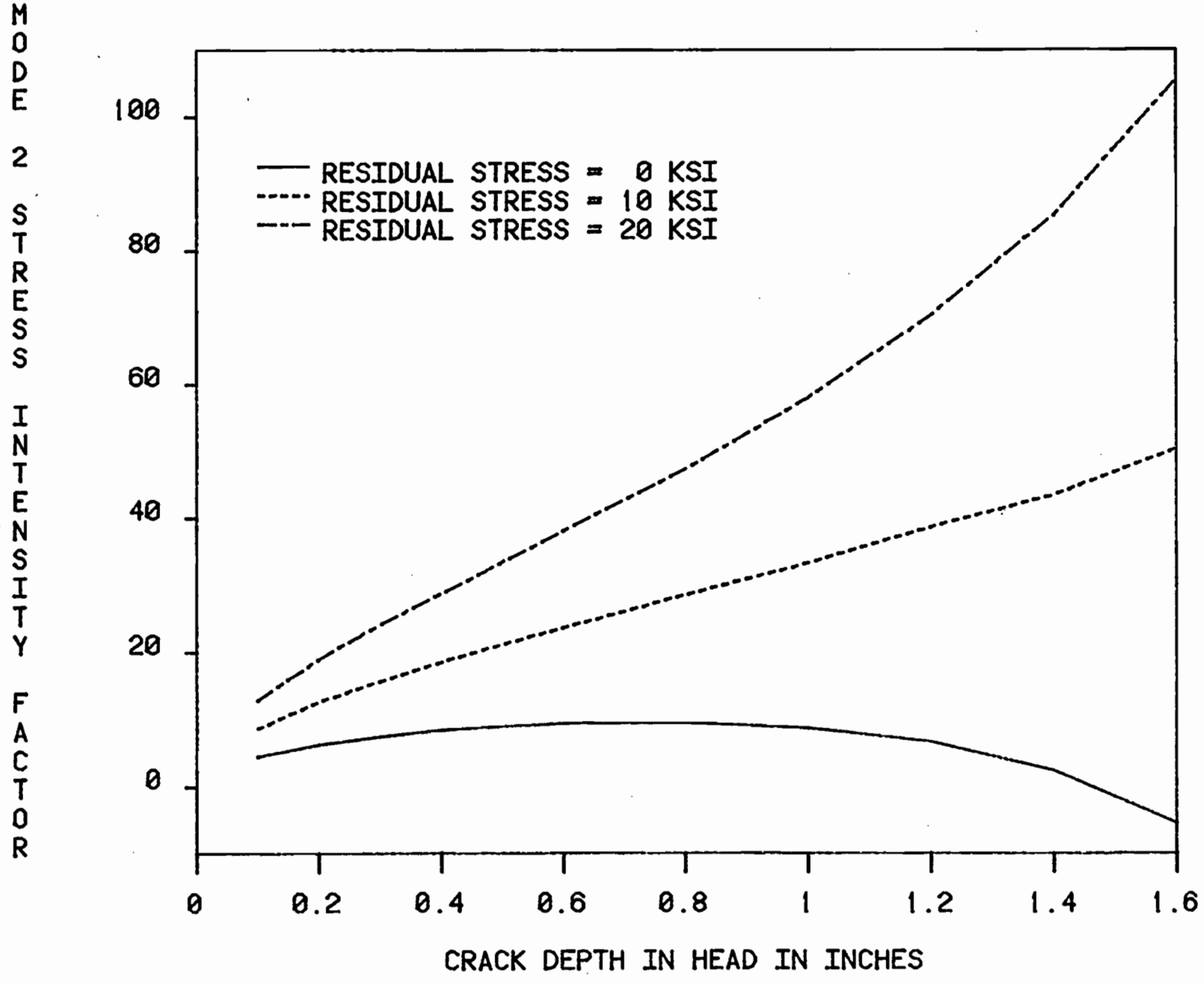

Figure 3-14. Plots of K_{II} from Table 3-3.

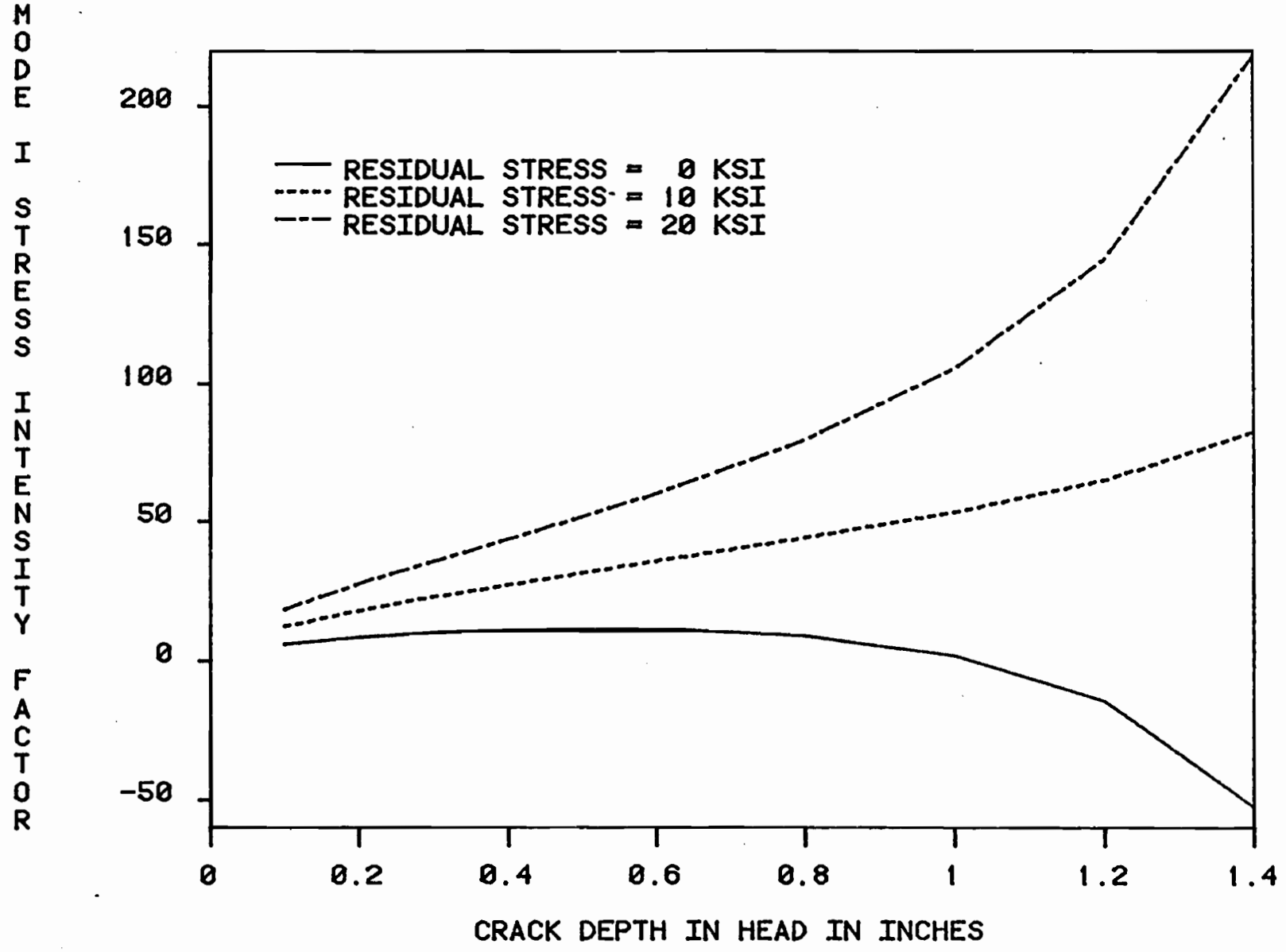

Figure 3-15. Plots of K_I from Table 3-4.

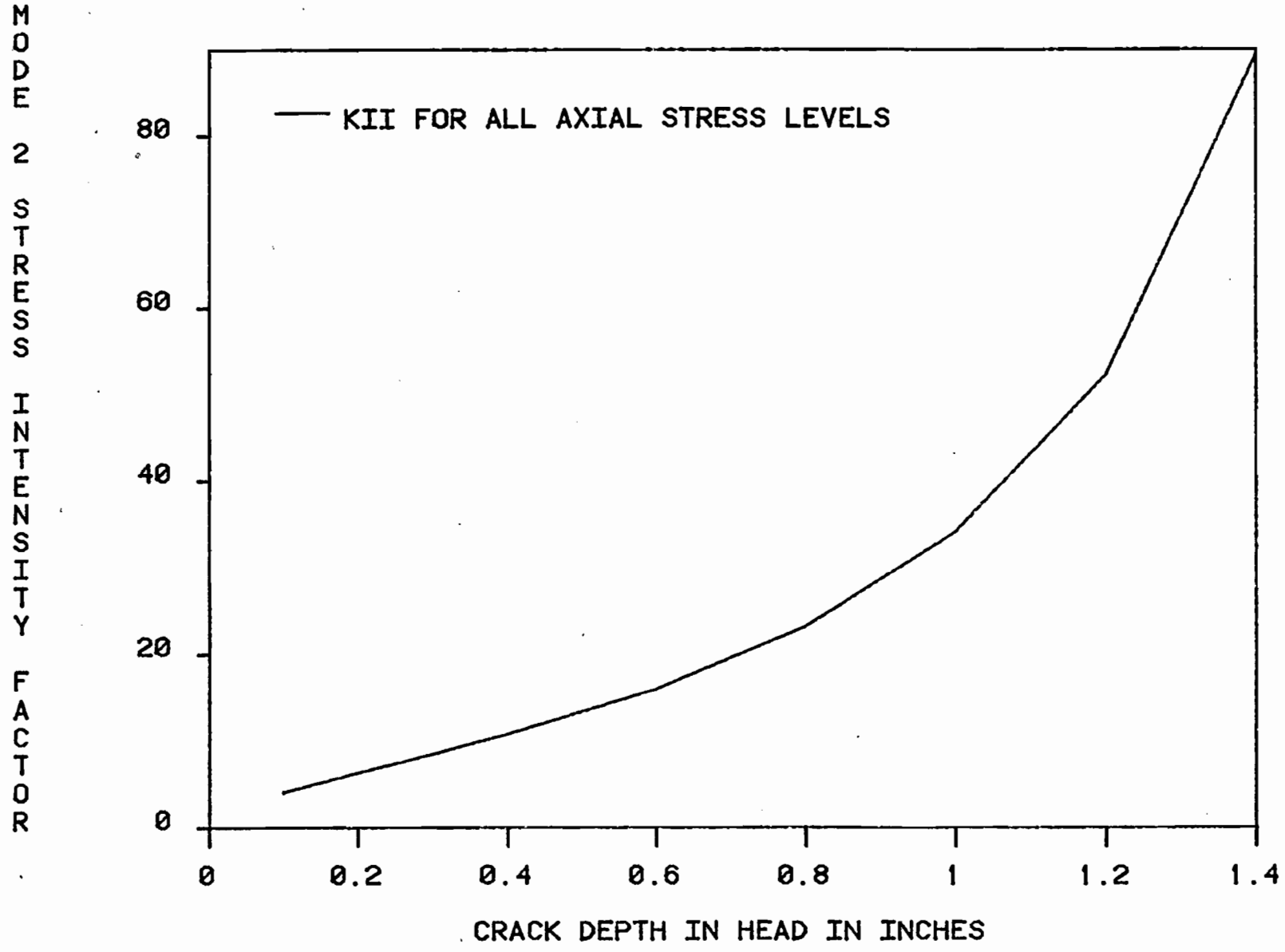

Figure 3-16. Plot of K_{II} from Table 3-4.

The method for obtaining stress intensity factors in the head-web fillet region is based on the assumption that locally, the crack behaves as an appropriate portion of a semielliptical flaw. The stress intensity factors for the edge of the flaw will be obtained from results of Wu [34], one of many who have tackled the semielliptical surface flaw problem. Three locations along the fillet will be considered; these are shown in Figure 3-17(a), together with plausible crack shapes. For simplicity and consistency, the semielliptical idealization used will assume a/c = 0.5 (see Figure 3-17(b)). For each crack, c is taken to be the distance from the rail centerline to the most remote point along the crack front.

The stress state giving rise to the stress intensity factors is assumed to be that which prevails at the fillet. This stress state, due to the free boundary, differs from that predicted in the head-on-web analysis. Here, the shear stresses in the fillet are obtained from the analysis of Section 3.3, while the axial stresses are in fact those from the head-on-web analysis, since axial stresses are not affected by the free boundaries. Residual stresses are assumed insignificant near the fillet. These stresses are then converted to principal stresses. In all three cases in Figure 3-17(a), the maximum principal stress is tensile and is oriented almost longitudinally. This tensile stress is used directly in a K_I calculation on the assumption that the actual crack would be oriented very closely normal to this stress.

The local stress state and corresponding principal stresses for the three points indicated in Figure 3-17(a) are given in Table 3-5. The corresponding stress intensity factors are also shown in the Table. A comparison of these results with those in Tables 3-3 and 3-4 indicates that if a crack does indeed enter the head, it can be expected to grow rapidly, if not immediately, up to the running surface, where severe compression may or may not arrest it. This kind of effect is prominent in the first rail fracture examined in Appendix A. In any case, one would expect the growth to be confined primarily to the center of the head, due to the lower stress intensity factors in the fillet region.

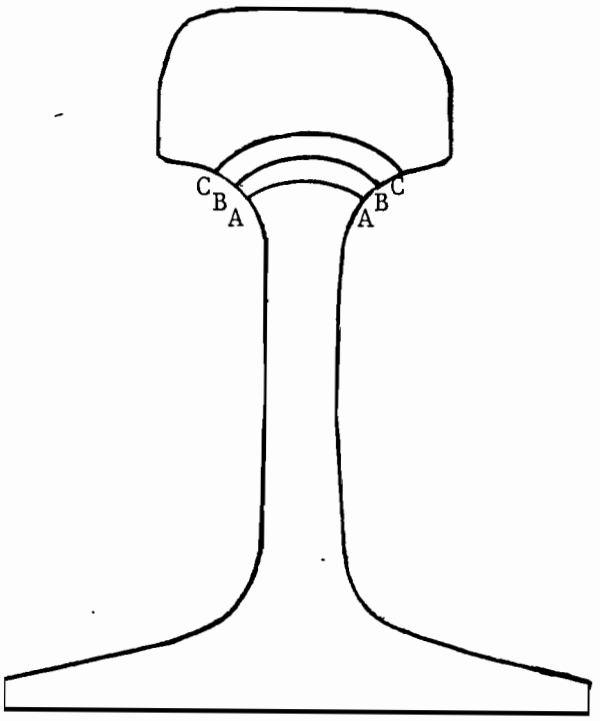

(a)

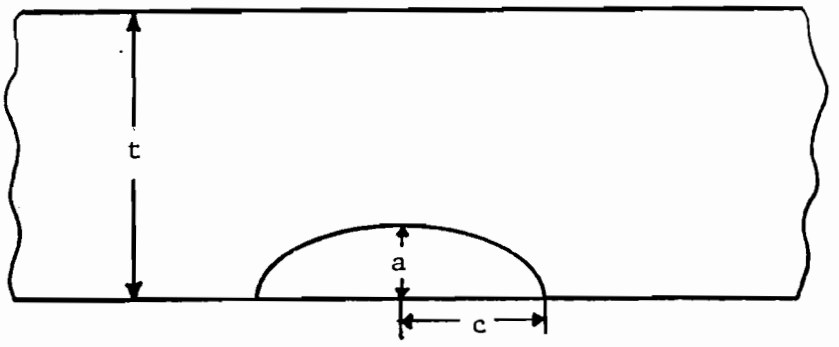

(b)

Figure 3-17. (a) Crack configurations for analyzing stress intensity factors in the head-web fillet. (b) Geometric parameters for semielliptical flaw.

Table 3-5. Stress Intensity Factors for Figure 3-17

	Stress State (ksi)			Principal Stresses and Eigenvectors			Flaw Parameters		
Location	τ_{xz}	τ_{yz}	σ_{zz}	$P_1, \hat{e}_1$	$P_2, \hat{e}_2$	$P_3, \hat{e}_3$	a(in.)	c(in.)	K_I(ksi$\sqrt{in}$)
A	2.67	5.84	11.3	-2.90 (.38,.83,-.41)	0.0 (.91,-.42,0)	14.20 (.17,.37,.91)	.25	.59	9.03
B	3.02	2.08	9.6	-1.24 (.78,.54,-.32)	0.0 (-.57,.82,0)	10.84 (.26,.18,.95)	.37	.74	8.39
C	1.47	0.38	8.7	-0.26 (.95,.25,-.17)	0.0 (-.25,.97,0)	8.96 (.16,.04,.99)	.56	1.02	8.53

Crack growth is thus not particularly favorable from the center of the head to either its gauge or field sides.

The primary aim of this section has been to provide methodology for addressing long cracks which emanate from a bolt hole. For simplicity, a conservative approach has been taken to estimating important components of stress in the rail head. Given the methodology here, further work could address, in a quantitative fashion, the variation of stress intensity factors during the passage of an entire car or train. Residual stresses, reversed bending, and head-on-web effects could all be incorporated as appropriate.

3.5 Finite Element Analyses of a Long Bolt Hole Crack

Six three-dimensional finite element analyses, using the program APES3D [35], were carried out in support of the calculations in the previous section. The calculations were performed for a 136 lb/yd rail section extending four feet from the rail end. Since no eccentric or lateral loading was considered here, symmetry conditions were applied along the rail centerline, and only half the rail section was modeled. The finite element mesh for this geometry is shown in Figure 3-18. A crack extends from the first bolt hole (the only bolt hole modeled) up to the rail head. The crack is inclined at 45° to the horizontal away from the rail end in accord with the most frequently observed instances of bolt hole cracking (cf. Figure 1-2). The six analyses performed correspond to six different positions of the wheel load along the rail; the primary result of these calculations is the variation of stress intensity factors with wheel position.

The boundary conditions for the four foot section of rail depicted in Figure 3-18 present some unique problems. In particular, the joint bar forces and foundation behavior require special attention. A joint bar efficiency of 0.75 for both moment and shear forces was assumed for all analyses here. The joint bar forces were taken to be separated by 11.875 inches, a distance in reasonable agreement with the Talbot reports [36] and convenient to the actual mesh design. Joint bar forces

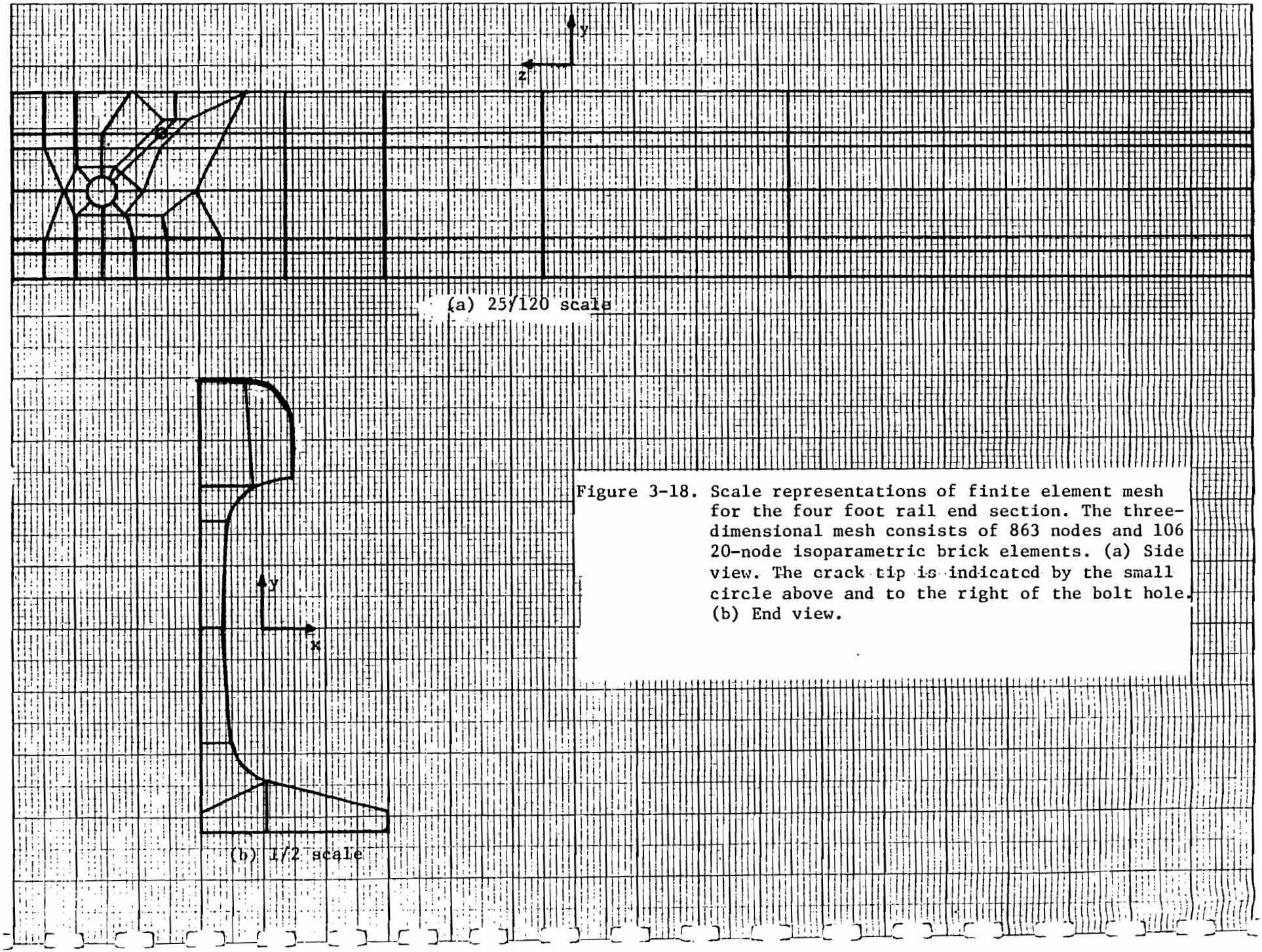

Figure 3-18. Scale representations of finite element mesh for the four foot rail end section. The three-dimensional mesh consists of 863 nodes and 106 20-node isoparametric brick elements. (a) Side view. The crack tip is indicated by the small circle above and to the right of the bolt hole. (b) End view.

were then calculated for a given wheel load by the scheme outlined in [5]. Each of the two joint bar forces were distributed as uniform tractions over a single element face. The force in the positive y direction was applied near the rail end under the head; the centroid of the loaded element face was 0.625 inches from the rail end. The force in the negative y direction was imposed over the rail base; the centroid of the loaded element face was 12.5 inches from the rail end. The wheel load itself was 33 kips, and this was applied as a point load of 16.5 kips (due to symmetry) at the top of the rail.

Since APES3D does not provide the capability to model an elastic foundation directly, an alternative approach was devised. A small computer program was written to furnish displacements of a rail idealized as a semi-infinite beam on an elastic foundation. The foundation modulus was assumed to be 3000 psi. The rail was loaded with the train wheel and the corresponding joint bar forces, and displacements were determined for the locations of the nodes along the rail base in the finite element mesh. Thus for the three-dimensional calculations, y displacements reflecting the effects of an elastic foundation were prescribed along the rail base.

The small computer program also provided the moment and shear force at any desired point along the rail. In particular, values were obtained at the rail position four feet from the rail end and applied to the remote end of the finite element grid in Figure 3-18. The moment was applied as a set of point loads at the top of the rail head and the bottom of the rail base. The shear force was applied as a set of point loads which had peak values in the web and diminished to zero in the head and base, in accord with Figure 3-7. By St. Venant's principle, the precise method by which these moment and shear forces were distributed has little effect on the solution features near the bolt hole, which lies at the opposite end of the section analyzed.

The remaining boundary conditions were symmetry constraints along the symmetry plane through the center of the rail, and longitudinal constraint of two nodes on the rail end to prevent rigid translation in

the z direction. For the 136 lb/yd rail modeled here, additional data included Young's modulus = 30 x 10^6 psi, Poisson's ratio = 0.3. A summary of the joint bar forces and moment and shear values four feet from the rail end, which served as input for the six analyses, is furnished in Table 3-6. The finite element calculations were performed on a Control Data Corporation 7600 series computer operated by Los Alamos National Laboratory.

Table 3-6

Loading Conditions for Finite Element Analyses

	Distance of Wheel Load (33 kips) From Rail End					
	4.5"	5.74"	6.1"	7.55"	10.5"	0(Wheel on Other Rail)
Shear force at remote end (kips)	-2.45	-2.15	-2.15	-2.64	-3.44	-2.0
Moment at remote end (kip-inches)	-101	-114	-115	-102	-81.2	-34.8
Joint bar force Q_1	29.3	28.4	27.4	26.3	23.0	10.4
Joint bar force Q_2	18.7	17.6	17.3	16.0	13.5	22.6

The finite element results were checked by examining calculated loads along the rail base and calculated stresses at different locations within the rail. Where comparisons were appropriate, these quantities showed good agreement with beam theory predictions. Confidence was therefore established in the values of stress intensity factors output by APES3D.

As mentioned previously, six positions of wheel load were analyzed. The focus here is on the effect of the changing position of a wheel on the driving force for the long bolt hole crack considered. Stress intensity factors for all of Modes I, II, and III were obtained at each of three points through the rail thickness: the center, the surface, and a point midway in between. The average values of K_I, K_{II}, and K_{III} through the thickness are plotted against wheel position (given as distance in inches from the rail end) in Figure 3-19. Symmetry requires that K_{III} vanish at the middle of the crack front; because Figure 3-19 shows that all the K_{III} values are indeed quite small compared to the K_I and K_{II} values, K_{III} will be neglected in the remainder of this discussion.

The parameter $|K| = (K_I^2 + K_{II}^2)^{\frac{1}{2}}$ is used here to characterize crack driving force since both modes I and II are important. As in Section 3.4, the contribution of K_I is neglected if $K_I < 0$. A plot of this driving force parameter at each of the three nodal locations along the crack front is furnished in Figure 3- 20. Several aspects of this and the previous figure are well worth noting. Although the data is quite discrete, the figures show that a definite peak in crack driving force is associated with passage of the wheel over the bolt hole crack. The leftmost point on the curves actually corresponds to a wheel on the opposite rail before it has crossed the joint. Only after the wheel crosses onto the receiving rail do the stress intensity factors develop significant magnitudes. The stress intensity factors diminish quickly after the wheel has passed the crack, but K_I seems to persist longer than K_{II}. The change in $|K|$ associated with the wheel passage is in excess of 10 ksi$\sqrt{\text{in}}$, which is certainly capable of supporting fatigue

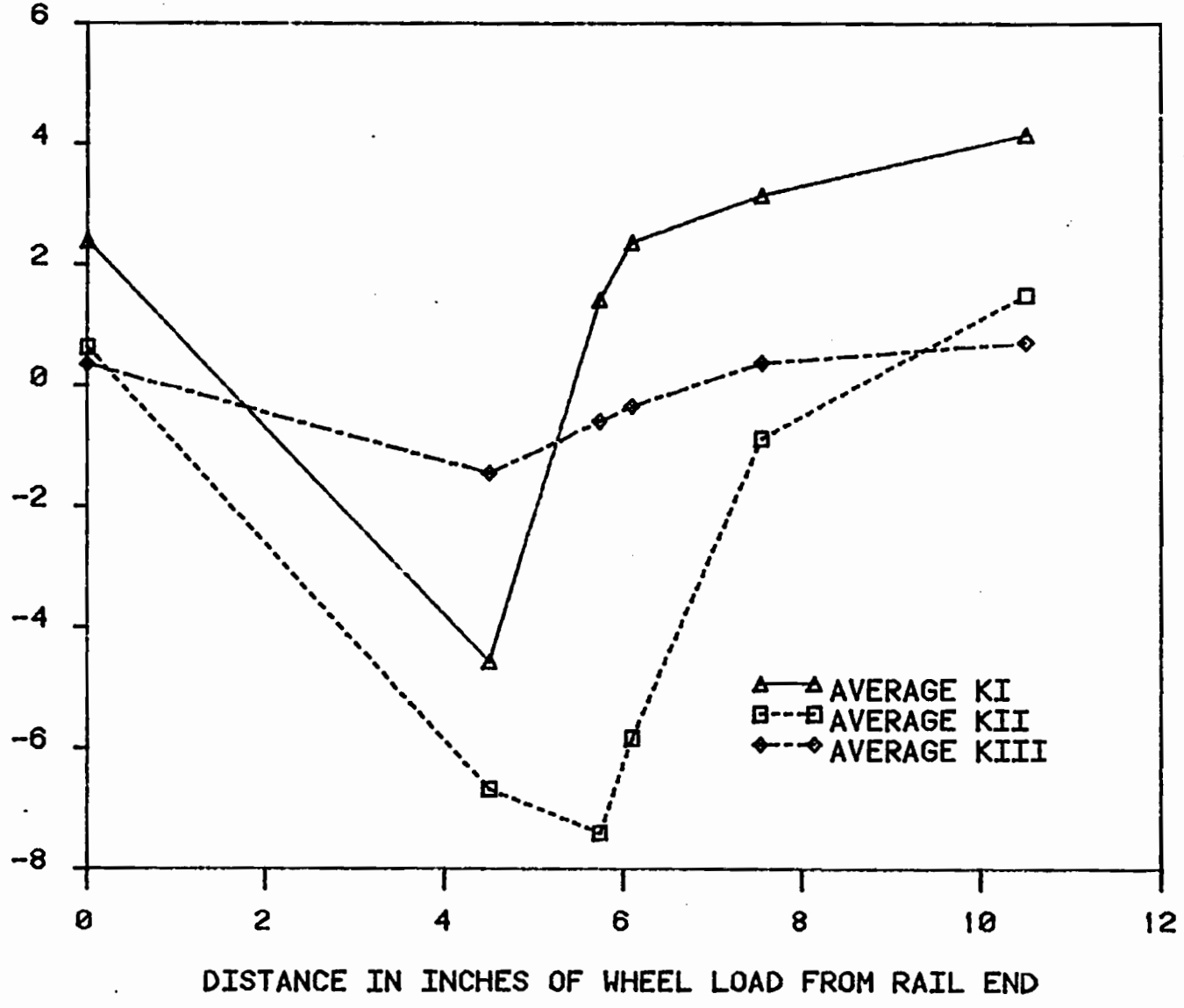

Figure 3-19. Through-thickness averages of stress intensity factors for Figure 3-18 measured in ksi$\sqrt{in.}$

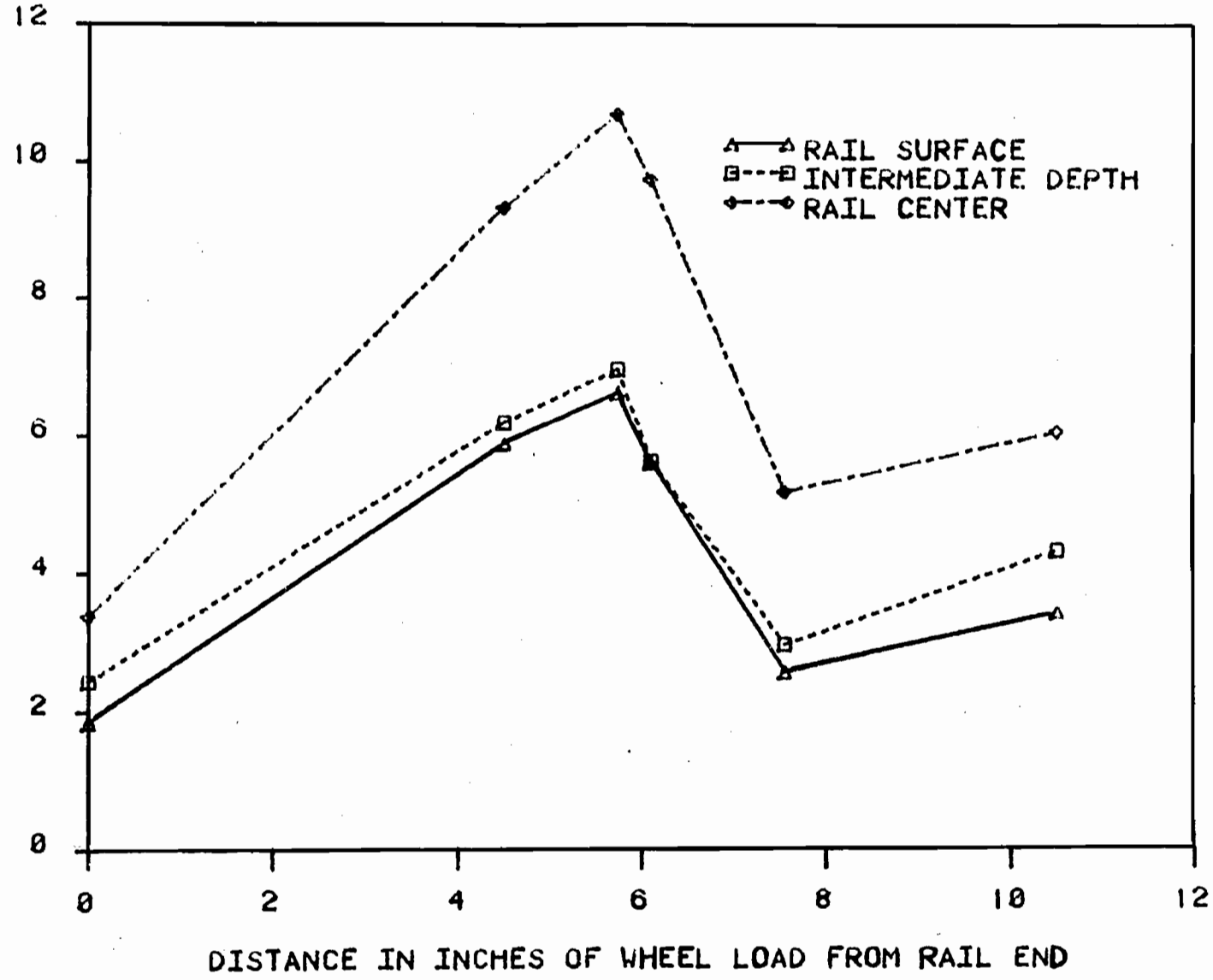

Figure 3-20. Values in ksi$\sqrt{in}$ of $|K| = (K_I^2 + K_{II}^2)^{\frac{1}{2}}$ at three positions along the crack front.

crack growth in rail steel. The growth would proceed even faster in the presence of residual tensile stresses and/or dynamic load amplification.

Figure 3-20 also shows that the crack driving force is markedly higher in the center of the rail than it is nearer the lateral surfaces. This corroborates the conjecture in Section 3.4 that crack growth in the head tends to proceed upward rather than outward. The broken rails shown in Figures A1 and A4 demonstrate this tendency as well since the cracks grew very deep into the head before changing direction in the face of high compression near the running surface. Only after this change in direction did growth seem to proceed to the outer portions of the head.

The finite element calculations from which these results were obtained required less than five minutes of processor time on the aforementioned CDC 7600 computer. Due to the reasonable computer costs involved, additional analyses for other rail load parameters could be performed if necessary. Parameter studies to assess the effects of joint efficiency or foundation modulus, for example, would be possible with the existing mesh. Lateral or eccentric loadings, however, would require a mesh on both sides of the rail centerline. Studies of crack length and crack shape effects would require more extensive efforts in mesh design.

4. DISCUSSION AND CONCLUSIONS

This report, together with our previous work summarized in Section 3.0, has sought to provide a unified understanding of rail end bolt hole cracking from initiation through to complete fracture. The ultimate objective of these analyses is to set appropriate inspection practices for rail joints; while substantial progress has been achieved in understanding crack development from corner cracking through to final fracture, the timing and causes for crack initiation and certain stages of growth must be researched further.

In Chapter 1, it was observed that the endurance strength of the steel in the rail web was sufficient to preclude fatigue crack initiation at the rail end bolt hole under normal operating conditions. Indeed, this explains the integrity of the vast majority of bolt holes in existing rails. It was concluded that special conditions must exist if a fatigue crack is to initiate from a rail end bolt hole. Such conditions include fretting, which arises from contact between the joint bar bolts and the bolt hole surface, and corrosion, which may occur preferentially in tunnels, and near bridges and crossings. Both fretting and corrosion significantly reduce the endurance limit of the steel in the web. At the same time, especially severe dynamic loads can contribute to an increase in the usual alternating stress levels, and such loads are likely to occur at inefficient or dipped rail joints. Further research aimed at quantifying reductions in endurance strength due to fretting and corrosion would help determine which of these conditions favor initiation the most.

Chapter 2 turned the focus to the growth rates of bolt hole cracks shortly after initiation has taken place. Any slight wheel load eccentricity and/or lateral loading from the wheel flange contacting the rail head tend to favor the formation of a corner crack on one side of the web at the intersection with the bolt hole. The analysis carried out in Section 2.2 for a particular coal transport situation suggests that a corner crack can grow through to the other side of the rail web in about a month, assuming heavy traffic of roughly 3.3 MGT per day.

For the 0.2 inch radius corner crack considered, its maximum depth was about two thirds the web thickness of 0.675 inches when it penetrated the opposite web surface. If the prevailing loads are severely asymmetric, initial growth of the corner crack is accelerated, but greater compression on the opposite side of the web inhibits the complete penetration of the crack through the web thickness.

Chapter 3 went on to analyze deeper through cracks in the rail web, including cracks which approach and enter the rail head. Our earlier study [5] determined that crack growth rates for the most common type of bolt hole crack, shown in Figure 1-2, are relatively constant for two to three inches of crack growth from the bolt hole up to the rail head. For typical rail parameters with a wheel load of 33 kips, this growth rate was calculated to be 6.2 MGT per inch of growth. Cracks of this size may also be affected by rail tension due to bolt bearing in cold weather, and this possibility was considered in Section 3.2. Here also the Mode I stress intensity factor did not vary much with crack length, staying in the range of a nonalternating 15 ksi $\sqrt{\text{in.}}$ This value is less in both magnitude and frequency of occurrence than the alternating 25 ksi $\sqrt{\text{in}}$ that reference [5] associated with train passages, but prolonged cold weather combined with heavy traffic might subject a bolt hole crack to frequent stress intensity factors near 40 ksi $\sqrt{\text{in.}}$ Since a typical K_{IC} for rail steel is 35 ksi $\sqrt{\text{in,}}$ the analysis predicts that fracture should occur more often during sustained cold spells, as is observed.

As bolt hole cracks approach the rail head, they may grow along the head-web boundary or penetrate the head at an arbitrary angle. Further analysis was performed in Sections 3.3 through 3.5 to determine stress intensity factors for a number of such cases. The results indicated that, especially in the presence of modest residual stresses, stress intensity factors for cracks growing deep into the rail head are much greater than for those which remain in the web or along the head-web boundary. Lateral crack growth to the outer portions of the head, however, is subject to a much lesser driving force. Thus a crack entering the rail head may rapidly penetrate to a depth just below the running surface, at which point final fracture of the rail occurs when

the lateral portions of the rail head separate as well. This behavior is consistent with fracture surfaces observed in the rails in Appendix A.

The relative invariance of stress intensity factor with respect to crack length in the upper portion of the web, as described in [5], leads one to the conclusion that, when the crack is in the web, a critical load situation rather than a critical crack length is most often responsible for a complete bolt hole fracture. If a critical load does not occur, the bolt hole crack may eventually grow by fatigue into the rail head. Estimated stress intensity factors in the head-web fillet indicate that initial penetration of the rail head requires a great many additional load cycles after the crack has just reached the head. On the other hand, complete fracture of the rail head seems to occur rapidly after penetration of the head, with or without a critical load condition. The rail fractures discussed in Appendix A are consistent with this scenario.

Because cracks entering the rail head are so critical, it is important to know how much time (or tonnage) is necessary for a crack to initiate, grow to a through crack, and propagate up to the rail head. Unfortunately, the timing of the degradation processes which are required for fatigue crack initiation remain poorly understood. On the other hand, we can make some estimate of the time required for a corner crack to grow to a through crack and then grow up to the base of the rail head. For the heavy traffic example referred to earlier, it takes one month ($\sim$ 10 MGT) for a corner crack to grow through the web, and two months ($\sim$ 20 MGT) for the crack to propagate up to the rail head. Because such heavy traffic is not typical, three months is probably a minimum time required for a corner crack to grow through the web and up to the head. Final fracture through the head may then occur quickly, but there could be a substantial delay before the crack actually enters the head.

Much of the data on which these conclusions are based are extremely variable. Actual crack growth could proceed either more slowly or more quickly depending on actual traffic and joint conditions. Further strain data on actual rail joints would provide needed confirmation

of the joint mechanics used for the predictions here. In addition, the processes of fatigue crack initiation and crack penetration of the rail head require further study. Tests on fretting, both with and without a corrosive environment, are needed to understand better the time required for crack initiation under these conditions. Fatigue tests on bolt hole cracks extending to the base of the rail head would provide important insight into the time to fracture once a crack has reached the head. The initiation and growth data furnished by these programs would prove invaluable in a calculation of the total time required for a crack to initiate, grow, and fracture the rail.

APPENDIX A: EXAMINATION OF THREE RAIL END BOLT HOLE CRACKS REMOVED FROM SERVICE

The Boston and Maine Corporation provided us with three rail pieces that contained bolt hole cracks for our examination. The pieces had been removed from service less than one month before examination. Each of the three rails was manufactured in 1929, and all joints were formed with four hole, 24 in. joint bars. Only the cracked rail end was given to us; we did not obtain the mating rail end, the joint bars or the bolts.

Rail Joint No. 1

This rail was 100 lb/yd rail in which the crack initiated from the first bolt hole and caused complete fracture of the rail end. A photograph is shown in Figure A1. The crack extended from two sides of the bolt hole at 40° to the rail axis on the upper part and 30° to the rail axis on the lower part. The fracture was apparently completely brittle and the locations of initiation were identified as small surface defects which may or may not be fatigue cracks. A magnified photograph of the defect for the upper crack is shown in Figure A2. Contact between the bolts and the hole surfaces was evident from fresh surface located adjacent to the upper crack on the first bolt hole. The regions of contact for the two holes in the broken rail are illustrated in Figure A3. This type of contact appears to be caused by movement of the joint bars or misalignment. There was some evidence of fretting debris--reddish powder--on the first bolt hole surface, but it was located about 0.25 in. from the crack site. Other parts of the bolt hole surface and much of the web had suffered considerable pitting corrosion.

Deep impressions in the rail base and rail head underside, where the joint bar contact points were located, indicated great joint bar forces. This was true of all of the rail pieces. The fracture propagated at almost 90° to the rail axis as the crack entered the rail

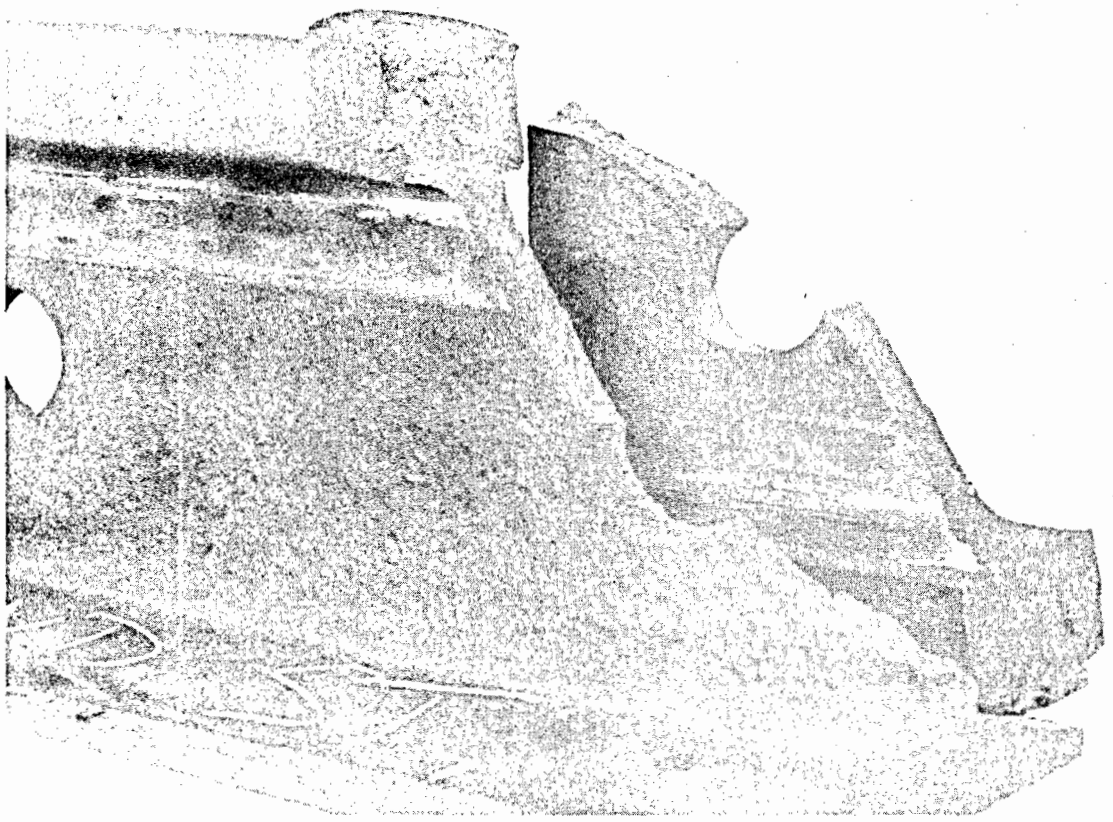

Figure A1: A Bolt Hole Fracture from the First Hole in a 100 lb/yd Standard Carbon Rail.

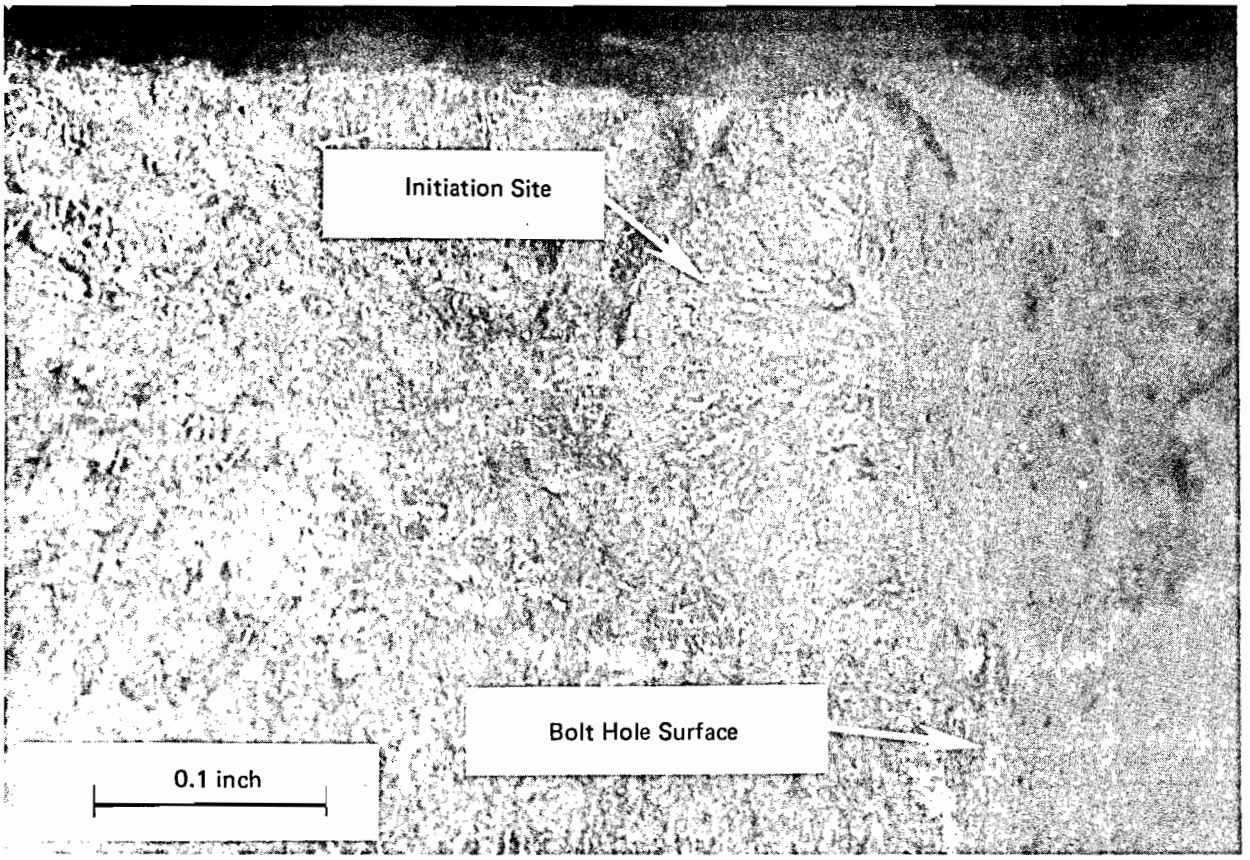

Figure A2: A Magnified Photograph of the Apparent Fracture Origin of the Bolt Hole Fracture Shown in Figure A1; the Origin is on the Gage Side of the Rail.

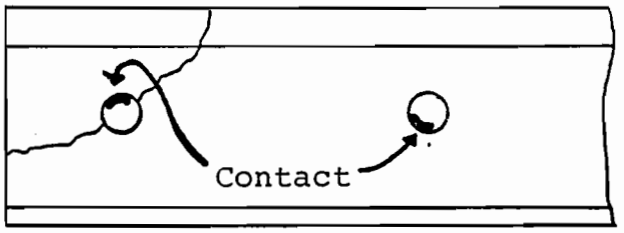

(a) Rail No. 1

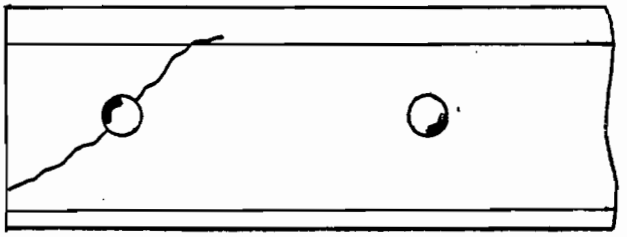

(b) Rail No. 2

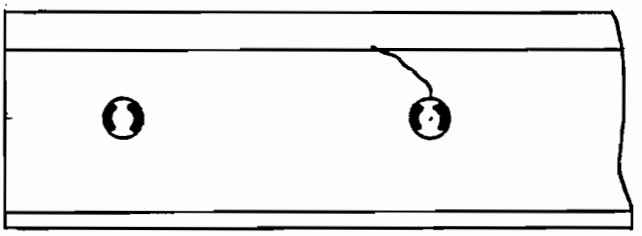

(c) Rail No. 3

Figure A3: Regions of Contact Between Bolt and Bolt Hole Surface in the Three Rails With Bolt Hole Cracks Provided by Boston and Maine.

head. The fracture surface revealed that crack advance was fastest in the center of the rail head: the crack propagated up the center of the head then turned around and propagated down to the outer, undersides of the head resulting in a nonplanar fracture surface.

Rail Joint No. 2

This rail was 130 lb/yd rail in which the crack also initiated at the first bolt hole and caused complete fracture of the rail end. However, in this case it was evident that several trains had passed the joint after fracture because the rail head had plastically deformed at the crack making it very difficult to separate the two pieces. Photographs of the rail as received and after being broken open are shown in Figure A4. The crack extended from two locations on the bolt hole surface: at 45° to the rail axis on the upper part and at 24° on the lower part. The upper crack was clearly a fatigue crack that extended up to the head-web fillet and then at a slight angle to the rail axis along the head-web fillet into the head. It was necessary to make three cuts into the rail piece in order to reveal the part of the crack that grew along the head-web fillet. This is shown in Figure A5. The lower crack occurred by either brittle fracture or rapid fatigue crack propagation based on its fracture surface roughness. The initiation site for the upper crack was a small surface defect very similar to the defects in the first rail piece but different from the rest of the fatigue fracture surface. These defects may not be due to fatigue but may be a result of the hole boring operation. Contact was evident on both bolt holes at the regions shown in Figure A3(b). The contact regions in this case showed some signs of rust but were not nearly as corroded as the remaining part of the bolt hole surface.

Rail Joint No.3

This 130 lb/yd rail piece cracked at the top of the second bolt hole at an angle of about 50° to the rail axis toward the rail end. A photograph of the rail piece is shown in Figure A6. The crack was not broken open so details of the fracture surface are not available. The

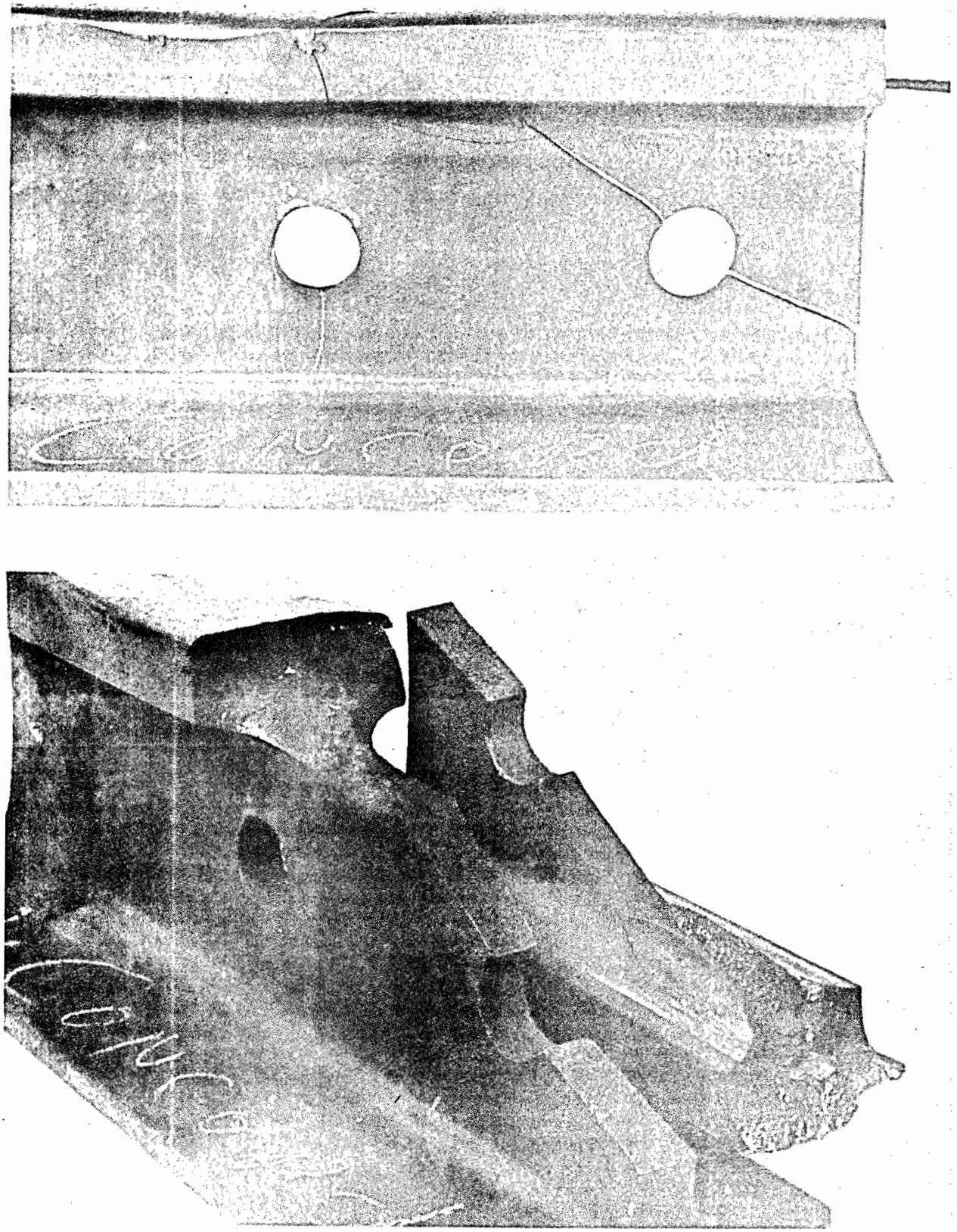

Figure A4: A Bolt Hole Fracture from the First Hole in a 130 lb/yd Standard Carbon Rail; the Upper Photograph Shows the Rail as Received, and the Lower Photograph Shows the Rail After Being Broken Open.

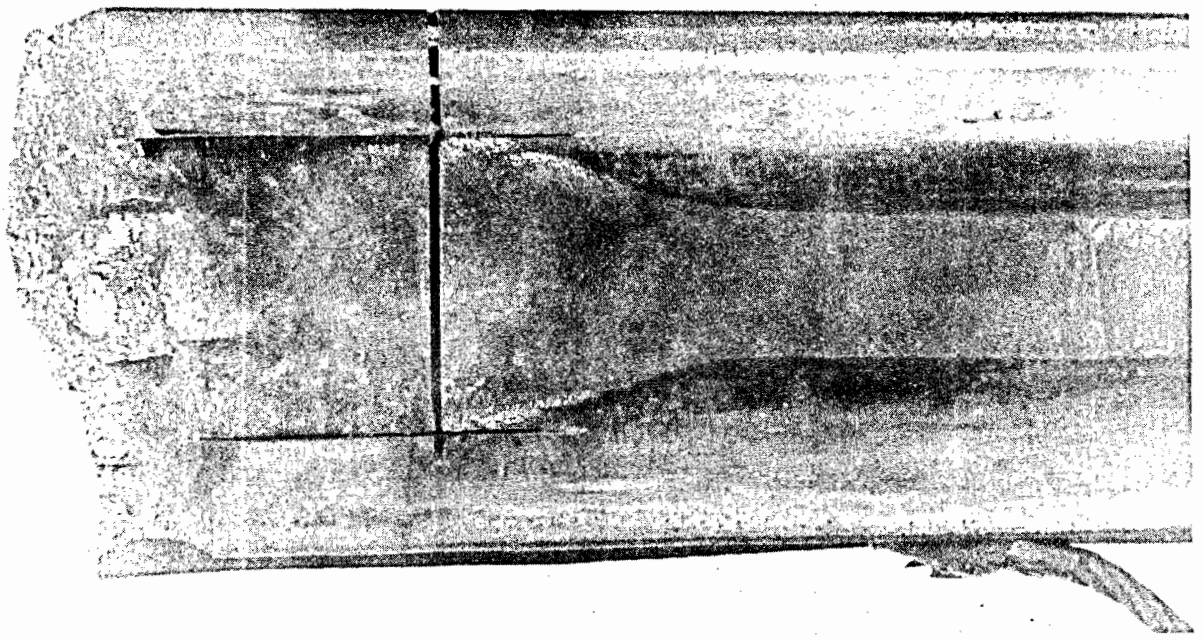

Figure A5: A section of the Part of the Bolt Hole Crack Shown in Figure A4 that Entered the Rail Head; the End of the Crack is Nearly Parallel to the Running Surface.

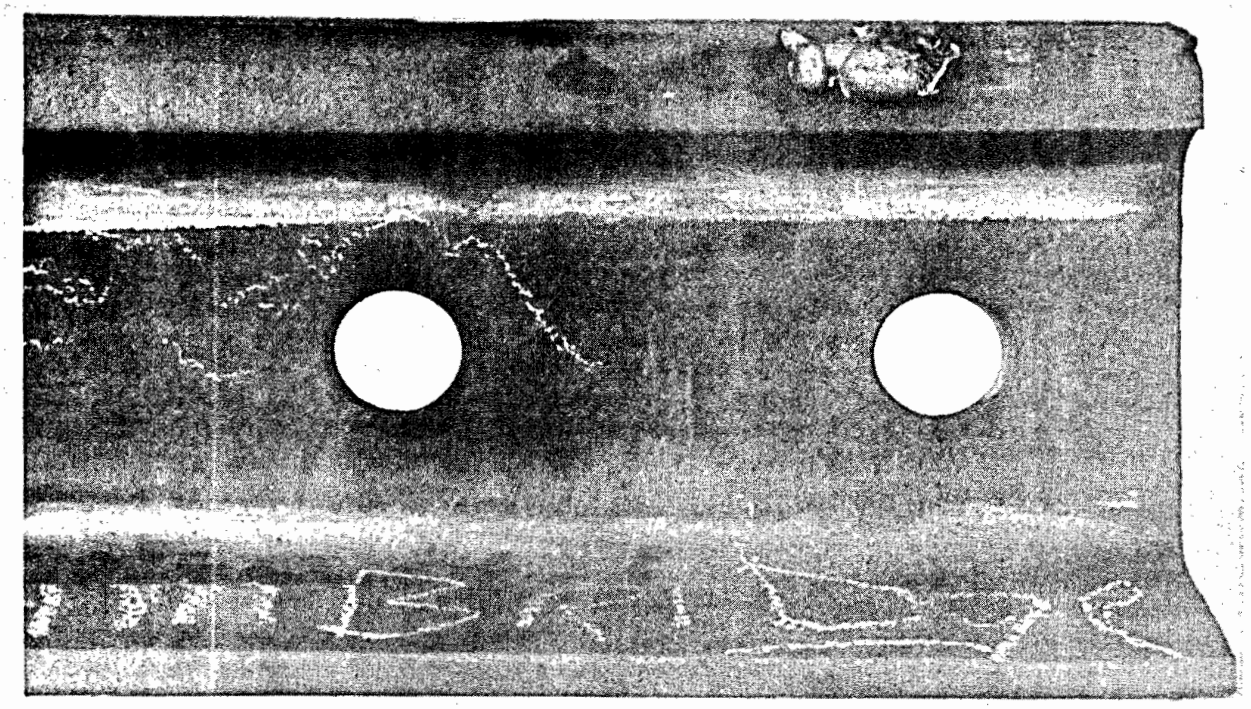

Figure A6: A Bolt Hole Crack from the Second Hole in a 130 lb/yd Standard Carbon Rail.

crack grew at 40° to the rail axis about halfway into the head after which it appears to have turned parallel to the rail axis. There are four zones of contact evident on the bolt hole surfaces as shown in Figure A3(c). None of these are close to the crack site, and the contact surfaces closest to the rail end show significant plastic deformation. This indicates that cracking may have occurred while the rail was under severe tension in winter.

APPENDIX B: DESIGN OF A FIXTURE TO DETERMINE THE BREAKING STRENGTH OF RAILS CONTAINING BOLT HOLE CRACKS

The FASTKRAX project includes determination of bolt hole crack growth rates in simulated service tests at the AAR Transportation Test Center and determinations of the breaking strength for rails that contain the defects. The purpose of determining breaking strength is to establish the margin of safety that the defect-containing rail has in service, the wheel loads required to cause fracture and the applicability of the fracture mechanics analysis in predicting fracture for the particular type of defect. The objective is to load the rail in the way it would be loaded in service. The procedure for detail fractures is to load the rail in four-point bending with the head in tension. The Transportation Systems Center (TSC) has a testing machine and fixture to conduct these tests.

Several studies (cf.[5]) have shown that the primary driving force for fracture of the most common bolt hole crack geometry (see Figure 1-2) comes from the joint bar forces applied under the rail head at the rail end. The stress intensity factor for this crack orientation is greatest when the wheel is just beyond the first bolt hole. For cracks oriented 90° to the most common orientation, and for fast moving trains, the stress intensity factor is greatest when the wheel just crosses the joint and impacts the end of the cracked rail.

Three- or four-point bending of an assembled joint is a convenient method of determining the breaking strength of a rail containing a bolt hole crack. In this case, as in the case in which a foundation is present, the maximum shear force at the cracked bolt hole occurs when the central load is applied adjacent to the bolt hole on the side opposite the rail end. This can be shown as follows [5]. The joint bar transfers load to the rail in a four point bending mode in which the points of contact occur near the rail ends and near the ends of the joint bar. The magnitudes of these joint bar forces are determined by equilibrium with the bending moment and shear force at the joint center as shown in Figure B1(b). Finally, the shear force at the bolt hole is just the sum of the force Q at the rail end and the central load, P, if

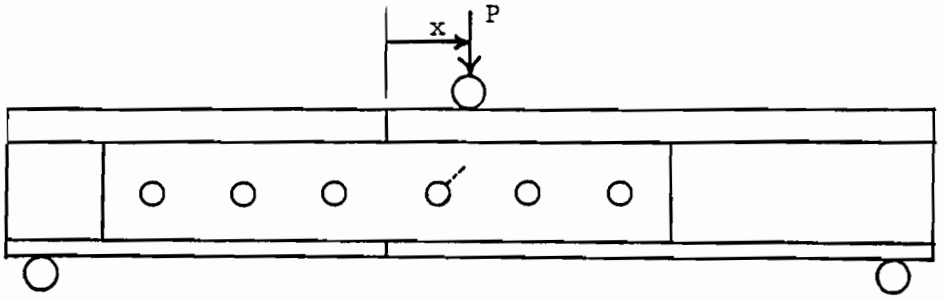

(a)

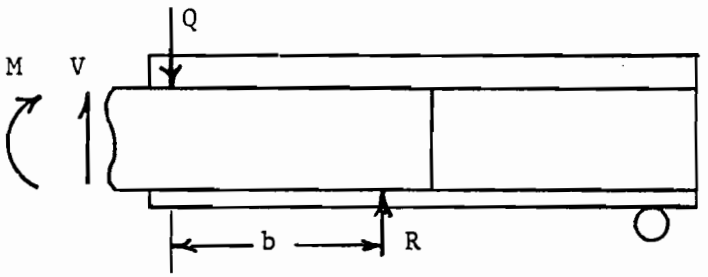

(b)

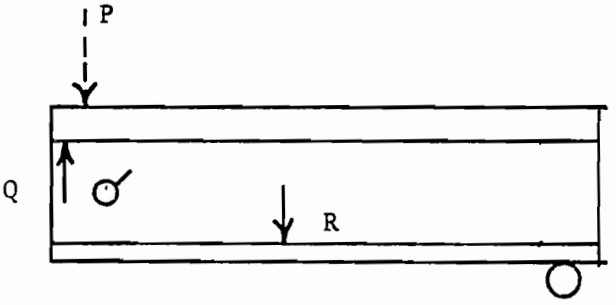

(c)

Figure B1: Shear Forces Produced in a Three or Four-Point Bend Fixture; (a) Proposed Set-up for TSC Rail Breaker; (b) Joint Bar Forces; (c) Rail End Forces.

the load is on the section of the rail between the rail end and the cracked bolt hole (see Figure B1(c)). Figure B2 shows the shear force at the first bolt hole as a function of the distance of the joint center from the central load. It has been assumed that the distance between the joint bar forces, b in Figure B1(b), is equal to 12 in., and the span of the loading fixture is 54 in. The figure shows that the maximum bolt hole shear force occurs when the central load is just to the right of the bolt hole. The shear force then has a magnitude of almost 1.5 times the centrally applied load. This shear force is also in a direction that will cause the most common bolt hole crack to fracture. For cracks oriented perpendicular to this orientation, a shear force of opposite sign is required to cause fracture. Figure B2 shows that there are only a few locations for which the applied load will result in bolt

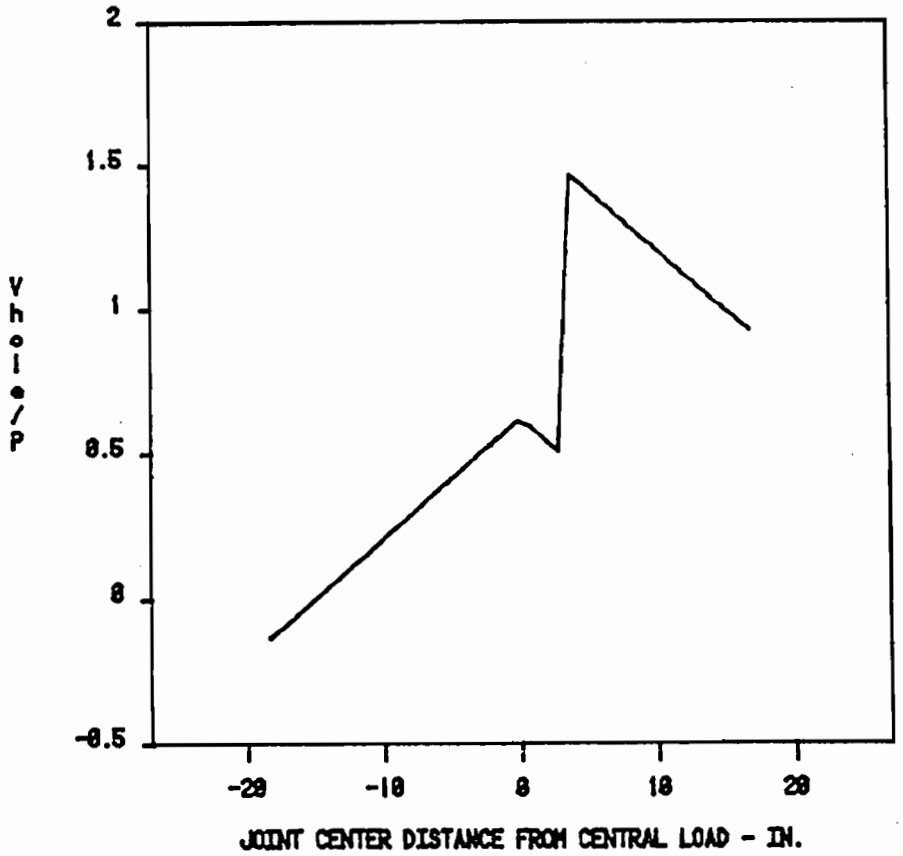

Figure B2: Shear Force at the First Bolt Hole in a Three or Four-Point Bend Fixture. Positive Distances are for Load Application Points to the Right of the Joint (see Figure B1).

hole shear force of opposite sign, and these only result in a low magnitude shear force. Therefore, the rail should be turned base up and loaded just to the right of the cracked bolt hole to cause fracture in cracks oriented perpendicular to the most common bolt hole crack.

The load required to cause fracture of the bolt hole cracks can be estimated from results of a previous investigation [5] in which rails containing bolt hole cracks were loaded in three-point bending. These tests, in which crack growth rates were measured and values of K_I inferred, showed that an 80 kip central load, or a 40 kip shear force, resulted in a value of $K_I \cong 25$ ksi $\sqrt{\text{in}}$ for crack lengths extending from 0.5 to 3 in. from the bolt hole. Rail steel fracture toughness seldom exceeds 50 ksi $\sqrt{\text{in.}}$ Therefore, since the bolt hole shear force for the rail breaker is about 1.5 times the central load, a central load of less than 100 kips should be sufficient to fracture the rail. A larger load may be required if the crack has just entered the rail head, since the value of K_I apparently decreases at this point. The analysis presented in [5] should be used to relate the breaking load in the four-point bend test to actual track conditions, because the bend test results in greater bending moments and shear forces at the joint than in track. Unfortunately, this analysis cannot be conducted with precision because the actual distance between the joint bar forces, b, is unknown.

The joint bars used in the joint assembly should be free of defects at their center outer fibers because the joint bars could be subjected to very high stresses. For example, if the central load is 100 kips applied 5 in. from the joint center, then the bending moment at the joint center is $(50\text{x}10^3)(27\text{-}5) = 1.1\text{x}10^6$ in-lb. Two joints bars have a section modulus of about 11 in^4 which gives a maximum stress of 100 ksi.

Before actually breaking the rail, about 100 fatigue cycles should be applied to the rail assembly to sharpen the crack. This should be done at a central load of about 25 kips.

ACKNOWLEDGEMENTS

The authors are grateful for the technical direction provided by Oscar Orringer and James Morris of the Transportation Systems Center. The financial support of the Department of Transportation is also gratefully acknowledged.

REFERENCES

1. Wise, S., Lindsay, D. and Duncan, I.G.T., "The Strength of Rails with Particular Reference to Rail Joints," Proceedings of the Institution of Mechanical Engineers, 174, 9 (1960) pp. 371-407.

2. Lindh, D.V., Taylor, R.Q. and Rose, D.M., "Sleeve Expansion of Bolt Holes in Railroad Rail," Vol. I, FRA/ORD-80/5, I (NTIS PB80 182181), Boeing Commercial Airplane Company (Dec. 1977) 67 pages.

3. Ahlbeck, D.R., Johnson, M.R., Harrison, H.D. and Tuten, J.M., "Measurements of Wheel/Rail Loads on Class 5 Track," Report FRA/ORD-80/19 (NTIS PB80 196868) (Feb. 1980) 292 pages.

4. Jenkins, H.H., Stephenson, J.E., Clayton, G.A., Morland, G.W. and Lyon, D., "The Effect of Track and Vehicle Parameters on Wheel/Rail Vertical Dynamic Forces," Railway Engineering Journal (Jan. 1974) pp. 2-26.

5. Mayville, R.A., Hilton, P.D. and Peirce, D.C., "An Analytical and Experimental Study of Fatigue Crack Growth from Rail End Bolt Holes," Arthur D. Little, Inc., Report 85560 to Transportation Systems Center, Department of Transportation (Feb. 1984) 39 pages.

6. Savin, G.N., Stress Concentration Around Holes, translated by W. Johnson (New York, Permagon Press) 1961.

7. Johns, T.G., Sampath, S.G., Bell, J.C. and Davies, K.B., "Engineering Analysis of Stresses in Railroad Rails," Report FRA/ORD-81/S1 (NTIS PB82 129610) Battelle - Columbus Laboratories (March 1981).

8. Timoshenko, S. and Langer, B.F., "Stresses in Railroad Track," Journal of Applied Mechanics, Trans. ASME, 54 (1932) pp. 277-302.

9. Jensen, R.S., "Fatigue Tests of Rail Webs," AREA Proceedings, 51 (1950) pp. 640-647.

10. Dabell, B.J., Hill, S.J. and Watson, P., "An Evaluation of the Fatigue Performance of Conventional British Rail Steels," in Rail Steels-Development, Processing and Use, ASTM STP 644, D.H. Stone and G.G. Knupp, eds. (1978) pp. 449-468.

11. Leis, B.N., "Cyclic Inelastic Deformation and Fatigue Resistance Characteristics of a Rail Steel," ibid, pp. 449-468.

12. Heller, W. and Schweitzer, R., "Untersuchungen zum Betriebsverhalten von Schienenstahl," (Investigations of the In-Service Behavior of Rail Steel), Archiv fuer Eisenbahntechnik, 28 (Dec. 1973) pp. 81-89.

13. Barsom, J.N. and Imhof Jr., E.J., "Fatigue and Fracture Behavior of Carbon-Steel Rails," ibid, pp. 387-413.

14. Fretting Fatigue, R.B. Waterhouse, ed. (London, Applied Science Pub. Ltd.) 1981.

15. Waterhouse, R.B., "Avoidance of Fretting Fatigue Failures," ibid, pp. 221-240.

16. Tada, H., Paris, P. and Irwin, G., "The Stress Analysis of Cracks Handbook," Del Research Corp. (1973).

17. Newman, J.C. and Raju, I.S., "Stress-Intensity Factor Equations for Cracks in Three-Dimensional Finite Bodies," Fracture Mechanics: Fourteenth Symposium - Volume I: Theory and Analysis, ASTM STP 791, J.C. Lewis and G. Sines, eds., American Society for Testing and Materials (March 1981) pp.I-238 - I-265.

18. McGowan, J.J. and Smith, C.W., "Stress Intensity Factors for Deep Cracks Emanating from the Corner Formed by a Hole Intersecting a Plate Surface," Mechanics of Crack Growth, ASTM STP 590, American Society for Testing and Materials (1976) pp. 460-476.

19. Rudd, J.L., "Part-Through Crack Growth Predictions Using Compact Tension Crack Growth Rate Data," Part-Through Crack Fatigue Life Prediction, ASTM STP 687, J.B. Chang, ed., American Society for Testing and Materials (1979) pp. 96-112.

20. Kobayashi, A.S. and Enetanya, A.N., "Stress Intensity Factor of a Corner Crack," Mechanics of Crack Growth, ASTM STP 590, American Society for Testing and Materials (1976) pp. 477-495.

21. Tracey, D.M., "3-D Elastic Singularity Element for Evaluation of K Along an Arbitrary Crack Front," International Journal of Fracture, Vol. 9, No. 3 (1973).

22. Atluri, S.N. and Kathiresan, K., "Influence of Flaw Shapes on Stress Intensity Factors for Pressure Vessel Surface Flaws and Nozzle Corner Cracks," ASME Paper 79-PVP-65 (1979).

23. Newman, J.C. and Raju, I.S., "Analysis of Surface Cracks in Finite Plates Under Tension and Bending Loads," NASA Technical Paper 1578 (1979).

24. Mayville, R.A. and Hilton, P.D., "Laboratory Analysis of Rails Containing Detail Fractures," Arthur D. Little, Inc. Report 85662-01 to Department of Transportation (March 1983).

25. "Stresses Around a Bolt Hole of a Rail With the Joint in Tension," AREA Proceedings, Vol. 54 (1953) pp. 1254-1267.

26. Pian, T.H.H., Mar, J.W., Orringer, O., and Stalk, G., "Numerical Computation of Stress Intensity Factors for Aircraft Structural Details by the Finite Element Method," Technical Report AFFDL-TR-76-12 to Wright-Patterson Air Force Base (1976).

27. Timoshenko, S.P. and Goodier, J.N., Theory of Elasticity, 3rd edition, McGraw-Hill, New York (1970).

28. Chavez, P.F., "Automatic Procedures in Evolutionary Finite Element Calculations," Ph.D. Thesis, Cornell University (1983).

29. Yang, W.H., Houssny-Emam, M. and Bassim, M.N., "An Experimental K-Analysis on the Fatigue Crack Near the Interface Where Plate Thickness Varies Discontinuously-Thin to Thick Type," Engineering Fracture Mechanics, Vol. 29, No. 2. (1984), pp. 295-303.

30. Suresh, S., "Crack Deflection: Implications for the Growth of Long and Short Fatigue Cracks," Metallurgical Transactions A , Vol. 14A (1983) p. 2375.

31. Cotterell, B. and Rice, J.R., International Journal of Fracture, Vol. 16 (1980) p. 155.

32. Kitugawa, H., Yuuki, R. and Ohira, T., "Crack-Morphological Aspects in Fracture Mechanics," Engineering Fracture Mechanics, Vol. 7 (1975) pp. 515-529.

33. Groom, J.J., "Residual Stresses in Railroad Rails," presented at the Fourth SESA International Congress on Experimental Mechanics, Boston, MA (May 1980).

34. Wu, X.R., "Stress Intensity Factors for Half-Elliptical Surface Cracks Subject to Complex Crack Face Loadings," Engineering Fracture Mechanics, Vol. 19 (1984) p. 387.

35. Hilton, P.C. and Peirce, D.C., "APES3D-Revision 1.0 Documentation and Theoretical Manual," Report to David Taylor Naval Ship R&D Center, Bethesda, Maryland (Jan. 1983).

36. "Stresses in Railroad Track - The Talbot Reports," reprinted reports of the Special Committee on Stresses in Railroad Track, 1918-1940, Prof. A.N. Talbot, Chairman, American Railway Engineering Association (1980), 1304 pages.